VIRGINIA TECH

CPES
Center for Power Electronics Systems

High Power Density Single Stage Auxiliary Power Module (APM) Design for Electric Vehicle: A Technical Review

Xiang Zhang, Dr. Liyan Zhu, Dr. Qiang Li

Feb. 3rd, 2025

On market 800V battery architecture Electric Vehicle

Taycan
610 V to 834 V

- Configuration = 198s 2p (LG Chem E66a)
- 33module X 12cells/module/(6s 2p)
- Nominal Voltage = 3.651V (723V)
- 2019 Porsche Taycan - Battery Design

e-Tron GT
594V(544V) to 841 V

- Configuration = 198s 2p (LG Chem E66a)
- 33module X 12cells/module/(6s 2p)
- Nominal Voltage = 3.657V (724V)
- 2021 Audi e-tron GT quattro - Battery Design

SU7 Max
594V(544V) to 871 V

- Configuration = 198s 2p (CATL Qilin CTP 3.0)
- 33module X 12cells/module/(6s 2p)
- Nominal Voltage = 3.67V (727V)
- Xiaomi SU7 Max Battery - Battery Design

Cybertruck
576V(528V) to 816 V

- Configuration = 192s 7p (Tesla 4680)
- 4module X 336cells/module (48s 7p)
- Nominal Voltage = 3.67V (705V)
- TESLA CYBERTRUCK and Battery Pack - Battery Design

EV6

Ioniq 5
480 V to 806 V

- Configuration = 192s 2p
- 32module X 12cells/module (6s 2p)
- Nominal Voltage = 3.63V (697V)
- 2022 Kia EV6 - Battery Design

G80 EV

- Configuration = 144s 3p
- 36module X 12cells/module (4s 3p)
- Genesis Electrified G80 Battery Pack Opened Up

LUCID AIR
525V to 882V

- Configuration = 210s 24p
- Nominal Voltage = 3.6V (756V)
- Formula E Battery 2019-21 - Battery Design

All Electric Vehicle

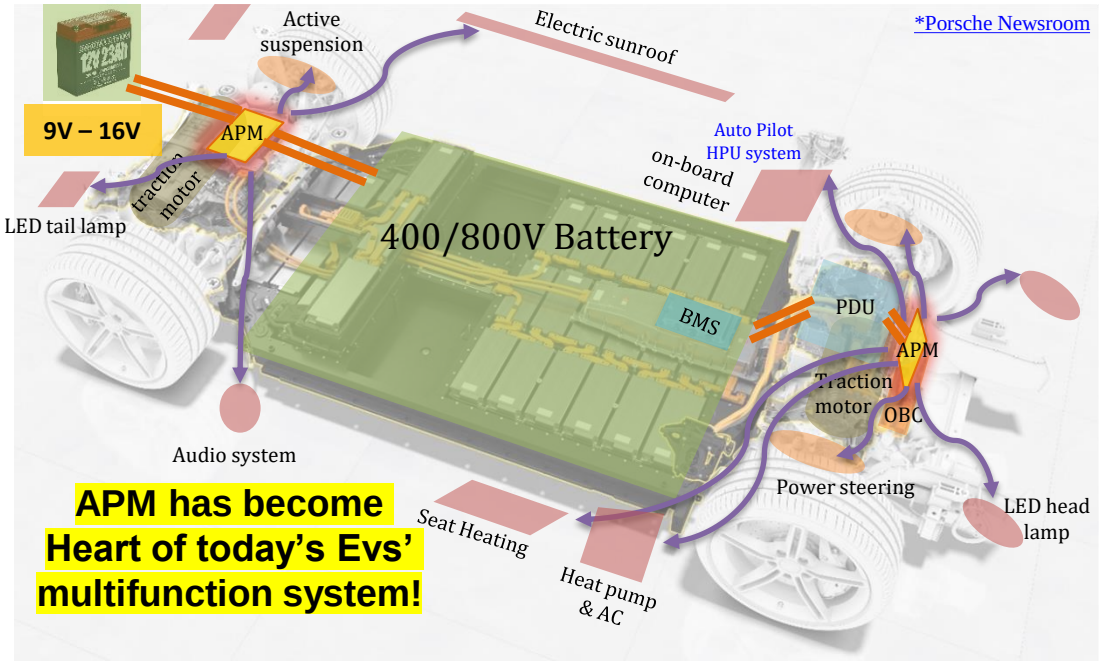

Strong/full-hybrid EV

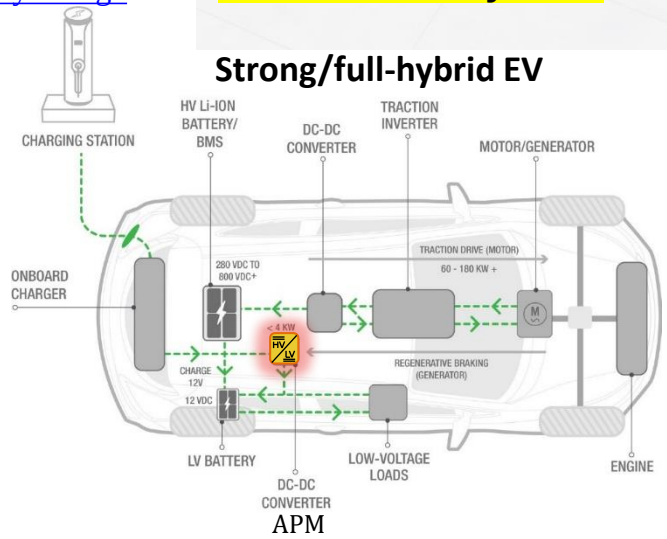

mild-hybrid EV

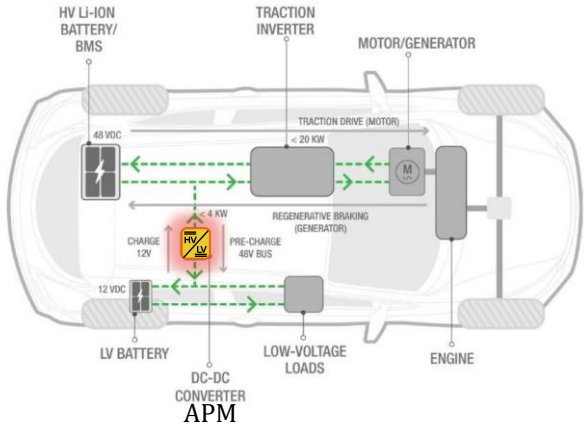

Challenge 1: High turns ratio & Ultra-Wide Gain range

400V Architecture APM

800V Architecture APM

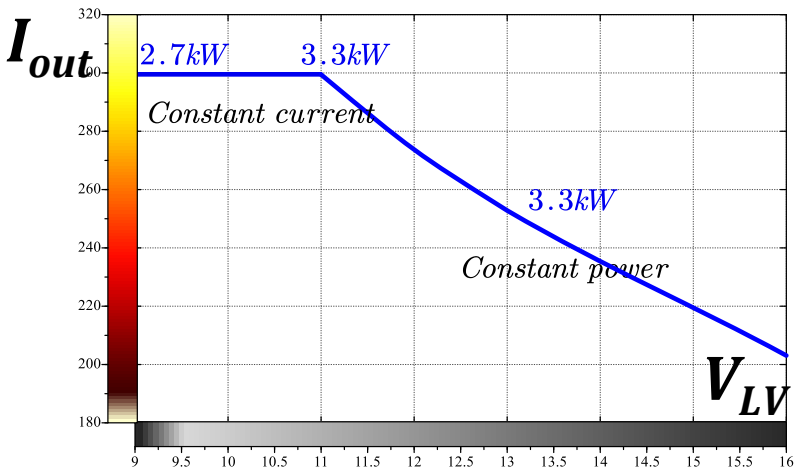

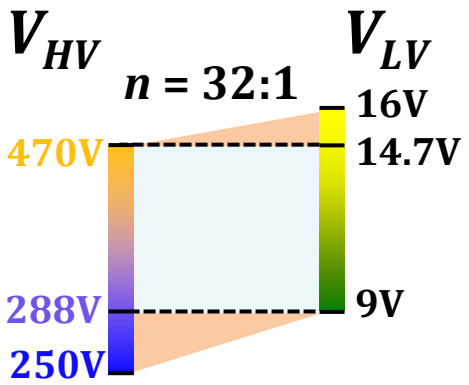

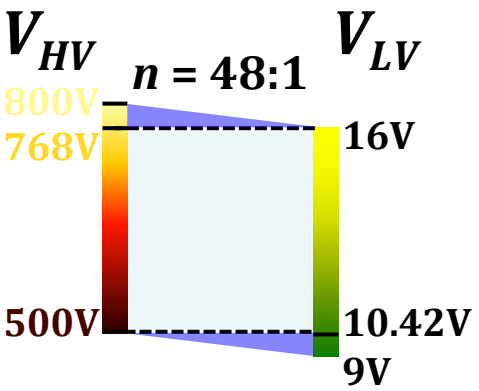

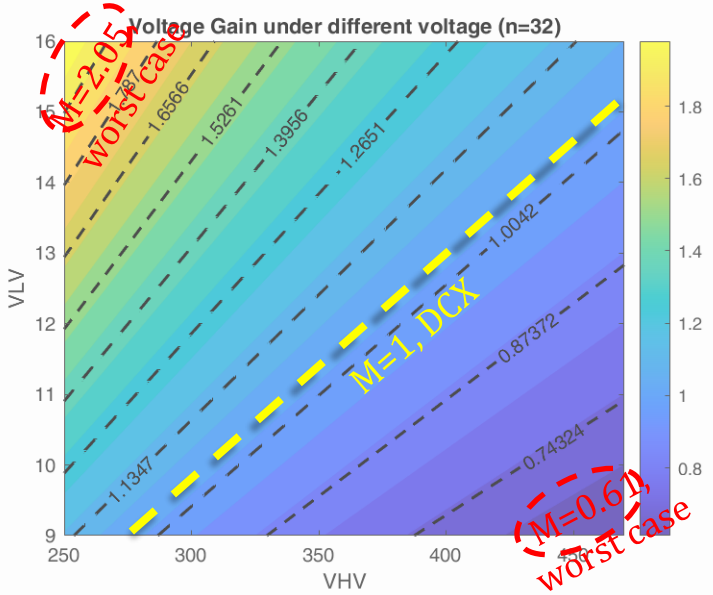

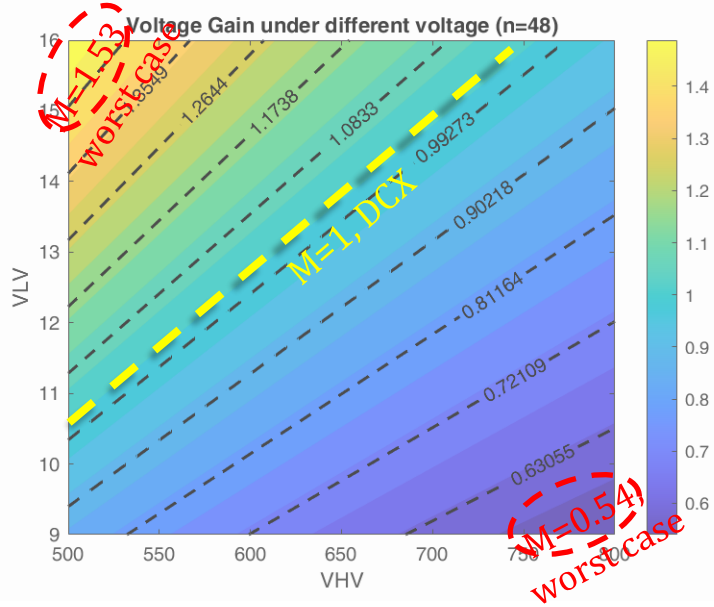

Challenge 2: High current stress & turn-off losses issue

800V Architecture APM

Operation Points (V|A)	Turn-ON (μJ)				Turn-OFF (μJ)			
	Simulation		Experimental		Simulation		Experimental	
	Switch	Scope	Delay Comp.	Scope	Switch	Scope	Delay Comp.	Scope
100 | 4.3	9.4	14.4	10.1	15.2	2.7	1.5	7.47	4.5
200 | 8.5	49.9	68.7	51.6	71.6	6.2	3.2	13.3	9.5
300 | 12.6	128.2	160.2	136.5	171.8	11.5	3.7	20.2	11.8
400 | 18.3	232.7	284.2	261.8	314.7	16.5	5.2	36.8	19.9

	80V/48A	80V/187A	
Technology	GaN	Si	
Part number	EPC2029	BSC025N08LS5	
$V_g(V)$	5	5	10
$C_{oss}(pF)$	820	840	840
$R_{dson-max}(m\Omega)$	3.2	3.2	2.5
$Q_g(nC)$	13	44	80

Assuming 3.6kW per module, the Secondary output current can exceed 300A!

6-12 devices is needed to handle the current, matrix transformer prefer

For Secondary rectifier, driver loss and conduction loss is a trade off

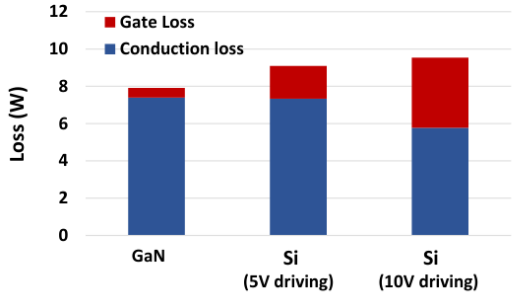

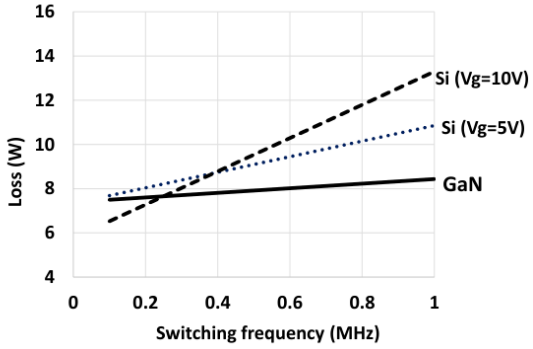

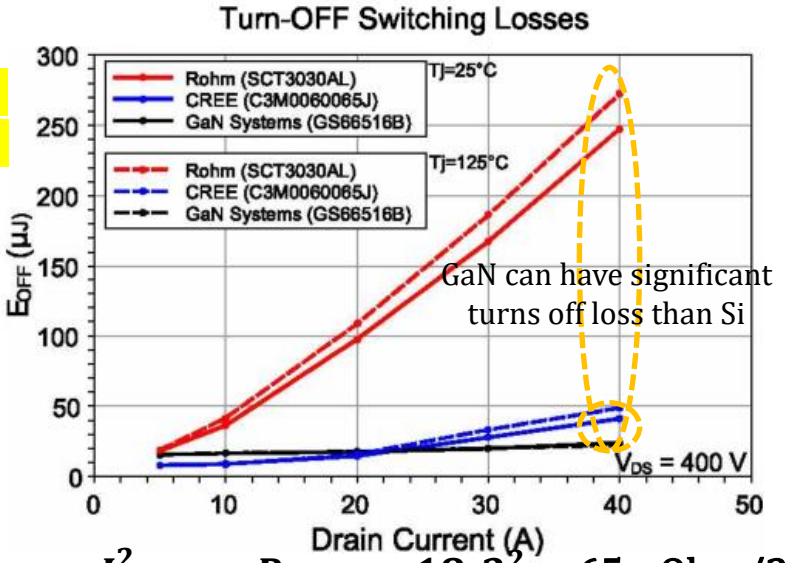

$$P_{condloss} = I_{sec(rms)}^2 R_{dson} = 18.3^2 \times 65\text{mOhm}/2 = 10.88\text{W}$$

$$E_{off} = E_{oss} + E_{offloss} = \frac{1}{2} C_{oss} V^2 + P_{offloss} T_s$$

$$P_{offloss} = \left(19.9\mu J - \frac{1}{2} \cdot 207pF \cdot (400V)^2\right) / 2\mu s = 1.67W$$

$$P_{onloss} = 0W\ (ZVS)$$

Even for GaN, Turn off loss can reach 1/6 of conduction loss !!!

J. Oliveira, A. Alhoussen, F. Loiselay, H. Morel, and D. Planson, "Switching Behavior and Comparison of Wide Bandgap Devices for Automotive Applications," in *2021 23rd European Conference on Power Electronics and Applications (EPE'21 ECCE Europe)*, Ghent, Belgium: IEEE, Sep. 2021, pp. 1–10. doi: 10.23919/EPE21ECCEEurope50061.2021.9570434.

Challenge 3: Global efficiency & High power density

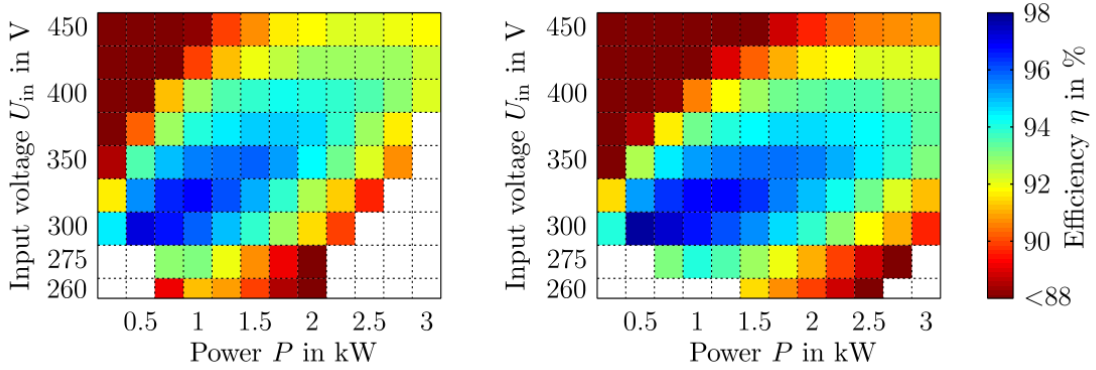

(a) SPS operation at $f_{sw} = 100\,\text{kHz}$

(b) SPS operation at $f_{sw} = 70\,\text{kHz}$

(c) TRI/TRAP-CM operation

(d) Operation mode combination

Figure 7.8: Efficiency of the different operation modes for $U_{out} = 14\,\text{V}$. Efficiency axes are cropped at 88 %.

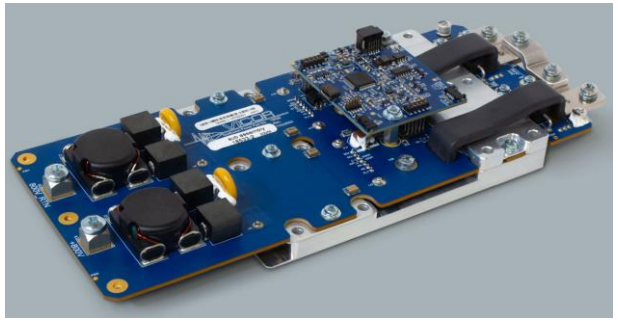

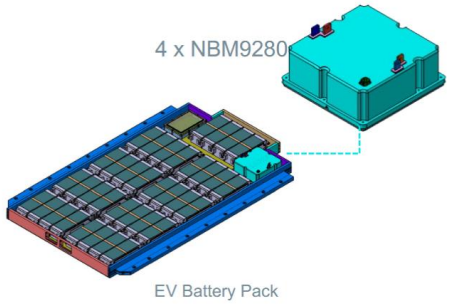

Device	Vicor Concept	Tesla Model X	Vitesco 4th Gen	Bright Loop DCDC LP
Output Power (W)	4000 @ 13.8V	2300 @ 12 V	3500 @ 14.5V	9600@?
Output Current (A)	290	193	240	480
Weight (kg)	1.4	2.1	2.6	3.5
Footprint (mm2)	24500	30520	50000	70272
Volume (L, w/o connectors)	1.1L (245 x 100 x 40)	1.8L (140 x 218 x 60)	1.8L (140 x 218 x 60)	3.0L (192 x 366 x 43)
Efficiency	95%	93% Estimate	96% Estimate	Global > 94%
Power Density (kW/liter)	**3.63**	**1.3**	**1.34**	**3.2**
Gravimetric Power Density (kW/kg)	2.85	1.1	1.5	2.7

https://www.vicorpower.com/resource-library/articles/automotive/power-modules-for-uncharted-ev-power-challenges

Comprehensive Review of state-of art APMs

REFERENCES

[1] S.-Y. Yu, C. Hsiao, and J. Weng, "A high frequency CLLLC bi-directional series resonant converter DAB using an integrated PCB winding transformer," in *2020 IEEE Applied Power Electronics Conference and Exposition (APEC)*, Mar. 2020, pp. 1074–1080.

[2] G. C. Knabben, J. Schafer, L. Peluso, J. W. Kolar, M. J. Kasper, and G. Deboy, "New PCB Winding "Snake-Core" Matrix Transformer for Ultra-Compact Wide DC Input Voltage Range Hybrid B+DCM Resonant Server Power Supply," in *2018 IEEE International Power Electronics and Application Conference and Exposition (PEAC)*. Shenzhen: IEEE, Nov. 2018, pp. 1–6.

[3] T. Jiang, J. Zhang, X. Wu, K. Sheng, and Y. Wang, "A Bidirectional Three-Level LLC Resonant Converter With PWAM Control," *IEEE Transactions on Power Electronics*, vol. 31, no. 3, pp. 2213–2225, Mar. 2016.

[4] X. Zhou, B. Sheng, W. Liu, Y. Chen, L. Wang, Y.-F. Liu, and P. C. Sen, "A high-efficiency high-power-density on-board low-voltage DC–DC converter for electric vehicles application," *IEEE Transactions on Power Electronics*, vol. 36, no. 11, pp. 12 781–12 794, Nov. 2021.

[5] M. Pahlevaninezhad, P. Das, J. Drobnik, P. K. Jain, and A. Bakhshai, "A Novel ZVZCS Full-Bridge DC/DC Converter Used for Electric Vehicles," *IEEE Transactions on Power Electronics*, vol. 27, no. 6, pp. 2752–2769, Jun. 2012.

[6] X. Yu, Z. Lan, J. Zeng, C. Tu, and D. He, "Time-domain based Superposition Analysis for Triple Active Bridge and its Application for ZVS and Current Stress Optimization," *IEEE Transactions on Power Electronics*, pp. 1–13, 2023.

[7] Z. Lin, S. Pan, M. Wang, W. Lin, J. Gong, L. Yao, and P. Jain, "A Three-Port LCC Resonant Converter for the 380-V/48-V Hybrid DC System," *IEEE Transactions on Power Electronics*, vol. 37, no. 9, pp. 10 864–10 876, Sep. 2022.

[8] H. van Hoek, M. Neubert, and R. W. De Doncker, "Enhanced modulation strategy for a three-phase dual active bridge—boosting efficiency of an electric vehicle converter," *IEEE Transactions on Power Electronics*, vol. 28, no. 12, pp. 5499–5507, Dec. 2013.

[9] Z. Wang and H. Li, "A soft switching three-phase current-fed bidirectional DC-DC converter with high efficiency over a wide input voltage range," *IEEE Transactions on Power Electronics*, vol. 27, no. 2, pp. 669–684, Feb. 2012.

[10] P. Purgat, S. Bandyopadhyay, Z. Qin, and P. Bauer, "Zero Voltage Switching Criteria of Triple Active Bridge Converter," *IEEE Transactions on Power Electronics*, vol. 36, no. 5, pp. 5425–5439, May 2021.

[11] D. Moon, J. Park, and S. Choi, "New interleaved current-fed resonant converter with significantly reduced high current side output filter for EV and HEV applications," *IEEE Transactions on Power Electronics*, vol. 30, no. 8, pp. 4264–4271, Aug. 2015.

[12] H. Yu, Y. Wang, H. Zhang, and Z. Chen, "Impedance Modeling and Stability Analysis of Triple-Active-Bridge-Converter-Based Renewable-Electricity-Hydrogen-Integrated Metro DC Traction Power System," *IEEE Transactions on Industrial Electronics*, vol. 70, no. 12, pp. 12 340–12 353, Dec. 2023.

[13] I. Kim and J.-W. Park, "New integrated DC–DC conversion system for electric vehicles," *IEEE Transactions on Industrial Electronics*, pp. 1–10, 2023.

[14] X. Tang, H. Wu, W. Hua, Z. Yu, and Y. Xing, "Three-Port Bidirectional Series-Resonant Converter With First-Harmonic-Synchronized PWM," *IEEE Journal of Emerging and Selected Topics in Power Electronics*, vol. 9, no. 2, pp. 1410–1419, Apr. 2021.

[15] J. Andrade, D. S. Y Rosas, D. Frey, and J.-P. Ferrieux, "Modified triple active bridge DC/AC three-phase converter with a series-resonant LC circuit on the AC-side," in *2017 IEEE Southern Power Electronics Conference (SPEC)*. Puerto Varas, Chile: IEEE, Dec. 2017, pp. 1–6.

[16] K. Wang, W. Liu, and F. Wu, "Topology-Level Power Decoupling Three-Port Isolated Current-Fed Resonant DC-DC Converter," *IEEE Transactions on Industrial Electronics*, vol. 69, no. 5, pp. 4859–4868, May 2022.

[17] F. Wu, W. Liu, K. Wang, and G. Wang, "Modeling and Closed-Loop Control of Three-Port Isolated Current-Fed Resonant DC–DC Converter," *IEEE Transactions on Transportation Electrification*, vol. 9, no. 1, pp. 1341–1349, Mar. 2023.

[18] N. D. Dao, D.-C. Lee, and Q. D. Phan, "High-Efficiency SiC-Based Isolated Three-Port DC/DC Converters for Hybrid Charging Stations," *IEEE Transactions on Power Electronics*, vol. 35, no. 10, pp. 10 455–10 465, Oct. 2020.

[19] P. Wang, X. Lu, W. Wang, and D. Xu, "Hardware Decoupling and Autonomous Control of Series-Resonance-Based Three-Port Converters in DC Microgrids," *IEEE Transactions on Industry Applications*, vol. 55, no. 4, pp. 3901–3914, Jul. 2019.

[20] Y.-K. Tran, F. D. Freijedo, and D. Dujic, "Open-Loop Power Sharing of Three-Port DC-DC Resonant Converters," in *2019 IEEE Applied Power Electronics Conference and Exposition (APEC)*, Mar. 2019, pp. 2138–2144.

[21] J. Wu, X. Yan, X. Sun, X. Su, H. Du, and X. Wang, "A Series Resonant Three-Port DC–DC Converter With Decoupling Function and Magnetic Integration," *IEEE Transactions on Power Electronics*, vol. 37, no. 12, pp. 14 720–14 737, Dec. 2022.

[22] X. Zhang, H. Liu, P. Wheeler, and F. Wu, "Research on Power Decoupling and Parameter Mismatch of Three-Port Isolated Resonant DC–DC Converter Applied Switch-Controlled Capacitor," *IEEE Transactions on Industrial Electronics*, vol. 70, no. 8, pp. 8098–8107, Aug. 2023.

[23] S. S. Chakraborty, S. Dey, and K. Hatua, "Design of a Three-Winding Transformer for Power Decoupling of a Three-Port Series Resonant Converter for an Integrated On-Board EV Charger," *IEEE Transactions on Power Electronics*, vol. 38, no. 11, pp. 14 262–14 273, Nov. 2023.

[24] H. Tao, A. Kotsopoulos, J. L. Duarte, and M. A. M. Hendrix, "Transformer-Coupled Multiport ZVS Bidirectional DC–DC Converter With Wide Input Range," *IEEE Transactions on Power Electronics*, vol. 23, no. 2, pp. 771–781, Mar. 2008.

[25] H. Cao, G. Zhu, F. Diao, and Y. Zhao, "Novel Power Decoupling Methods for Three-Port Triple-Active-Bridge Converters," in *2022 IEEE Applied Power Electronics Conference and Exposition (APEC)*, Mar. 2022, pp. 1833–1837.

[26] L. Wang, Z. Wang, and H. Li, "Asymmetrical Duty Cycle Control and Decoupled Power Flow Design of a Three-port Bidirectional DC-DC Converter for Fuel Cell Vehicle Application," *IEEE Transactions on Power Electronics*, vol. 27, no. 2, pp. 891–904, Feb. 2012.

[27] Y. Cai, C. Gu, J. Li, J. Yang, G. Buticchi, and H. Zhang, "Dynamic Performance Enhancement of a Triple Active Bridge With Power Decoupling-Based Configurable Model Predictive Control," *IEEE Transactions on Transportation Electrification*, vol. 9, no. 2, pp. 3338–3349, Jun. 2023.

[28] S. Goudarzitaemeh and M. Pahlevani, "A Bidirectional DC–DC Converter With Direct Power Transfer," *IEEE Open Journal of Power Electronics*, vol. 5, pp. 232–249, 2024.

[29] L. Zhu, H. Bai, and A. Brown, "Model and control of a current-fed dual active bridge based ultrawide-voltage-range auxiliary power module for 400 V/800 V electric vehicles," *IEEE Transactions on Power Electronics*, vol. 39, no. 3, pp. 3263–3276, Mar. 2024.

[30] M. Salato and P. Kowalyk, "Double-clamp ZVS converter interfaces high voltage traction batteries with 12V legacy system in hybrid and pure-electric vehicles," in *2012 IEEE Vehicle Power and Propulsion Conference*, Oct. 2012, pp. 667–670.

[31] A. M. Naradhipa, S. Kim, D. Yang, S. Choi, I. Yeo, and Y. Lee, "Power density optimization of 700 kHz GaN-based auxiliary power module for electric vehicles," *IEEE Transactions on Power Electronics*, vol. 36, no. 5, pp. 5610–5621, May 2021.

[32] C. C. D. Viana, M. Pathmanathan, and P. W. Lehn, "Auxiliary power module elimination in evs using dual inverter drivetrain," *IEEE Transactions on Power Electronics*, vol. 37, no. 10, pp. 12 513–12 524, Oct. 2022.

[33] R. Hou and A. Emadi, "Evaluation of integrated active filter auxiliary power modules in electrified vehicle applications," in *2015 IEEE Energy Conversion Congress and Exposition (ECCE)*, Sep. 2015, pp. 6314–6319.

[34] ——, "Applied integrated active filter auxiliary power module for electrified vehicles with single-phase onboard chargers," *IEEE Transactions on Power Electronics*, vol. 32, no. 3, pp. 1860–1871, Mar. 2017.

[35] D.-W. Lee, H.-S. Youn, and J.-K. Kim, "Development of phase-shift full-bridge converter with integrated winding planar two-transformer for LDC," *IEEE Transactions on Transportation Electrification*, vol. 9, no. 1, pp. 1215–1226, Mar. 2023.

[36] G. Yang, P. Dubus, and D. Sadarnac, "Double-phase high-efficiency, wide load range high- voltage/low-voltage LLC DC/DC converter for electric/hybrid vehicles," *IEEE Transactions on Power Electronics*, vol. 30, no. 4, pp. 1876–1886, Apr. 2015.

[37] L. Zhu, H. Bai, A. Brown, and A. Körner, "An ultra-high gain current-fed universal auxiliary power module for 400V/800V electric vehicles," in *2023 IEEE Applied Power Electronics Conference and Exposition (APEC)*, Mar. 2023, pp. 885–891.

Converter | Wolfspeed." [Online]. Available: https://www.wolfspeed.com/products/power/reference-designs/crd-60dd12n-k/

[78] "DC DC Converter 1500w | EMP EV MOBILITY." [Online]. Available: https://www.empevmobility.com/products/1.5kw-dc-dc-converter-unit.html

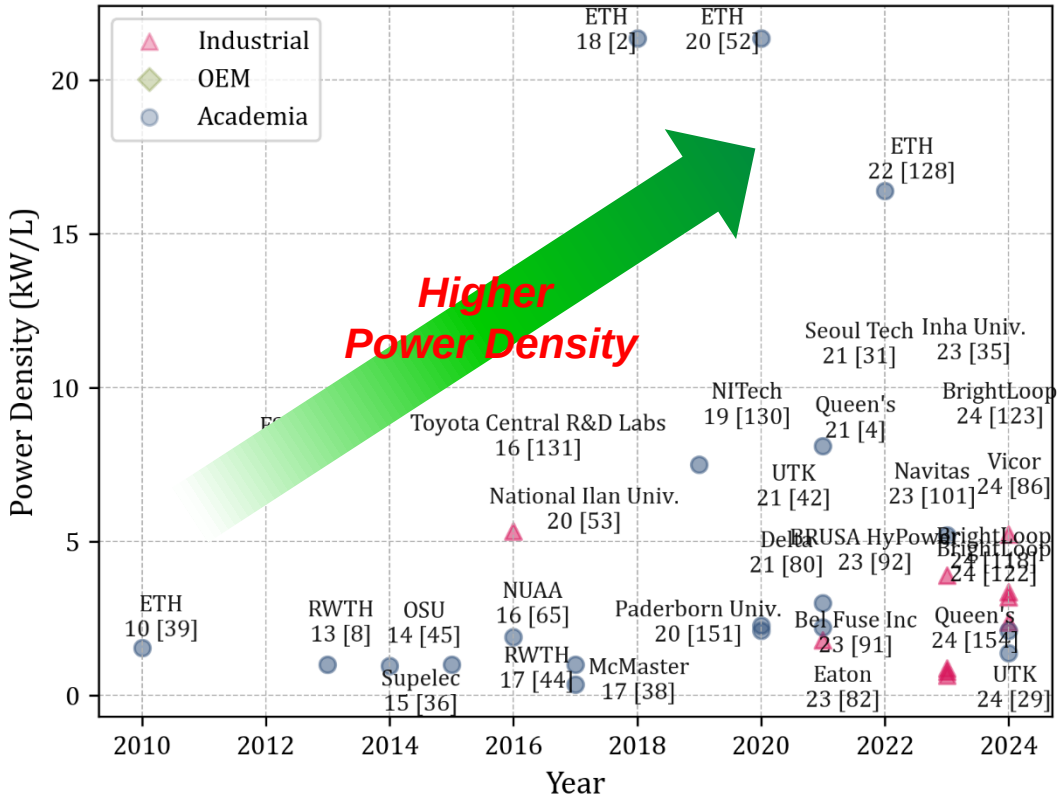

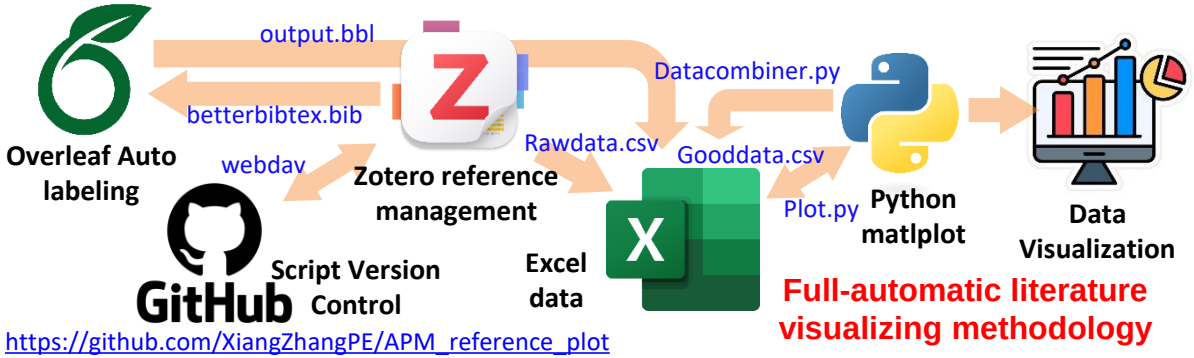

https://github.com/XiangZhangPE/APM_reference_plot

Comprehensive Review of state-of art APMs

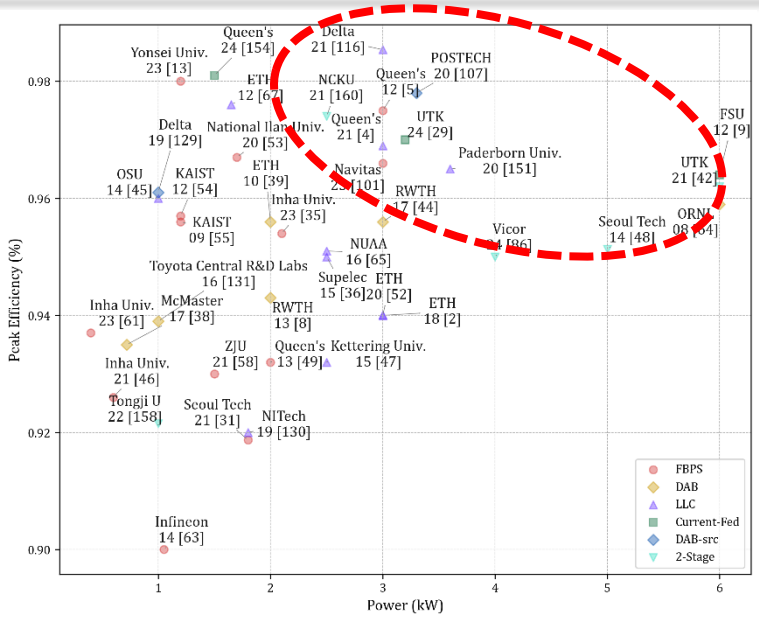

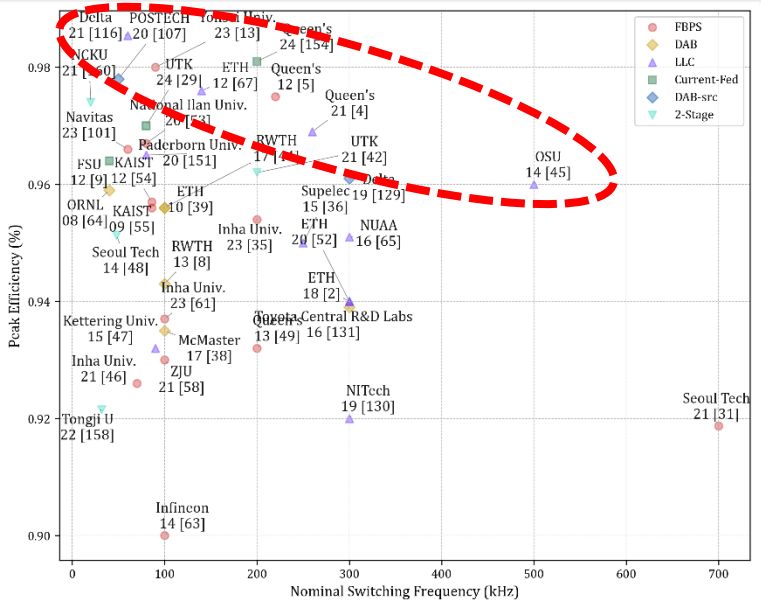

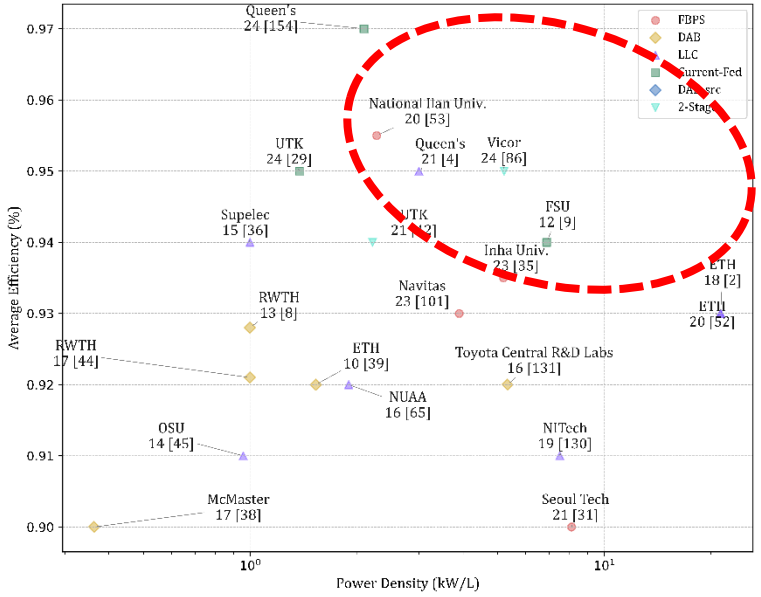

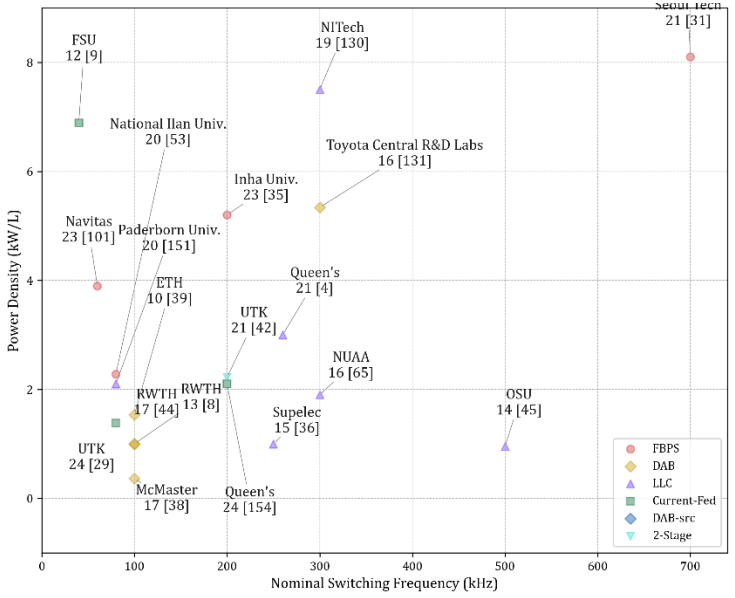

Five main-stream APM topologies with the corresponding improvement are investigated:

- (FBPS) Full Bridge Phase Shift Converter with its rectifier, and magnetic integration
- (LLC/CLLC) LLC, multiphase LLC converter with variable frequency control for wide voltage gain
- (DAB) Non-resonant Dual Active Bridge and its variants
- (DAB-SRC) Series Resonant Converter with both primary and secondary active switch control
- (Current-Fed) Current-Fed DAB converter, non-resonant and resonant

APM topologies: ZVS FBPS + CD/CT/FB rectifier

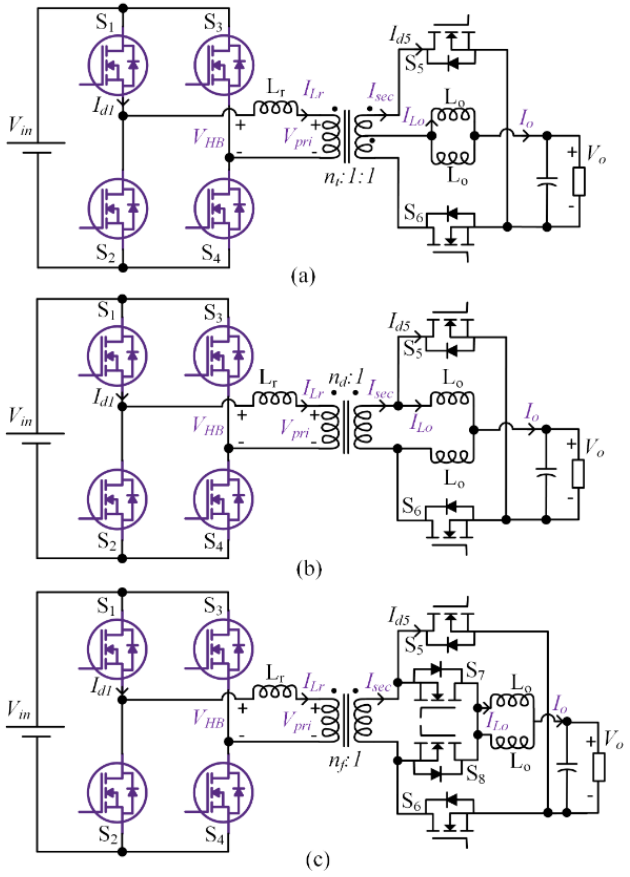

Fig. 2. Schematic figure for (a) PSFB_CT, (b) PSFB_CD, and (c) PSFB_FB

Identifying Suitable PSFB Topology for HVLV Auxiliary Power Supply (APS) Application in EVs

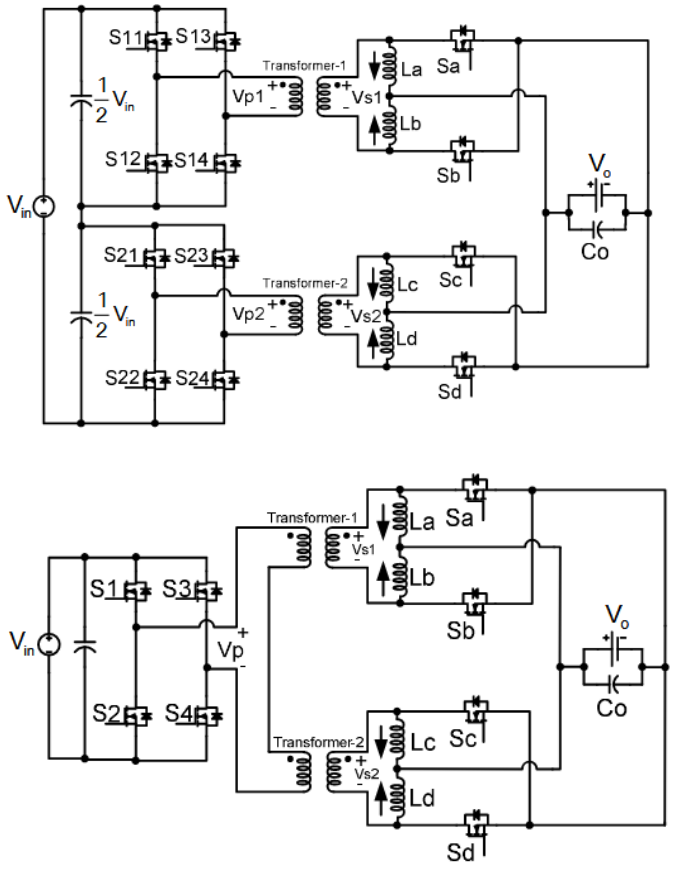

A Topological Evaluation of Isolated DC/DC Converters for Auxiliary Power Modules in Electrified Vehicle Applications

FBPS: main advantages

- wide range of output voltage
- operates at a fixed frequency, EMI can be delt easily
- Widely accepted topology, simpler component design
- good efficiency
- synchronous rectification with fixed frequency
- Low switch counts, economy for EV OEM customers

FBPS: main drawbacks

- ZVS only at heavy load condition
- Duty cycle lost at light load
- High circulating current at primary
- High component stress due to hard switch and oscillation

doi: 10.1109/APEC48139.2024.10509472.

doi: 10.1109/APEC.2015.7104525.

FBPS APM : ZVS and circulating current minimize

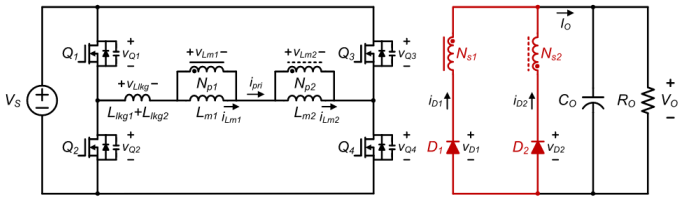

Fig. 1. Circuit diagram of the two-transformer PSFB converter [13].

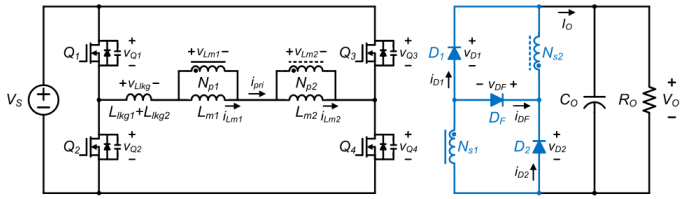

Fig. 2. Circuit diagram of the proposed converter.

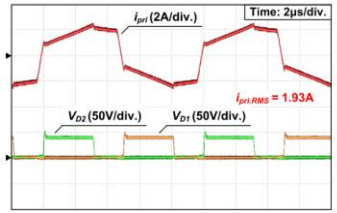

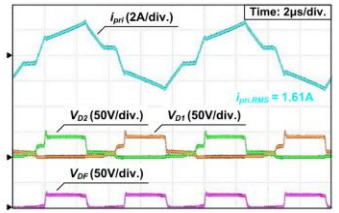

Two-Transformer Phase-Shift Full-Bridge Converter With a New Rectifier for Reducing Conduction Loss

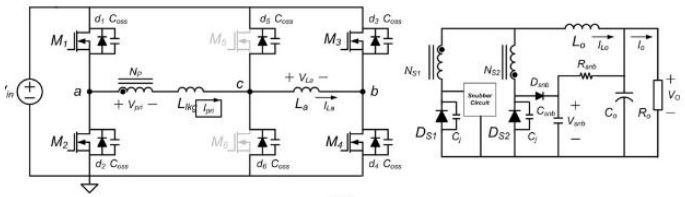

(a)

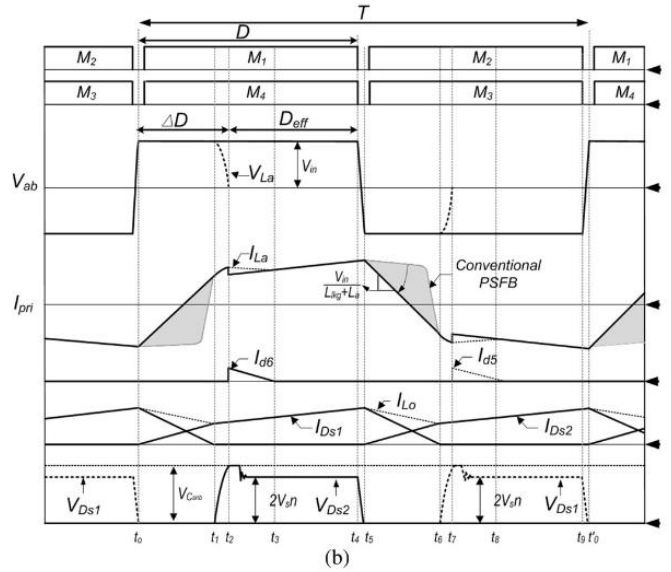

(b)

Wide-Range ZVS Phase-Shift Full-Bridge Converter With Reduced Conduction Loss Caused by Circulating Curren

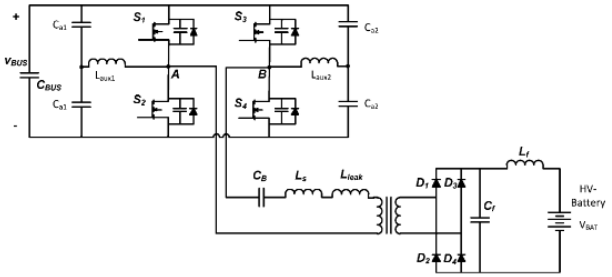

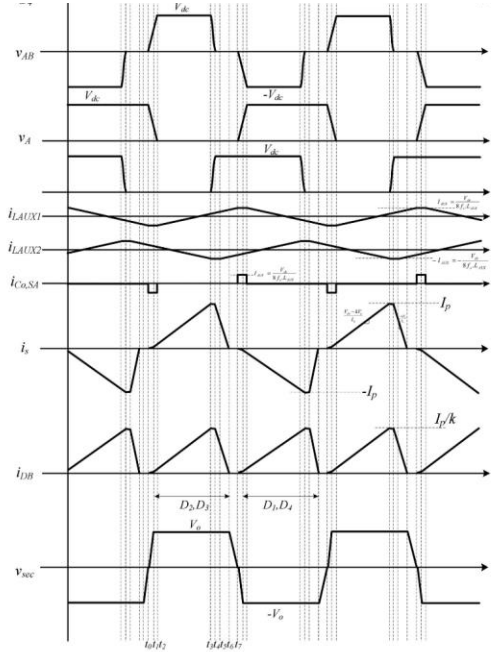

A Novel ZVZCS Full-Bridge DC/DC Converter Used for Electric Vehicles

doi: 10.1109/TPEL.2023.3303917.

doi: 10.1109/TPEL.2012.2227280.

doi: 10.1109/TPEL.2011.2178103.

FBPS APM: magnetics integration

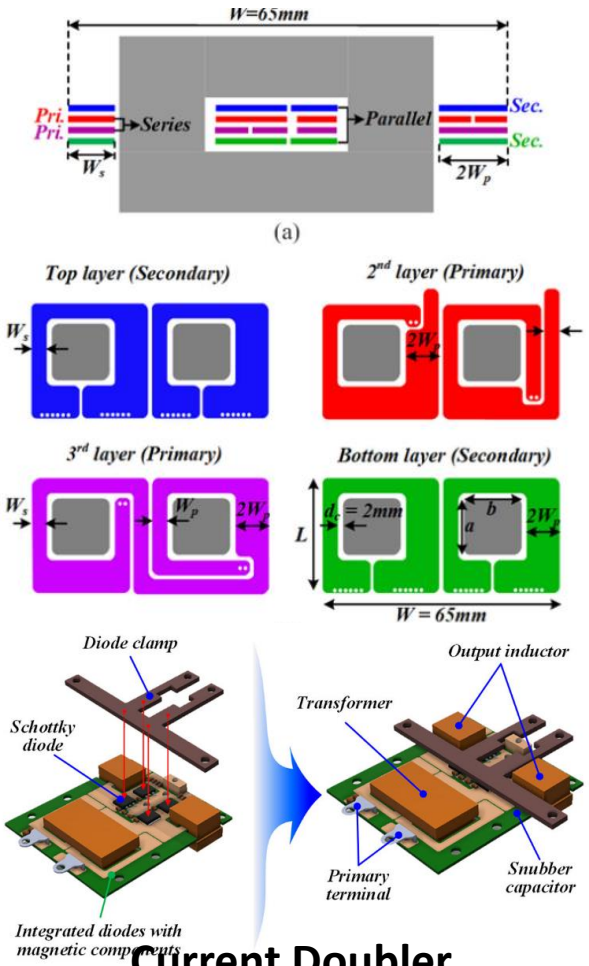

Current Doubler

1.8kW, 8.1kW/L, 700kHz

Power Density Optimization of 700 kHz GaN-Based Auxiliary Power Module for Electric Vehicles

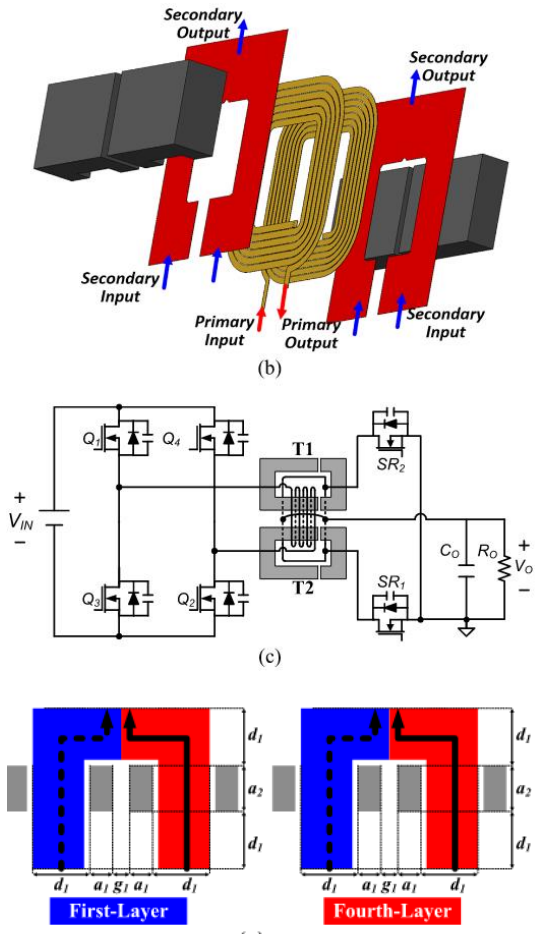

Two Transformers (Center Tap)

2.1kW, 5.2kW/L, 200kHz

Development of Phase-Shift Full-Bridge Converter With Integrated Winding Planar Two-Transformer for LDC

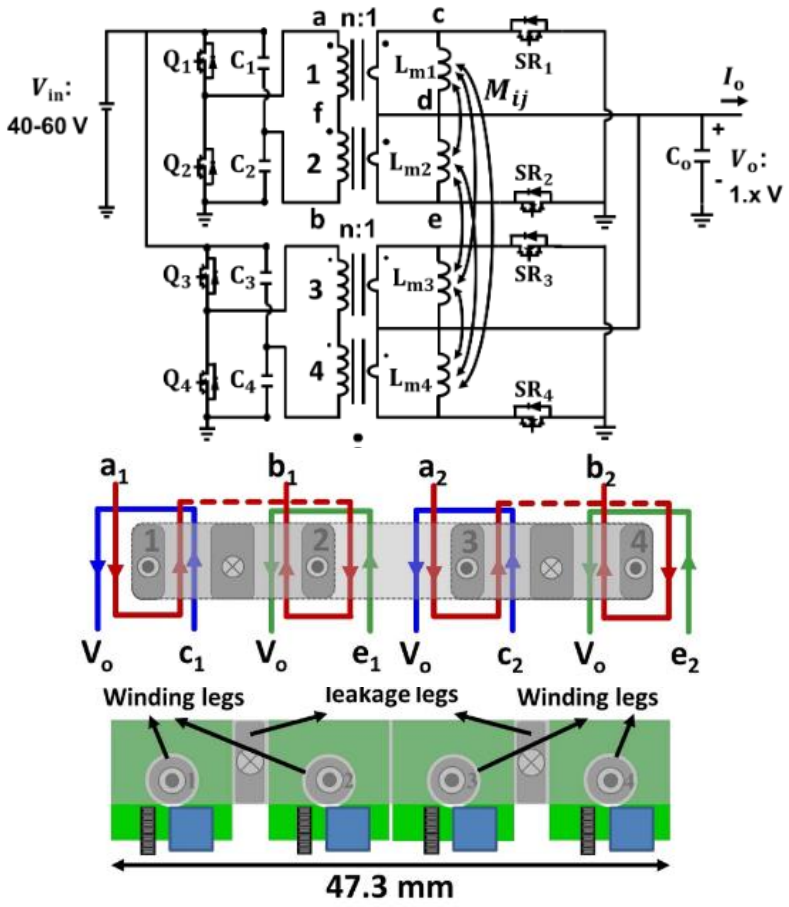

4-matrix-XFMR (Current Doubler)

2.1kW, 63.28kW/L, 600kHz

Single-Stage 48 V/1.8 V Converter With a Novel Integrated Magnetics and 1000 W/in3 Power Density

doi: 10.1109/TPEL.2020.3026328.

doi: 10.1109/TTE.2022.3190968.

doi: 10.1109/TIE.2023.3310020.

Resonant APM : topology modification

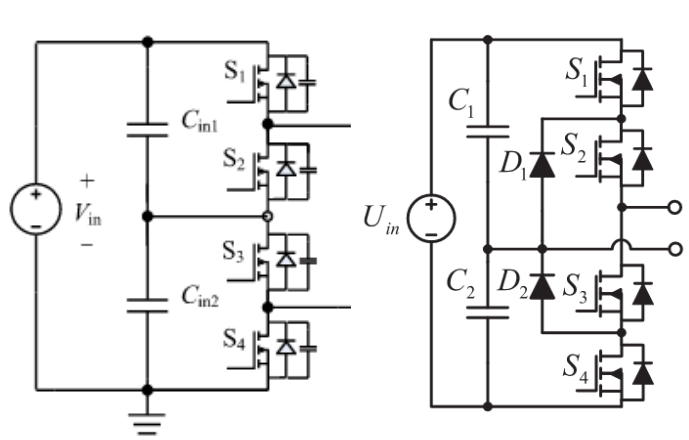

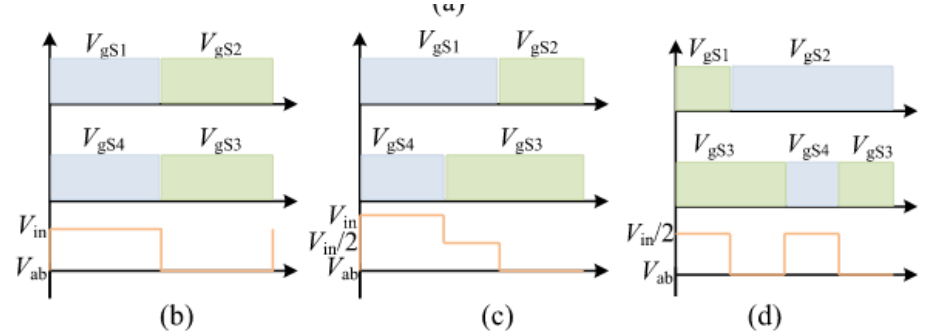

Fig. 6. Stacked structure resonant converter with various operation modes. (a) Stacked structure inverter. (b) HB. (c) Three-level. (d) FD.

Mutli-level phase-shifting high gain resonant converters

Modified primary/secondary structure high gain resonant converters

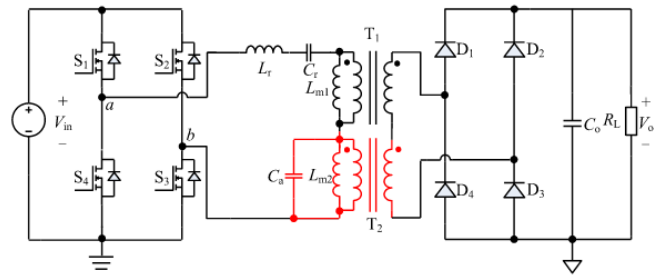

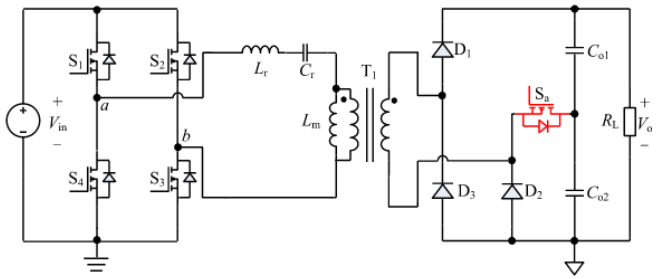

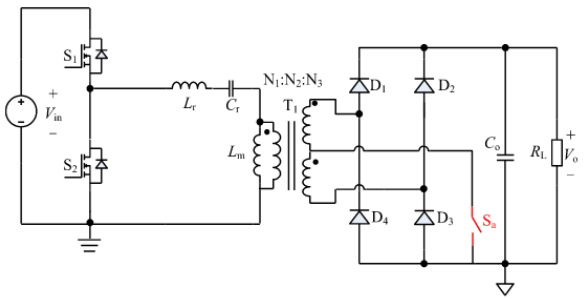

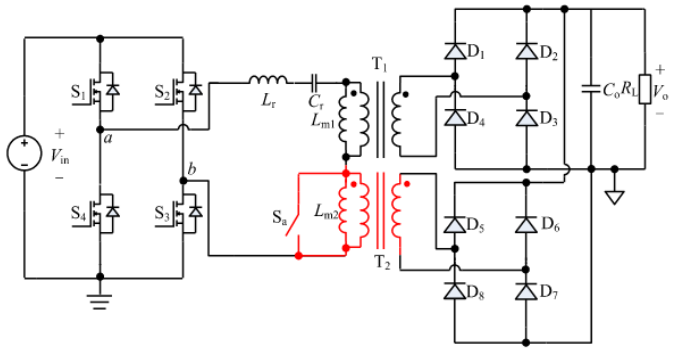

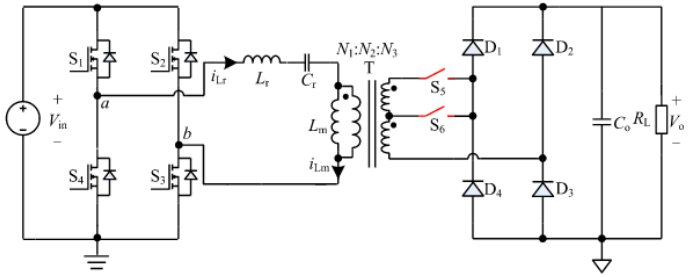

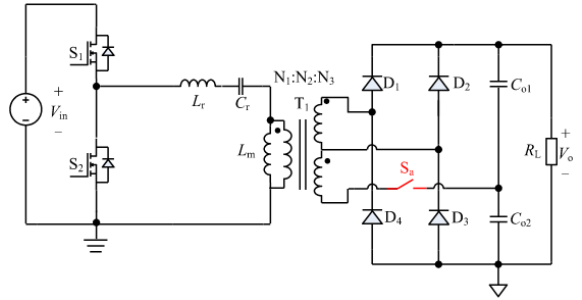

Resonant LLC APM: multi-resonant and multiphase

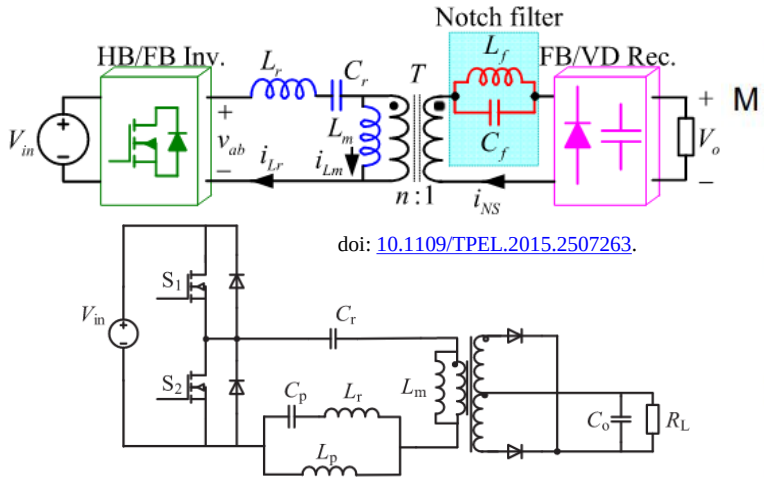

doi: 10.1109/TPEL.2015.2507263.

High-Order CL-LLC DC/DC Converter

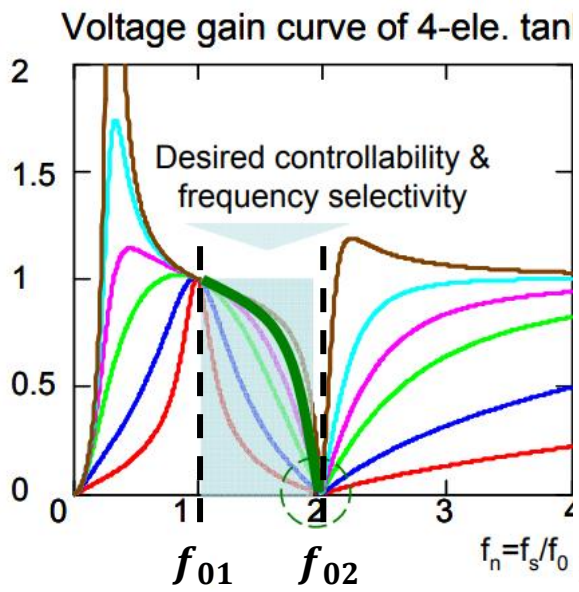

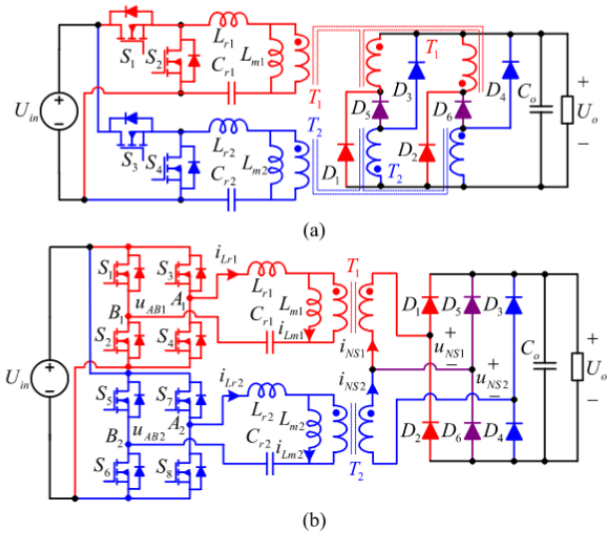

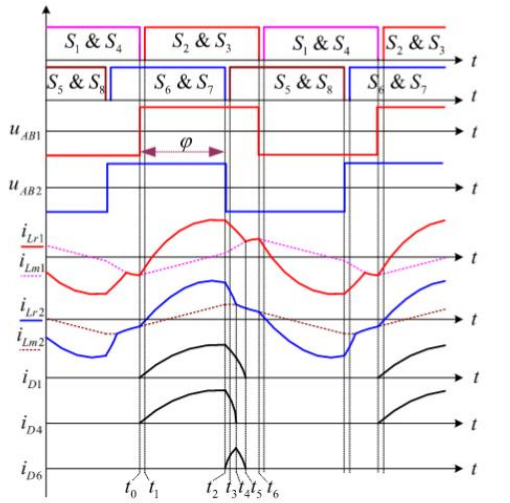

Key waveforms of the iLLC converter in the phase-shift mode.

Fig. 4. Examples of iLLC resonant converter with hybrid rectifier, (a) half-bridge and (b) full-bridge.

Hybrid Rectifier Plus Phase-Shift Control

doi: 10.1109/TPEL.2021.3067715.

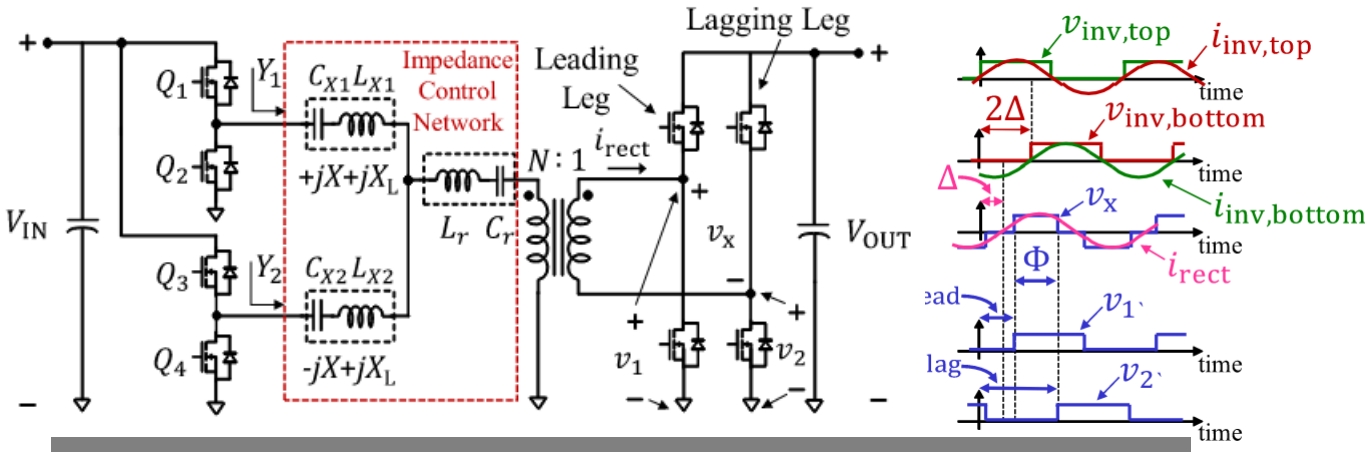

Step-Down Impedance Control Network Resonant DC–DC Converter Utilizing an Enhanced Phase-Shift Control for Wide-Input-Range Operation

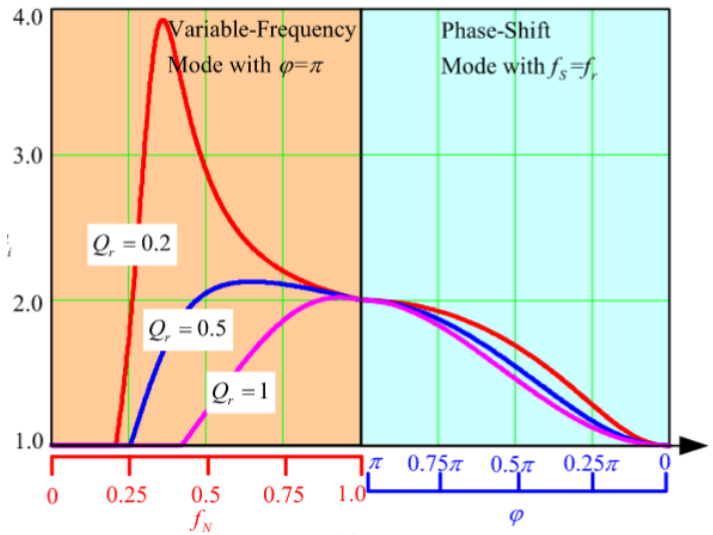

doi: 10.1109/TPEL.2018.2832176.

doi: 10.1109/TPEL.2016.2602545.

Resonant LLC APM : topology morphying and magnetics

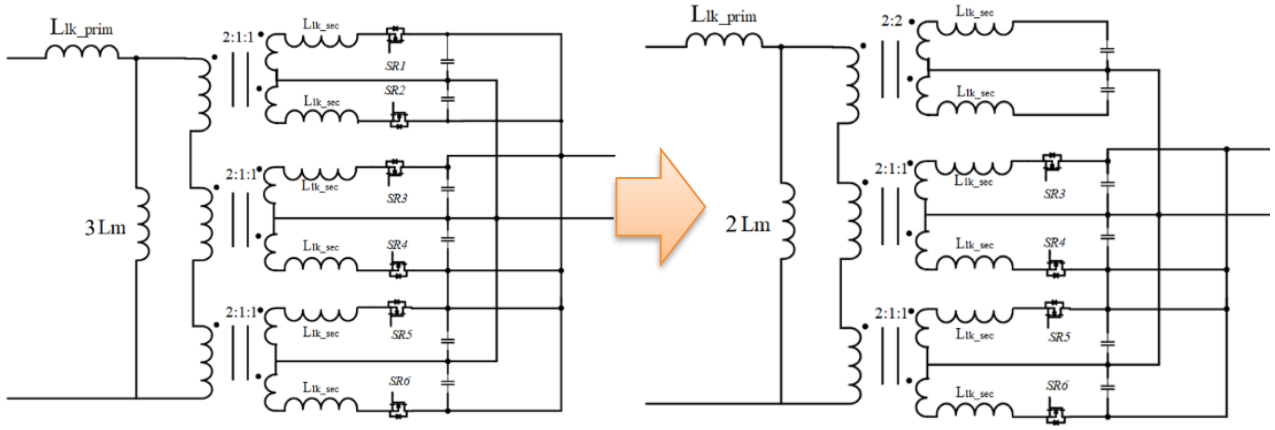

Variable ratio matrix transformer [60]
N=6:1:1

Variable ratio matrix transformer [60]
N=4:1:1

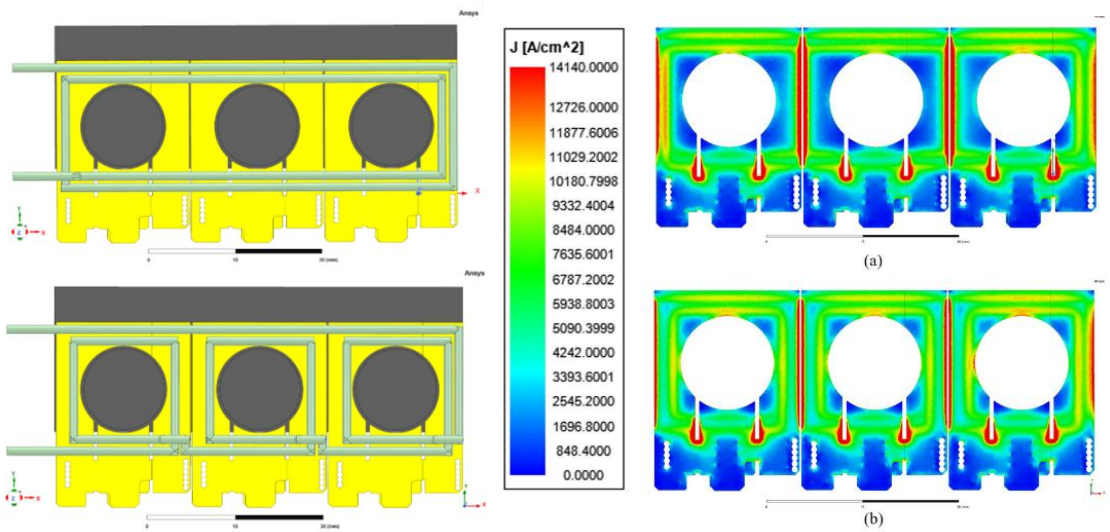

Z. Hou, D. Jiao, and J.-S. Lai, "An Ultra-Wide Range Pulse Width Modulated LLC Converter with Voltage Multiplier Rectifiers," *IEEE Transactions on Power Electronics*, pp. 1–14, 2024, doi: 10.1109/TPEL.2024.3519387.

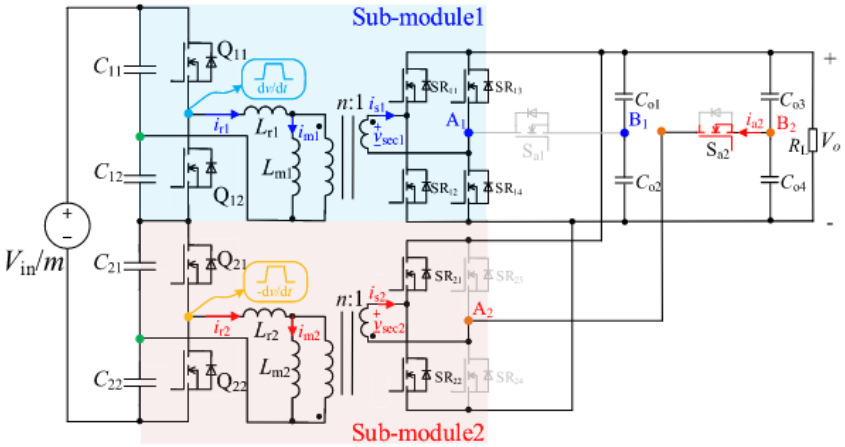

Wide Voltage Gain ISOP-LLC Converter

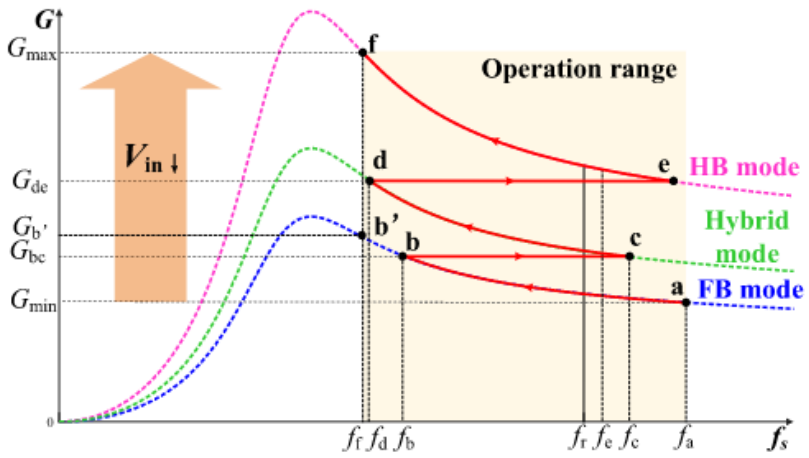

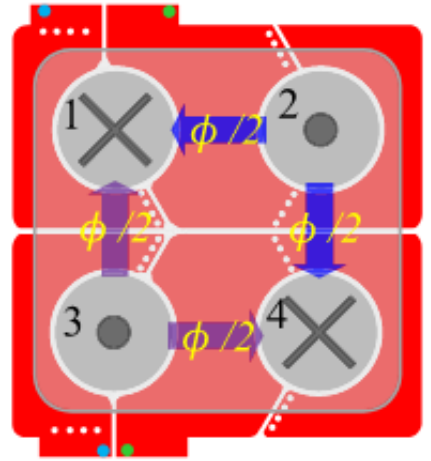

Y. Wang, C. Chen, R. Ji, B. Chen, and L. Tao, "A Novel Integrated Magnetic for Wide Voltage Gain ISOP-LLC Converter," *IEEE Transactions on Industrial Electronics*, pp. 1–10, 2023, doi: 10.1109/TIE.2023.3319735.

Resonant LLC APM : multiphase and phase-shedding

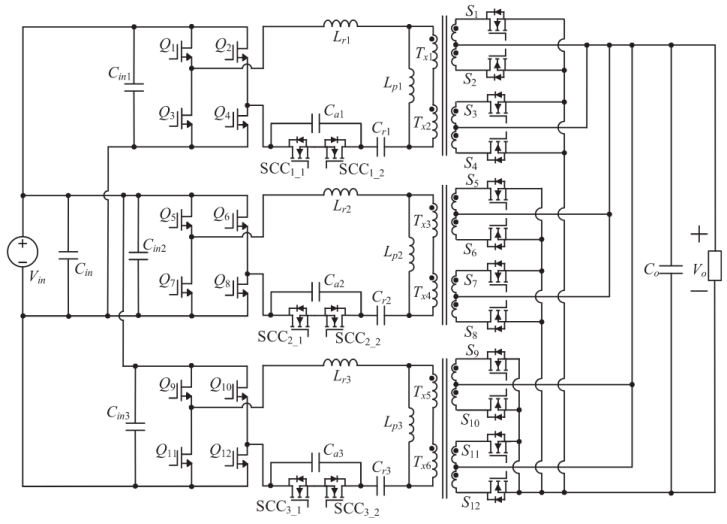

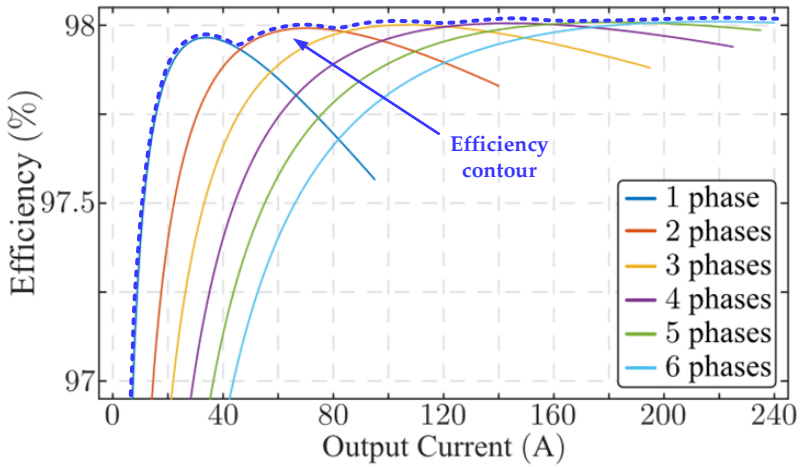

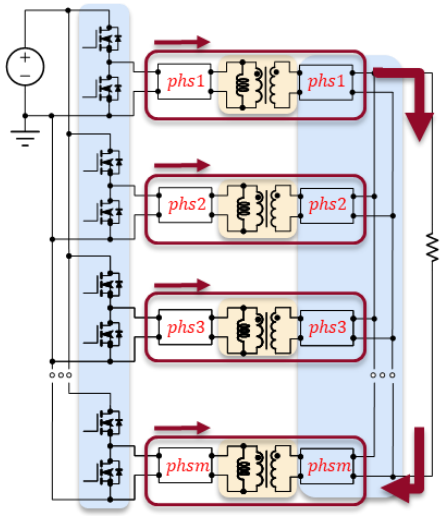

Full Load

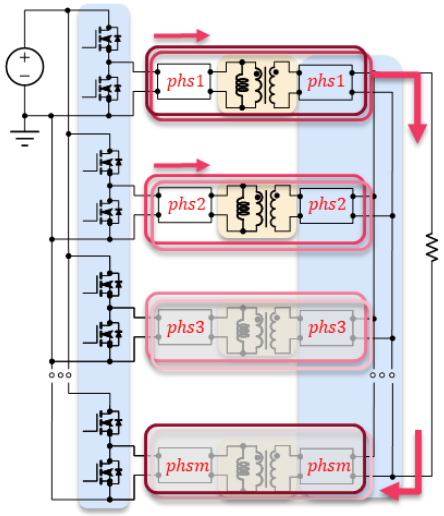

Half Load

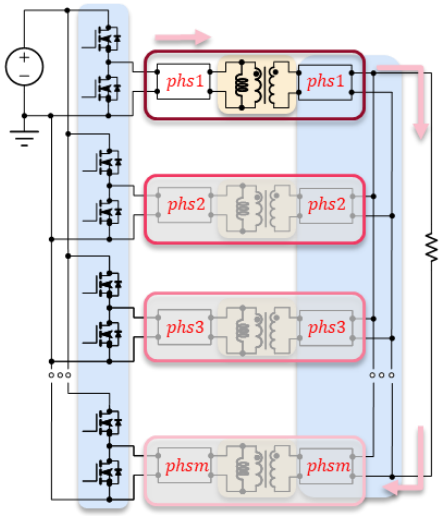

Light Load

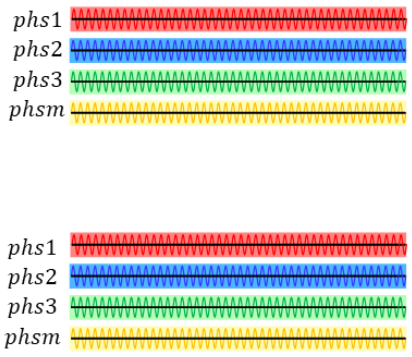

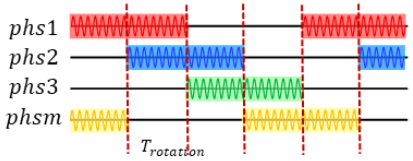

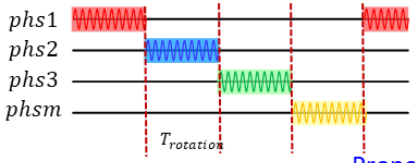

Proposed rotation phase-shedding

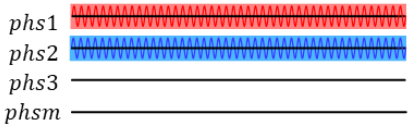

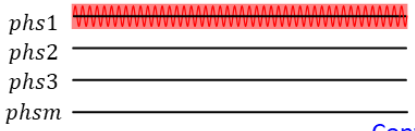

Conventional phase-shedding

X. Zhou *et al.*, "A high-efficiency high-power-density on-board low-voltage DC–DC converter for electric vehicles application," *IEEE Transactions on Power Electronics*, vol. 36, no. 11, pp. 12781–12794, Nov. 2021, doi: 10.1109/TPEL.2021.3076773.

Wide gain implementation of LLC resonant converter

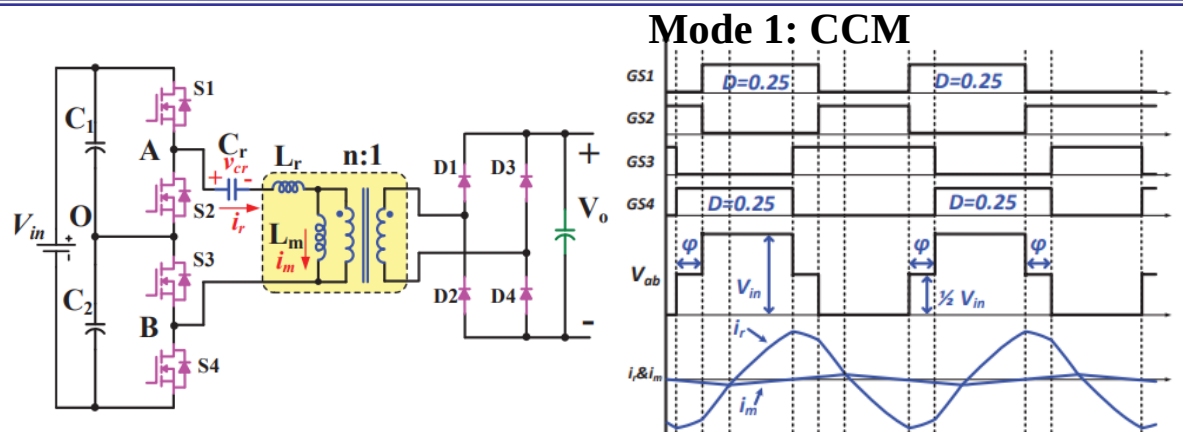

Leg B devices phase-shifted to 3-level primary voltage, can expand V_o range by toggling different operating modes

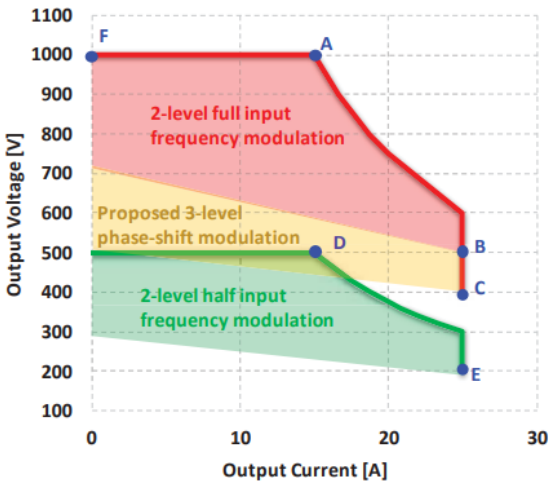

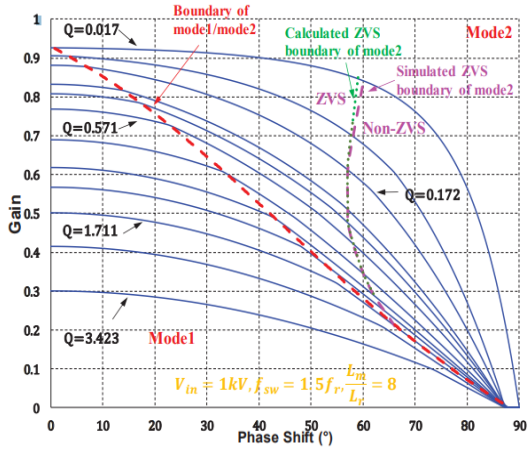

Fig. 4. DC gain characteristics of the SHB LLC converter under three-level phase-shift modulation

At $f_n=1.5f_o$

Buck Gain with FM and primary 3-level operation

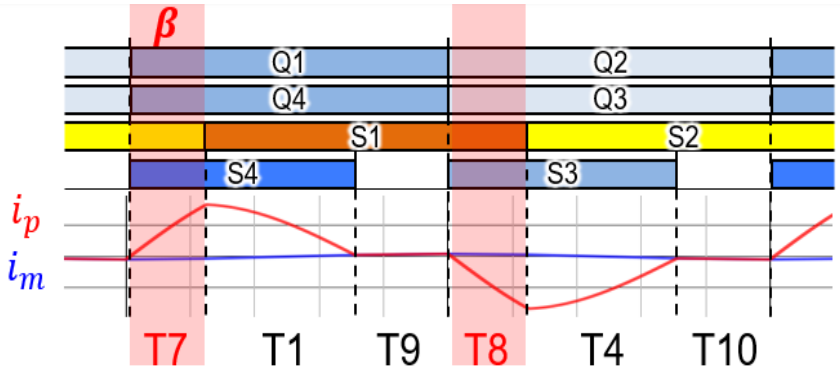

$$\beta = \frac{T_7}{T_s} \times 360^{\circ}$$

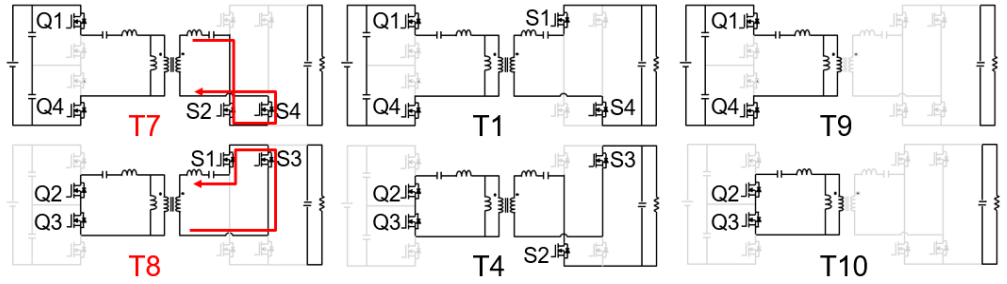

$V_{DC} = 500\sim675\ V, V_{Bus} = 600\ V, P = 30\ kW$

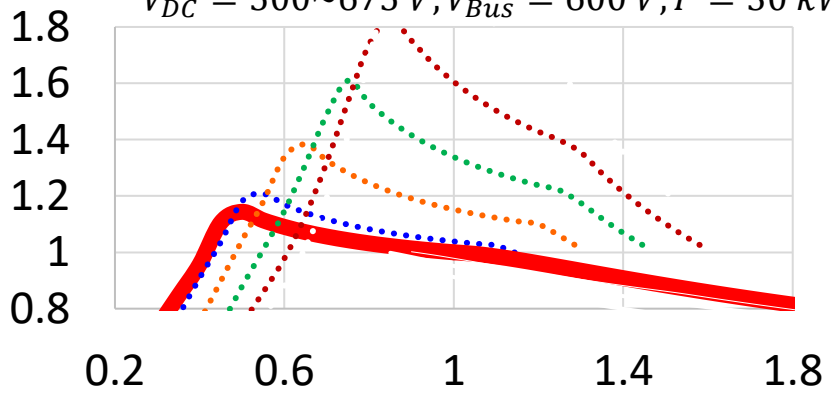

Boost Gain with FM and SR Shorting control

C. Zhang, P. Barbosa, Z. Shen and R. Wang, "A Novel Three-level Phase-Shift Modulation for Serial Half Bridge LLC Resonant Converter," *2021 IEEE Applied Power Electronics Conference and Exposition (APEC)*, 2021, pp. 355-362, doi: 10.1109/APEC42165.2021.9487111.

C. Zhao, F. Jin, Z. Li, Y.-H. Hsieh, F. C. Lee, and Q. Li, "Design Consideration for CLLC Converter with High Power and Wide Gain Range," in *2023 IEEE Applied Power Electronics Conference and Exposition (APEC)*, Orlando, FL, USA: IEEE, Mar. 2023, pp. 1–6. doi: 10.1109/APEC43580.2023.10131583.

PWM LLC control patent review (primary phase shift 3level)

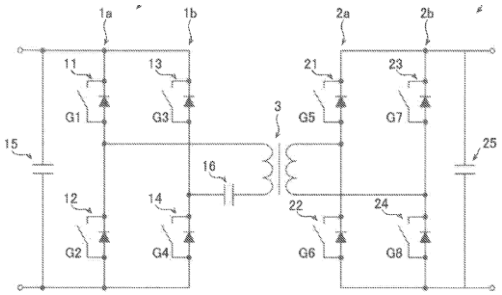

Fuji Electric Co Ltd

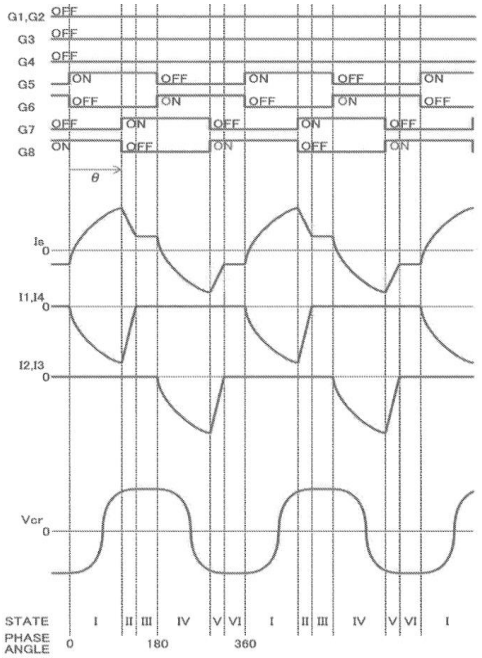

Y. Nishikawa, "Power conversion device," US20210399644A1, Dec. 23, 2021. [Online]. Available: https://patents.google.com/patent/US20210399644A1/en?oq=US20150229225A1

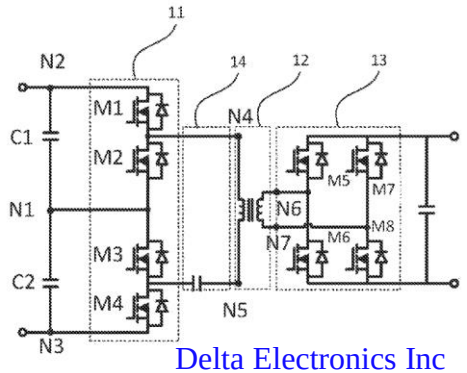

Delta Electronics Inc

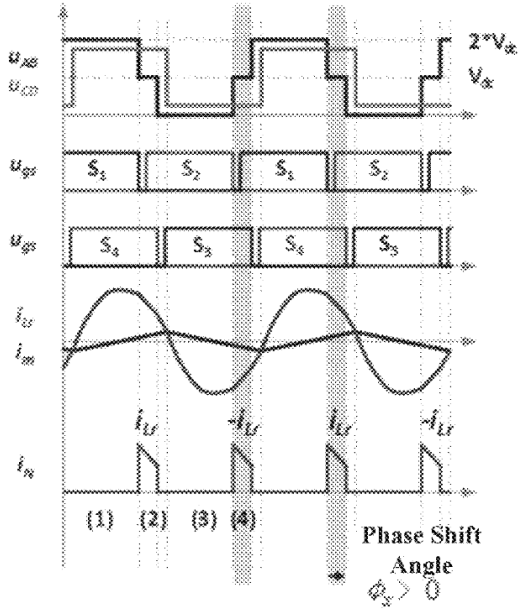

W. Hu and C. Lu, "DC/DC converter and control method thereof," US11063523B2, Jul. 13, 2021. [Online]. Available: https://patents.google.com/patent/US11063523B2/en?oq=US20150229225A1

Delta Electronics Inc

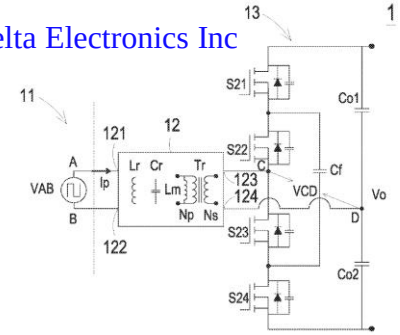

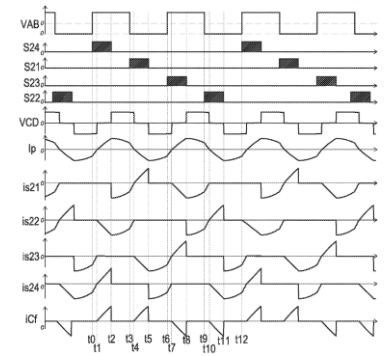

FIG. 3A

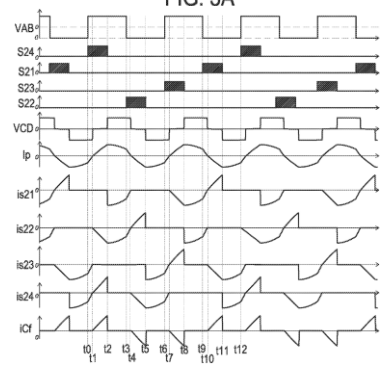

FIG. 3B

M. Jia, H. Sun, C. Zhang, J. Zhang, and P. M. BARBOSA, "Three-level rectification dc/dc converter," US20230179108A1, Jun. 08, 2023. [Online]. Available: https://patents.google.com/patent/US20230179108A1/en?oq=US20150229225A1

Delta Electronics Inc

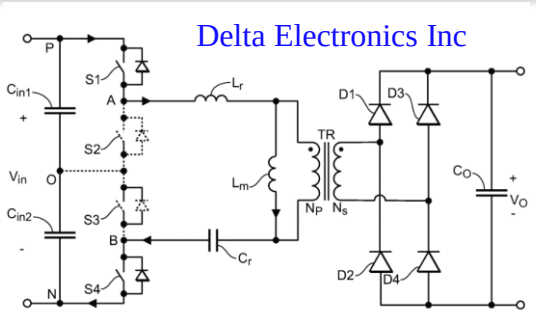

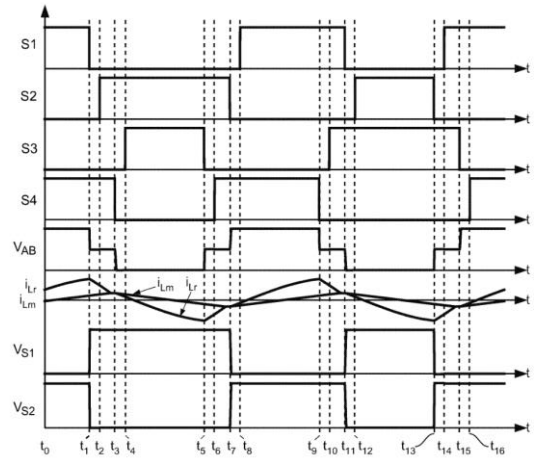

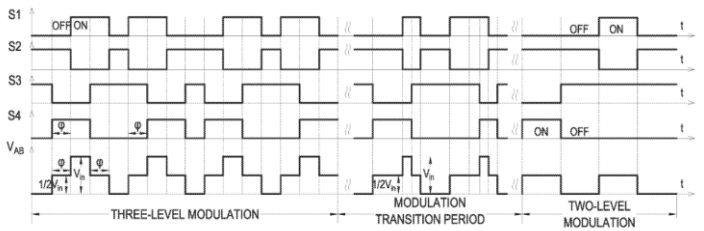

C. Zhang and P. Barbosa, "Isolated DC/DC converters for wide output voltage range and control methods thereof," US11901826B2, Feb. 13, 2024. [Online]. Available: https://patents.google.com/patent/US11901826B2/en?oq=US20150229225A1

PWM LLC control patent review

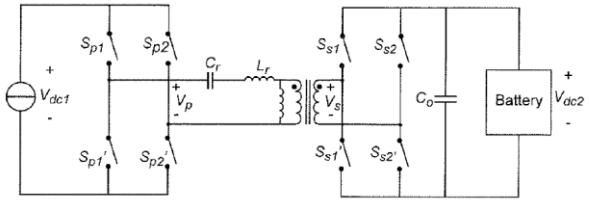

CPES@VT

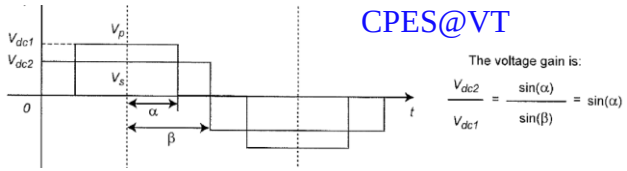

The voltage gain is:

$$\frac{V_{dc2}}{V_{dc1}} = \frac{\sin(\alpha)}{\sin(\beta)} = \sin(\alpha)$$

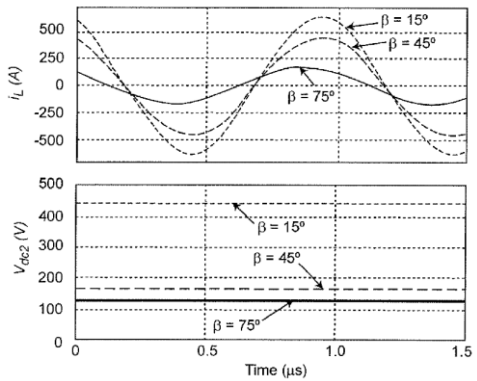

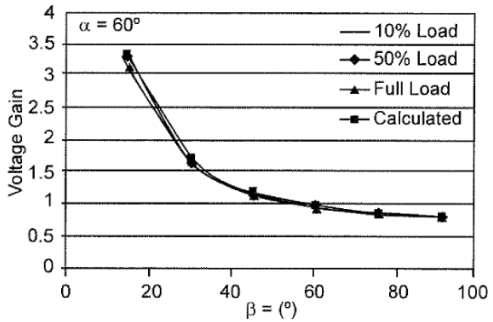

K. D. T. Ngo, X. Cao, and Y. Wang, "Pulse width modulated resonant power conversion," US20120014138A1, Jan. 19, 2012. [Online]. Available: https://patents.google.com/patent/US20120014138A1/en?oq=US+Patent+10%2c756%2c617+

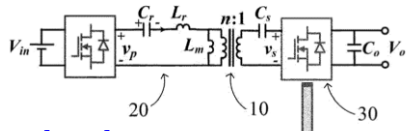

Delta Electronics Inc

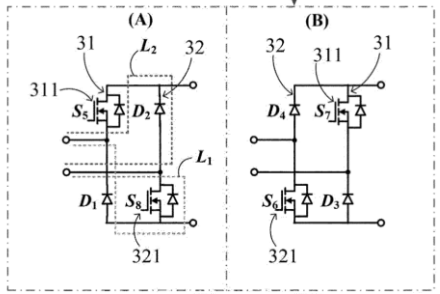

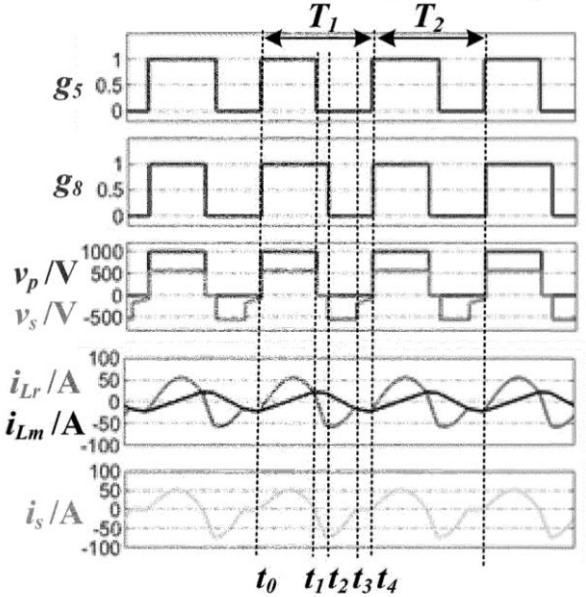

H. Liu, B. SONG, S. OUYANG, and C. Lu, "Resonant converter, and controlling method for the same," EP4322382A1, Feb. 14, 2024. [Online]. Available: https://patents.google.com/patent/EP4322382A1/en?oq=US+Patent+10%2c756%2c617+

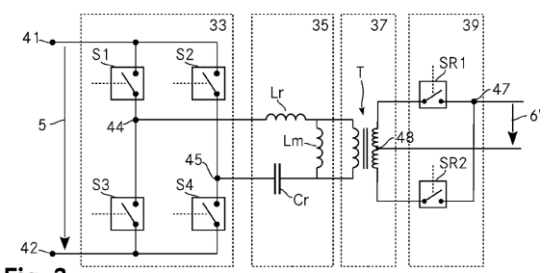

Fig. 3

Delta Electronics Inc

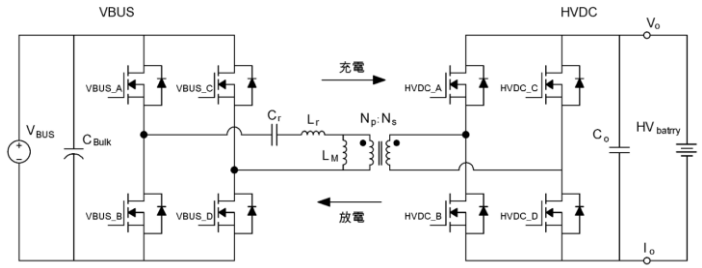

Delta Electronics Inc

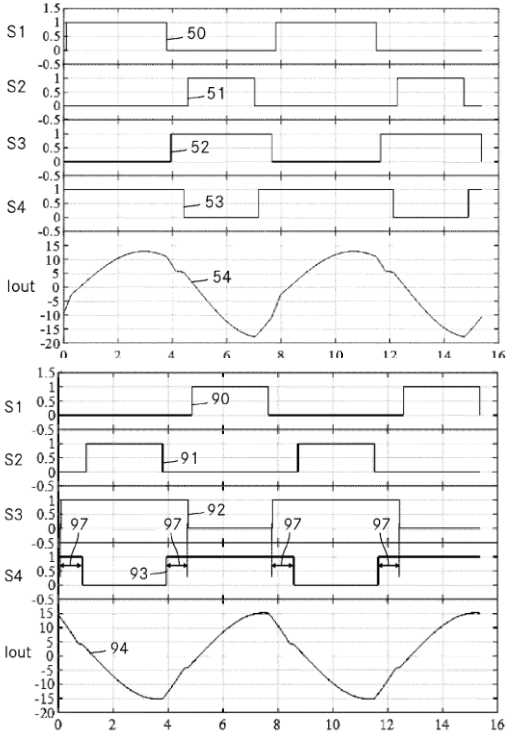

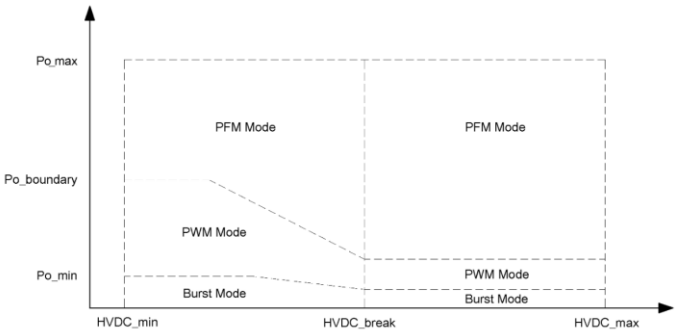

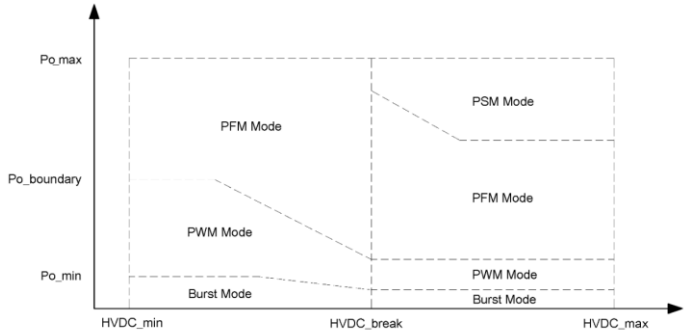

P. REHLAENDER, F. Schafmeister, and J. Boecker, "Power balancing in interleaved llc converters via duty cycle variation," EP3965279A1, Mar. 09, 2022. [Online]. Available: https://patents.google.com/patent/EP3965279A1/en?oq=US20150229225A1

王璟, "混合模式控制方法," TWI816617B, Sep. 21, 2023. [Online]. Available: https://patents.google.com/patent/TWI816617B/en?oq=US20240333141A1

APM topologies: Non-resonant DAB converter

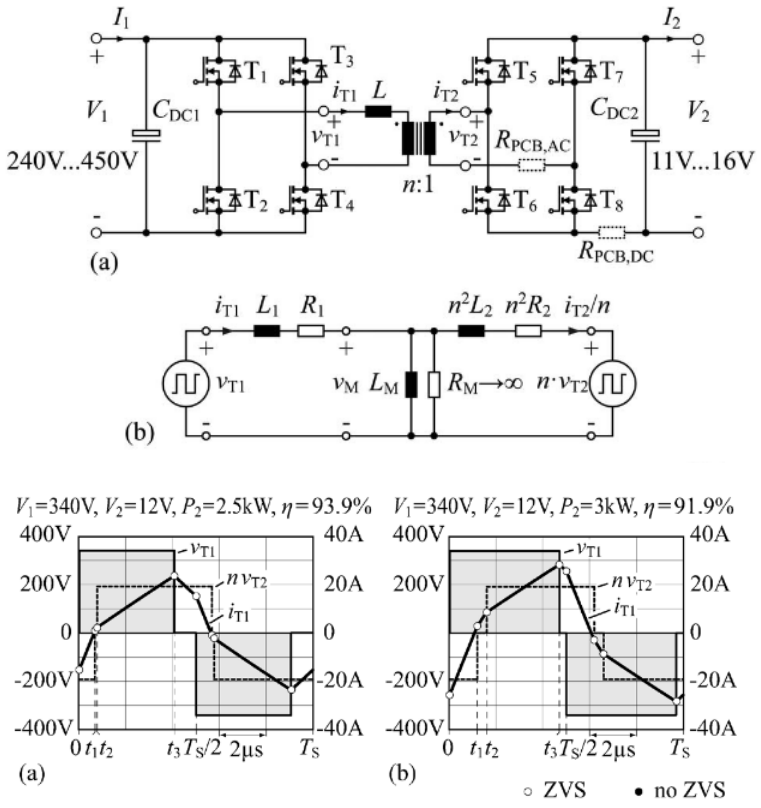

Fig. 9. Waveforms of v_{T1}, v_{T2}, and i_{T1} obtained for $V_1 = 340$ V, $V_2 = 12$ V, and efficiency-optimal operation at very high power levels (exceeding the rated power of 2 kW): (a) $P_2 = 2.5$ kW and (b) $P_2 = 3$ kW. Employed DAB converter: $n = 16$, $L = 22.4$ µH.

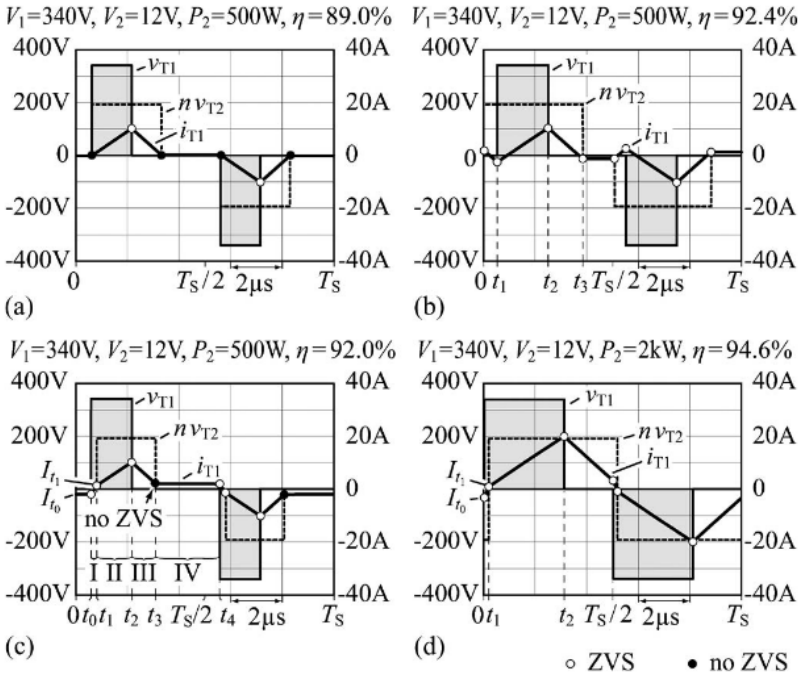

Fig. 6. Waveforms of v_{T1}, v_{T2}, and i_{T1} (cf. Fig. 1(a)) obtained for $V_1 = 340$ V, $V_2 = 12$ V, and different operating conditions; (a) triangular current mode modulation according to [19] and $P_{out} = 500$ W; (b), (c) modulation at $P_{out} = 500$ W: optimal and suboptimal converter efficiency, η_{opt} and η_{subopt} in Fig. 7(a), respectively; besides, (c) illustrates the modified triangular current mode modulation detailed in Section V-A1; and (d) optimal converter efficiency at $P_{out} = 2$ kW. Employed DAB: $n = 16$, $L = 22.4$ µH.

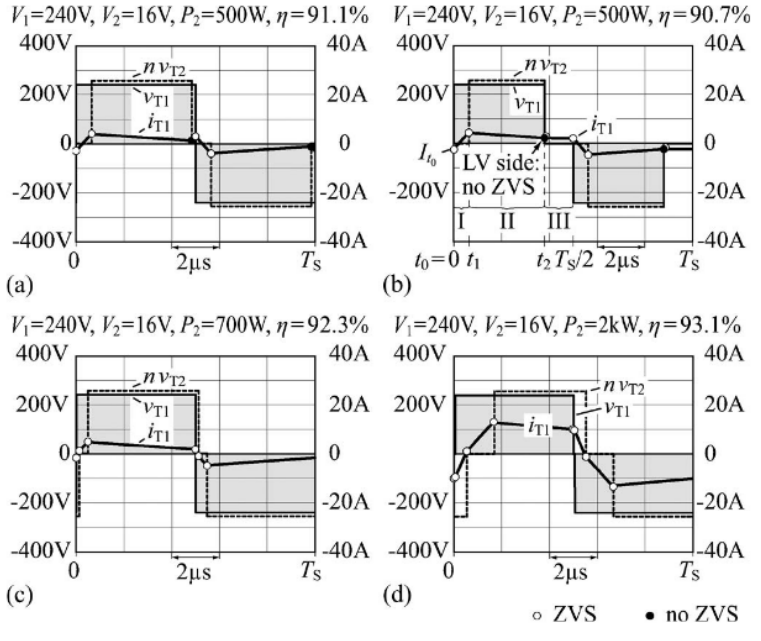

Fig. 11. Waveforms of v_{T1}, v_{T2}, and i_{T1} obtained for $V_1 = 240$ V, $V_2 = 16$ V, and different operating conditions; (a) efficiency-optimal modulation at $P_{out} = 500$ W (η_{opt} in Fig. 10(a)); (b) modified triangular current mode modulation detailed in Section V-A-2 at $P_{out} = 500$ W; (c), (d) modulation for optimal converter efficiency at $P_{out} = 700$ W (cf. Fig. 8(b)) and at $P_{out} = 2$ kW (η_{opt} in Fig. 10(d)), respectively. Employed DAB: $n = 16$, $L = 22.4$ µH.

Three-phase Non-resonant DAB APM

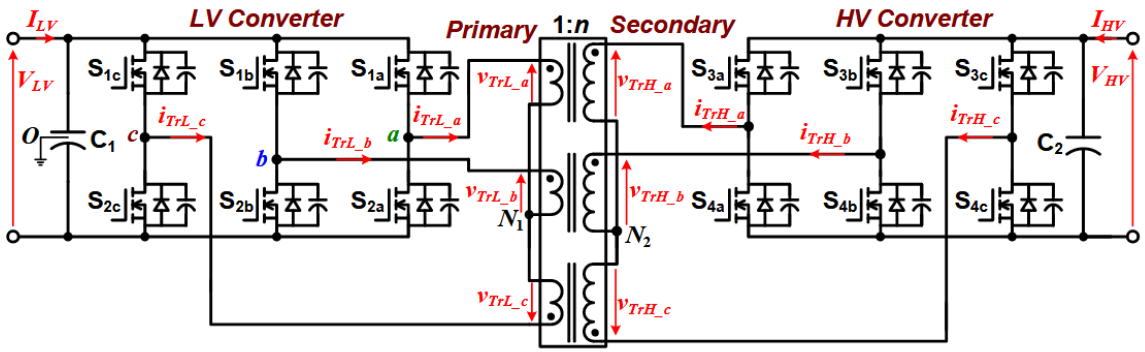

Figure 1. A three-phase soft-switching bidirectional dc-dc converter operating a duty cycle of 1/3.

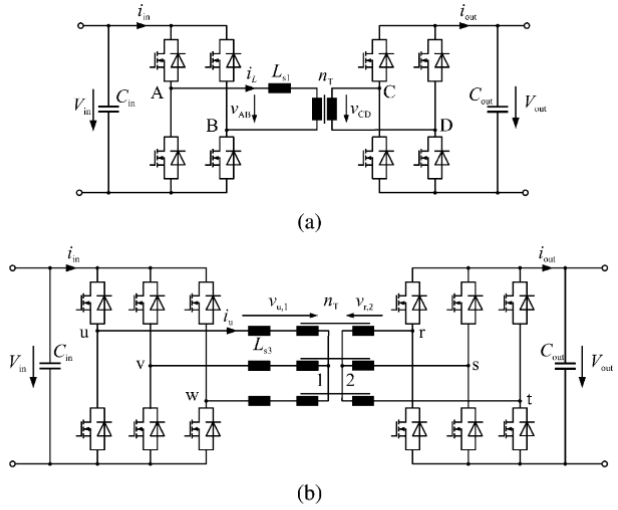

Fig. 2. Schematics of the dual active bridges. (a) Single-phase DAB (1p-DAB). (b) Three-phase DAB (3p-DAB).

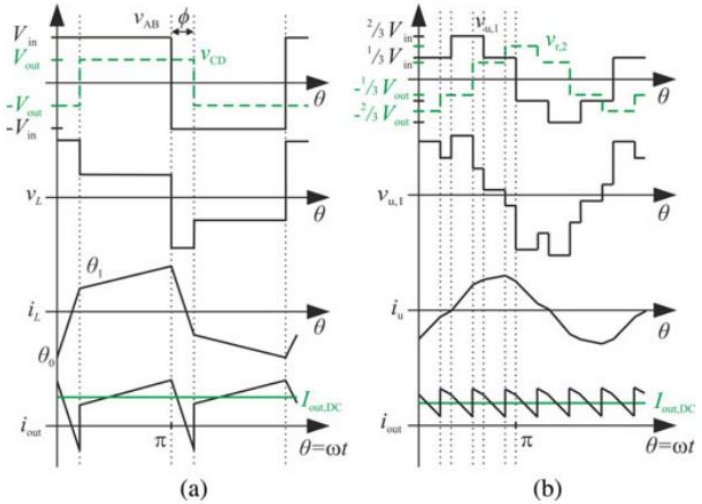

Fig. 3. Phase shift (PS) modulations. (a) 1p-DAB PS. (b) 3p-DAB PS.

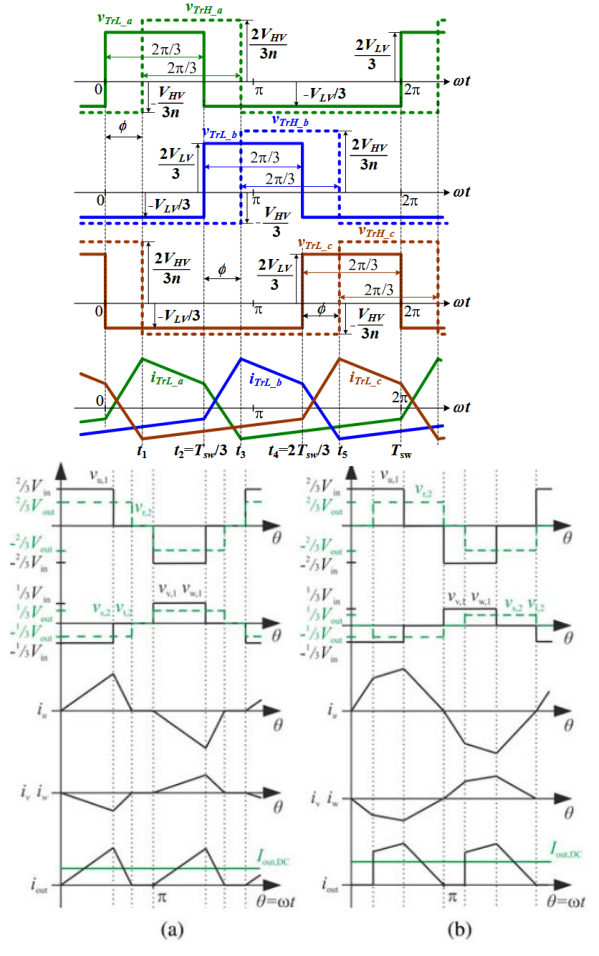

Fig. 6. Advanced modulation schemes for the 3p-DAB. (a) Triangular. (b) Trapezoidal.

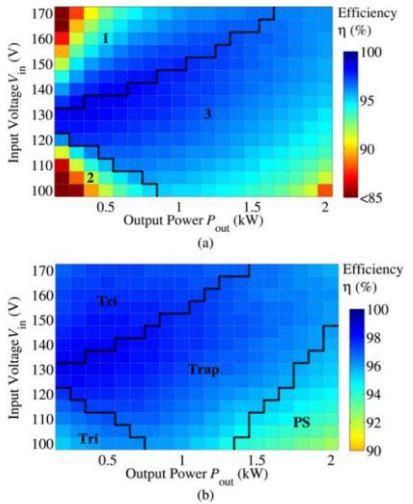

Fig. 7. Efficiency for the 3p-DAB at V_{out} = 14 V. (a) PS modulation: 1—Hard-switching (output bridge); 2—Hard-switching (input bridge); 3—Soft-Switching. (b) Combined modulation.

Enhanced Modulation Strategy for a Three-Phase Dual Active Bridge—Boosting Efficiency of an Electric Vehicle Converter

G.-J. Su and L. Tang, "A three-phase bidirectional DC-DC converter for automotive applications," in *2008 IEEE Industry Applications Society Annual Meeting*, Oct. 2008, pp. 1–7. doi: 10.1109/08IAS.2008.286.

H. van Hoek, M. Neubert, and R. W. De Doncker, "Enhanced modulation strategy for a three-phase dual active bridge—boosting efficiency of an electric vehicle converter," *IEEE Transactions on Power Electronics*, vol. 28, no. 12, pp. 5499–5507, Dec. 2013, doi: 10.1109/TPEL.2013.2251905.

DAB-SRC: achieve full power range ZVS

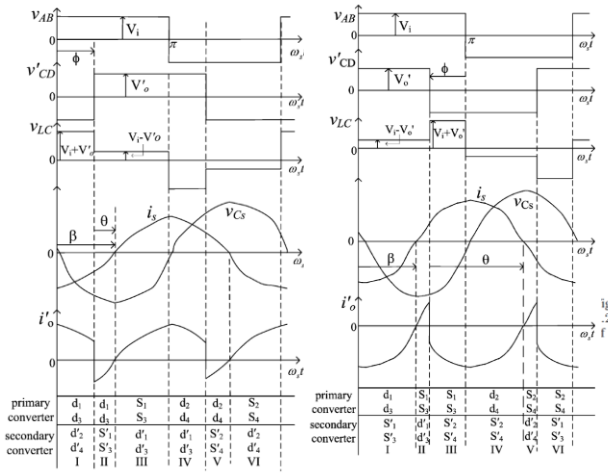

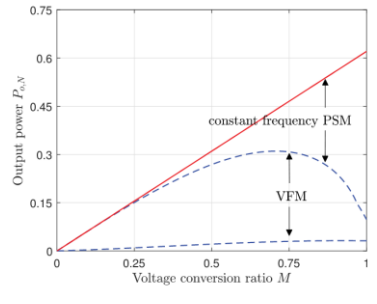

ig. 4. Normalized output power range of the VFM ($r_H = 0.85$, $r_L = 0.2$, and $J_{sw} = -0.1$) combined with the PSM ($r = 0.85$) as a function of M.

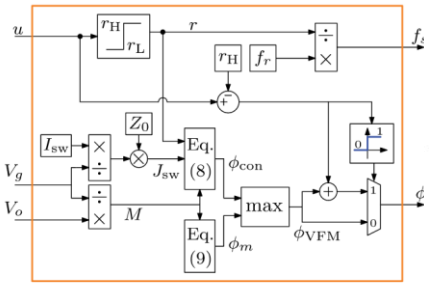

Fig. 5. Control block diagram of the proposed VFM+PSM technique.

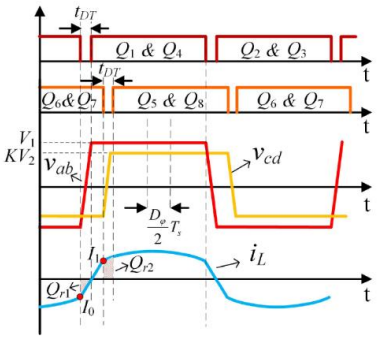

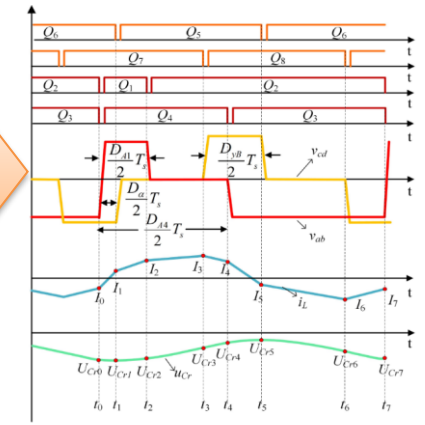

Fig. 8. Typical waveforms of the DALM scheme.

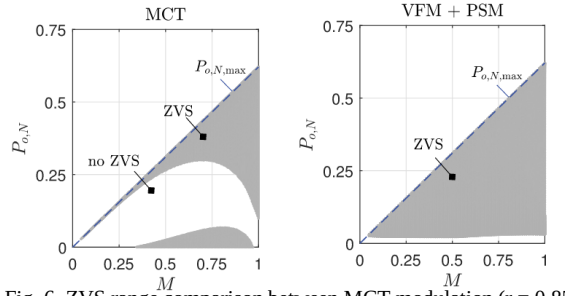

Fig. 6. ZVS range comparison between MCT modulation (r = 0.85) and VFM + PSM (Jsw = −0.1, rH = 0.85, and rL = 0.2).

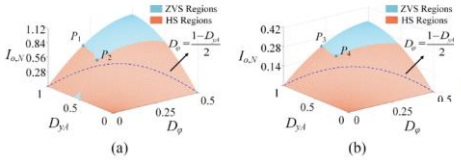

Fig. 4. ZVS regions with EPSM when $M = 0.74$. (a) $r = 0.75$. (b) $r = 0.43$.

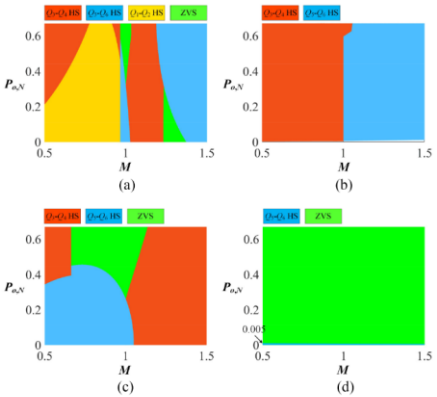

Fig. 13. ZVS performance for different control strategies. (a) MCT [2]. (b) 4-DOF [19]. (c) E-MCT [13]. (d) Proposed HLM scheme.

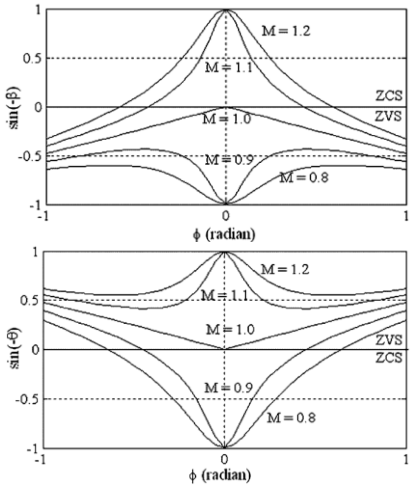

Fig. 9. Soft-switching range of (a) the primary-side converter and (b) the secondary-side converter.

For Voltage Source Load

$$i_{s,pu}(0) = \frac{4}{\pi X_{s,pu}}(-1 + M\cos\phi)$$

$$i_{s,pu}\left(\frac{\phi}{\omega_s}\right) = \frac{4}{\pi X_{s,pu}}(M - \cos\phi)$$

For Resistive Load

$$\sin(-\beta) = \frac{M\cos\phi - 1}{\sqrt{1 + M^2 - 2M\cos\phi}}$$

$$\sin(-\theta) = \sin(\phi - \beta) = \frac{M - \cos\phi}{\sqrt{1 + M^2 - 2M_o\cos\phi}}.$$

In summary, the proposed combination of the VFM and PSM (VFM+PSM) is formulated as

$$r = \begin{cases} r_L, & u < r_L \\ u, & r_L \le u \le r_H \\ r_H, & u > r_H \end{cases} \quad (19)$$

$$\phi = \begin{cases} \phi_{\text{VFM}}(r, M), & u \le r_H \\ \phi_{\text{VFM}}(r_H, M) + (u - r_H), & u > r_H. \end{cases} \quad (20)$$

$$I_{o,N} = \begin{cases} \dfrac{\sin\left(\frac{\pi r D_{yA}}{2}\right)\sin(\pi r D_\varphi)}{2r\cos\left(\frac{\pi r}{2}\right)}, & 0 < 2D_\varphi < 1 - D_{yA} \\ \dfrac{\cos\left[\pi r\left(D_\varphi - \frac{1}{2}\right)\right]\cos\left[\pi r\frac{\left(1 - D_{yA}\right)}{2}\right]}{2r\cos\left(\frac{\pi r}{2}\right)} - \frac{1}{2r}, & 1 - D_{yA} < 2D_\varphi < 1 \end{cases}$$

$$I_{om} = \frac{4KV_1}{\pi Z_0}.$$

Frequency Domain model based SPS controlled DAB-SRC ZVS operation

Frequency Domain model based VFM+PSM controlled half bridge DAB-SRC ZVS operation

Time Domain model based DALM scheme DAB-SRC ZVS operation

DALM is offered in (19). It is worth noting that the output current with the DALM scheme is independent of load, i.e., the output character can be seen as an adjustable current source with infinite voltage gain.

Xiaodong Li and A. K. S. Bhat, "Analysis and Design of High-Frequency Isolated Dual-Bridge Series Resonant DC/DC Converter," *IEEE Trans. Power Electron.*, vol. 25, no. 4, pp. 850–862, Apr. 2010, doi: 10.1109/TPEL.2009.2034662.

W. Han and L. Corradini, "Wide-Range ZVS Control Technique for Bidirectional Dual-Bridge Series-Resonant DC–DC Converters," *IEEE Transactions on Power Electronics*, vol. 34, no. 10, pp. 10256–10269, Oct. 2019, doi: 10.1109/TPEL.2019.2893282.

Y. Gao *et al.*, "Hybrid-Level Modulation Scheme for Dual-Bridge Series-Resonant Converter," *IEEE Transactions on Industrial Electronics*, vol. 70, no. 11, pp. 11205–11215, Nov. 2023, doi: 10.1109/TIE.2022.3225810.

DAB-SRC: tank current RMS minimizing control

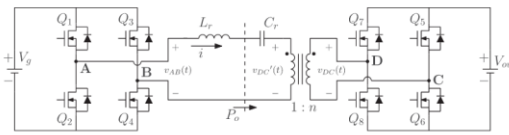

(a)

$$P_o = P_{o,\max} \sin\left(\frac{\varphi_{AB}}{2}\right) \sin\left(\frac{\varphi_{DC}}{2}\right) \sin\left(\varphi_{AD} + \frac{\varphi_{DC} - \varphi_{AB}}{2}\right).$$

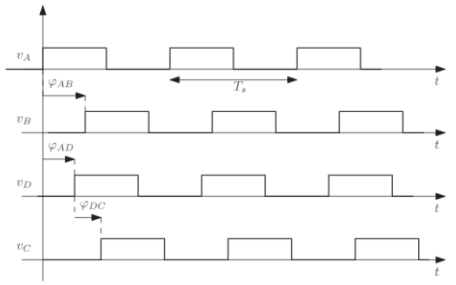

(b)

$$|I| = \frac{I_{\text{rms,max}}}{1+M} \times \sqrt{\sin^2\left(\frac{\varphi_{AB}}{2}\right) + M^2 \sin^2\left(\frac{\varphi_{DC}}{2}\right) - 2M \sin\left(\frac{\varphi_{AB}}{2}\right) \sin\left(\frac{\varphi_{DC}}{2}\right) \cos\left(\varphi_{AD} + \frac{\varphi_{DC} - \varphi_{AB}}{2}\right)} \quad (6)$$

$$\min_{\mathbf{v}_\varphi \in C_s} |I(\mathbf{v}_\varphi)| : \begin{cases} P_o(\mathbf{v}_\varphi) = \tilde{P}_o \\ -P_{o,\max} \le \tilde{P}_o \le +P_{o,\max} \end{cases}$$

Fig. 1. (a) Isolated bidirectional DBSRC. (b) Ideal switching node voltages with a three-angle phase-shift control.

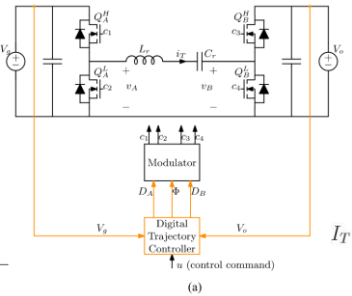

(a)

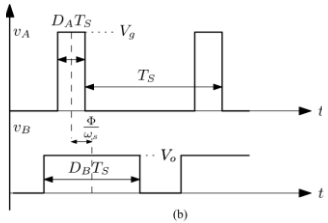

(b)

$$P_o = \frac{2}{M\pi^2} \frac{V_o^2}{|Z_T|} \sin(\pi D_A) \sin(\pi D_B) \sin(\Phi)$$

$$I_T = \frac{\sqrt{2}V_o}{\pi M |Z_T|} \sqrt{\begin{matrix} M^2 \sin^2(\pi D_B) \\ -2M \cos(\Phi) \sin(\pi D_A) \sin(\pi D_B) \\ +\sin^2(\pi D_A) \end{matrix}}$$

$$I_{T,N} = \begin{cases} \dfrac{P_{o,N}}{\sqrt{1+M^2}} & \text{if } |P_{o,N}| \le \sqrt{1-M^2} \\ \dfrac{\sqrt{1+M^2-2M\sqrt{1-P_{o,N}}}}{\sqrt{1+M^2}} & \text{otherwise} \end{cases}$$

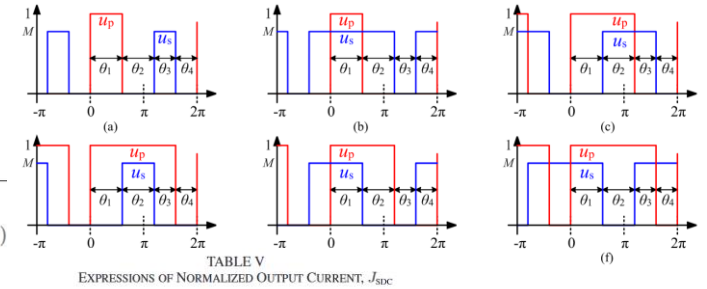

TABLE V
EXPRESSIONS OF NORMALIZED OUTPUT CURRENT, J_{sdc}

# of pattern	Expression
1	$\frac{1}{2\pi F_N \sin(F_N\pi)}\{2\sin(F_N D_p\pi)\sin(F_N D_s\pi)\sin(F_N(1-2D_\phi)\pi)\}$
2	$\frac{1}{2\pi F_N \sin(F_N\pi)}\{2\sin(F_N D_p\pi)\sin(F_N \overline{D_s}\pi)\sin(2F_N D_\phi\pi)\}$
3	$\frac{1}{2\pi F_N \sin(F_N\pi)}\begin{Bmatrix}-\sin(F_N\pi)+\cos(F_N(\overline{D_p}-2D_\phi)\pi)\sin(F_N D_s\pi) \\ +\cos(F_N(D_p-2D_\phi)\pi)\sin(F_N \overline{D_s}\pi)\end{Bmatrix}$
4	$\frac{1}{2\pi F_N \sin(F_N\pi)}\{2\sin(F_N \overline{D_p}\pi)\sin(F_N D_s\pi)\sin(2F_N D_\phi\pi)\}$
5	$\frac{1}{2\pi F_N \sin(F_N\pi)}\begin{Bmatrix}\sin(F_N\pi)-\sin(F_N D_p\pi)\cos(F_N(\overline{D_s}+2D_\phi)\pi) \\ -\sin(F_N \overline{D_p}\pi)\cos(F_N(D_s+2D_\phi)\pi)\end{Bmatrix}$
6	$\frac{1}{2\pi F_N \sin(F_N\pi)}\{-2\sin(F_N \overline{D_p}\pi)\sin(F_N \overline{D_s}\pi)\sin(F_N(1+2D_\phi)\pi)\}$

$$J_{\text{rms}} = \sqrt{\frac{1}{4F_N\pi}\sum_{k=1}^{4}(C_1+C_2+C_3)}$$

$$C_1 = \left(J_{L,k-1}^2 + (U_{c,k-1}-U_{T,k})^2\right)(F_N\theta_k)$$

$$C_2 = \left(J_{L,k-1}^2 - (U_{c,k-1}-U_{T,k})^2\right)\cos(F_N\theta_k)\sin(F_N\theta_k)$$

$$C_3 = -2J_{L,k-1}(U_{c,k-1}-U_{T,k})\sin^2(F_N\theta_k) \quad (9)$$

First-harmonic model based min RMS current trajectory of DAB-SRC

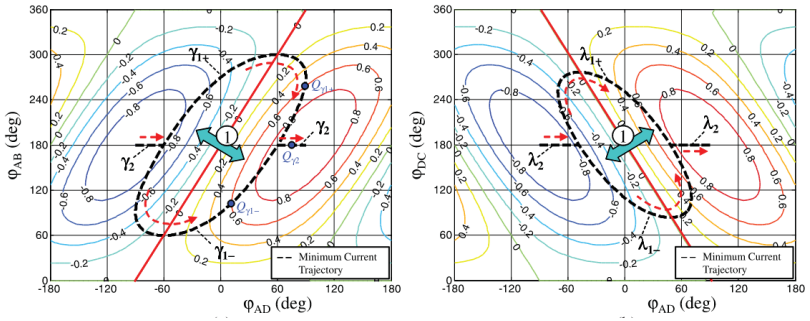

Fig. 4. Normalized rms current |I|/Irm s,m ax over the φD C = 180◦ plane for (a) M = 1 and (b) M = 0.5.

First-harmonic model based min RMS current trajectory of half bridge DAB-SRC

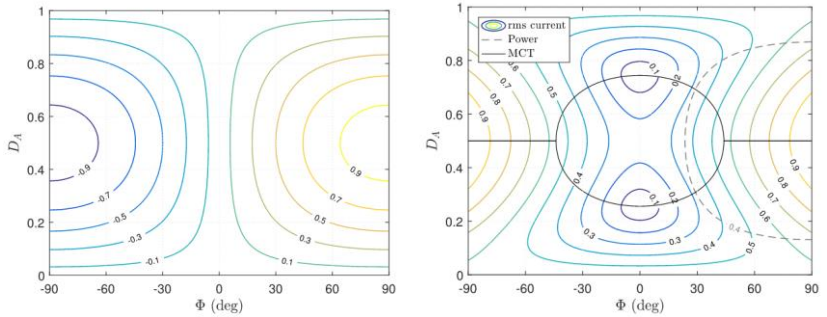

Fig. 2. (DA , Φ) plane (DB = 0.5) for M = 0.72: (a) normalized output power contours Po,N = Po /Po ,m ax , and (b) normalized tank rms current IT ,N = IT /IT ,m ax and MCT together with a single power contour Po ,N = 0.4.

Time domain model based 4-DoF min RMS current control of half bridge DAB-SRC

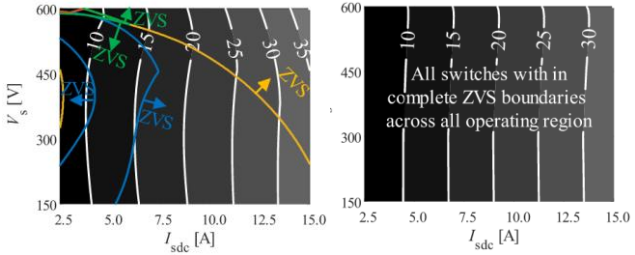

Comparison of rms current and ZVS boundaries in various modulation methods: (a) single phase shift modulation, (b) minimum current trajectory modulation, and (c) 4DOF modulation. The shaded contour illustrates the rms current, while the colored lines represent the boundary between complete ZVS and iZVS for each corresponding switch. The colored arrows indicate the ZVS operating regions.

L. Corradini, D. Seltzer, D. Bloomquist, R. Zane, D. Maksimović, and B. Jacobson, "Minimum Current Operation of Bidirectional Dual-Bridge Series Resonant DC/DC Converters," *IEEE Transactions on Power Electronics*, vol. 27, no. 7, pp. 3266–3276, Jul. 2012, doi: 10.1109/TPEL.2011.2181421.

F. Bez, W. Han, and L. Corradini, "A Low-Complexity Trajectory Controller for Reduced Conduction Losses in Series-Resonant Dual Half-Bridge Converters," *IEEE Transactions on Power Electronics*, vol. 33, no. 11, pp. 9963–9974, Nov. 2018, doi: 10.1109/TPEL.2018.2796141.

J.-S. Hong, S. Choi, and J.-I. Ha, "Modulation Method of Series-Resonant Dual-Active Half-Bridge Converter for ZVS and Minimum RMS Current," *IEEE Transactions on Industry Applications*, vol. 60, no. 1, pp. 694–708, Jan. 2024, doi: 10.1109/TIA.2023.3324316.

DAB-SRC: reactive power elimination optimization

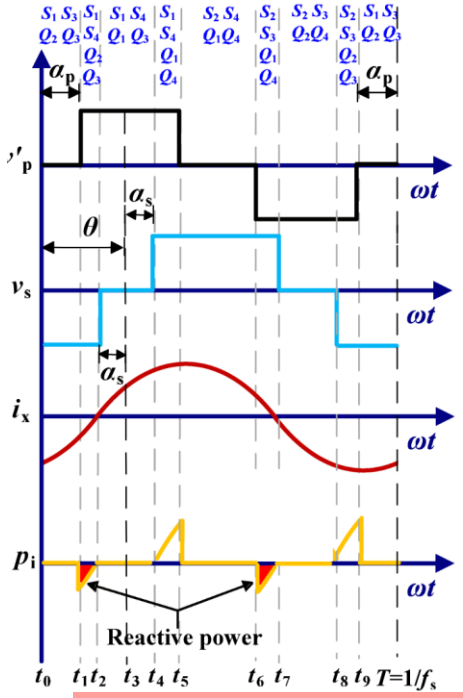

$$v'_{p,p.u}(t) = \frac{4\cos\alpha_p}{\pi}\sin\omega t \quad (1)$$

$$v_{s,p.u}(t) = \frac{4M\cos\alpha_s}{\pi}\sin(\omega t-\theta) \quad (2)$$

$$i_{x,p.u}(t) = \frac{4}{\pi X_{p.u}}(-\cos\alpha_p\cos\omega t + M\cos\alpha_s\cos(\omega t-\theta)) \quad (3)$$

$$P_{o,p.u} = \frac{1}{2\pi}\int_0^{2\pi} v_{p,p.u}(t)i_{x,p.u}(t)dt = \frac{8M\cos\alpha_p\cos\alpha_s}{\pi^2 X_{p.u}}\sin\theta$$

$$I_{o,p.u} = \frac{8\cos\alpha_p\cos\alpha_s}{\pi^2 X_{p.u}}\sin\theta.$$

A. Conditions for Achieving a Minimum Tank Current

$$I_{x,rms,p.u} = \frac{\pi I_{o,p.u}}{4\sin\theta\cos\alpha_p\cos\alpha_s} \times\sqrt{M^2+M^2\cos 2\alpha_s - 4M\cos\theta\cos\alpha_p\cos\alpha_s+\cos 2\alpha_p+1}. \quad (8)$$

C. Reactive Power Elimination

$$\begin{cases}\theta=\alpha_p=\sin^{-1}\sqrt{1-M} \text{ and } \alpha_s=0, & \text{for } M\le 1\\ \theta=\alpha_s=\sin^{-1}\sqrt{1-\frac{1}{M}} \text{ and } \alpha_p=0, & \text{for } M>1.\end{cases}$$

First-harmonic model based reactive power elimination for 4-DoF DAB-SRC

TABLE I
EFFECTIVE PHASE-SHIFT PARAMETERS FOR THE FORWARD POWER TRANSFER

M	α_{pe}	α_{se}	θ_e
$0.2\le M\le 0.95$	$\sin^{-1}(\sqrt{1-M})-\alpha_{dp}$	0	$\sin^{-1}(\sqrt{1-M})$
$0.95<M\le 1$	$\sin^{-1}(\sqrt{1-0.95})-\alpha_{dp}$	0	$\sin^{-1}(\sqrt{1-0.95})$
$1<M\le 1.05$	0	$\sin^{-1}(\sqrt{1-\frac{1}{1.05}})$	$\sin^{-1}(\sqrt{1-\frac{1}{1.05}})+\alpha_{dp}$
$M>1.05$	0	$\sin^{-1}(\sqrt{1-\frac{1}{M}})$	$\sin^{-1}(\sqrt{1-\frac{1}{M}})+\alpha_{dp}$

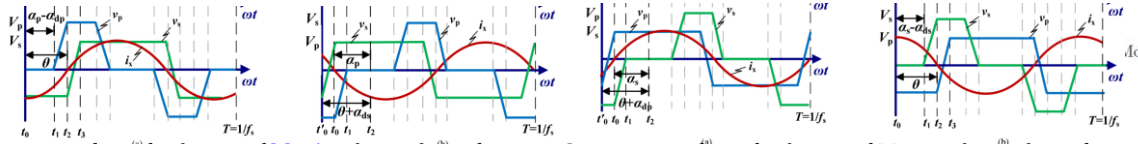

Operating waveforms for the case of $M \le 1$ with complete soft-switching transitions, minimum-tank-current operation, and reactive-power elimination. (a) Forward power flow. (b) Reverse power flow.

Operating waveforms for the case of $M > 1$ with complete soft-switching transitions, minimum-tank-current operation, and reactive-power elimination. (a) Forward power flow. (b) Reverse power flow.

M. Yaqoob, K. H. Loo, and Y. M. Lai, "A Four-Degrees-of-Freedom Modulation Strategy for Dual-Active-Bridge Series-Resonant Converter Designed for Total Loss Minimization," *IEEE Transactions on Power Electronics*, vol. 34, no. 2, pp. 1065–1081, Feb. 2019, doi: 10.1109/TPEL.2018.2865969.

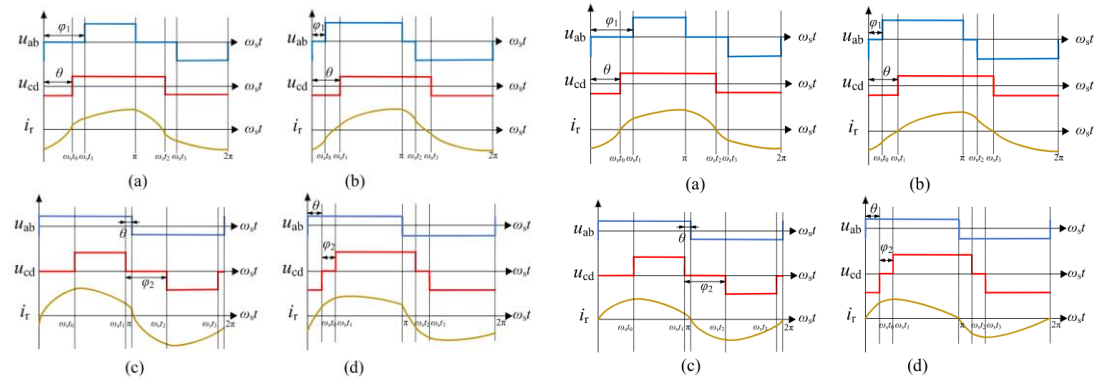

Fig. 3. Waveforms of the DBSRC under EPS control. (a) Mode I. (b) Mode II. (c) Mode III. and (d) Mode IV.

Fig. 4. Schematic diagram of zero-backflow power optimization method. (a) Mode I. (b) Mode II. (c) Mode III. and (d) Mode IV.

$$P_o = \begin{cases}\frac{2NU_iU_o}{\pi Z_r}F\sec\left(\frac{\pi}{2F}\right)\sin\left(\frac{2\theta-\varphi_1}{2F}\right)\sin\left(\frac{\pi-\varphi_1}{2F}\right) & \text{Mode I}\\ \frac{2NU_iU_o}{\pi Z_r}F\sec\left(\frac{\pi}{2F}\right)\left[\cos\left(\frac{\varphi_1}{2F}\right)\cos\left(\frac{\pi-2\theta+\varphi_1}{2F}\right)-\cos\left(\frac{\pi}{2F}\right)\right] & \text{Mode II}\\ \frac{2NU_iU_o}{\pi Z_r}F\sec\left(\frac{\pi}{2F}\right)\sin\left(\frac{\varphi_2}{2F}\right)\sin\left(\frac{\varphi_2-2\theta}{2F}\right) & \text{Mode III}\\ \frac{2NU_iU_o}{\pi Z_r}F\sec\left(\frac{\pi}{2F}\right)\left[\cos\left(\frac{\varphi_2}{2F}\right)\cos\left(\frac{\pi-2\theta-\varphi_2}{2F}\right)-\cos\left(\frac{\pi}{2F}\right)\right] & \text{Mode IV}\end{cases}$$

Mode I II $K<1, i_r(\theta)=0$

Mode III IV $K>1, i_r(0)=0$

Mode I
$$\begin{cases}Q_1=0\\ Q_2=\frac{NU_iU_o}{\pi^2Z_r}F\sec\left(\frac{\pi}{2F}\right)\begin{bmatrix}\sqrt{\sin^2\left(\frac{\varphi_1-\pi}{2F}\right)+K^2+2K\sin\left(\frac{\varphi_1}{2F}\right)\sin\left(\frac{\varphi_1-2\theta+2\pi}{2F}\right)}\\ -\sin\left(\frac{\varphi_1-2\pi}{2F}\right)\sin\left(\frac{\varphi_1-2\phi}{2F}\right)-K\cos\left(\frac{\pi}{2F}\right)\end{bmatrix}\end{cases}$$

Mode II
$$\begin{cases}Q_1=\frac{NU_iU_o}{\pi^2KZ_r}F\sec\left(\frac{\pi}{2F}\right)\begin{bmatrix}\cos\left(\frac{\varphi_1}{2F}\right)\cos\left(\frac{\pi-\varphi_1}{2F}\right)+K\cos\left(\frac{\pi-2\theta+2\varphi_1}{2F}\right)\\ -\sqrt{\sec\left(\frac{\pi}{2F}\right)\cos\left(\frac{\varphi_1}{2F}\right)\cos\left(\frac{\pi-\varphi_1}{2F}\right)+K^2+2K\cos\left(\frac{\varphi_1}{2F}\right)\cos\left(\frac{2\pi-2\theta+\varphi_1}{2F}\right)}\end{bmatrix}\\ Q_2=\frac{NU_iU_o}{\pi^2Z_r}F\sec\left(\frac{\pi}{2F}\right)\begin{bmatrix}\sqrt{\sec\left(\frac{\pi}{2F}\right)\cos\left(\frac{\varphi_1}{2F}\right)\cos\left(\frac{\pi-\varphi_1}{2F}\right)+K^2+2K\cos\left(\frac{\varphi_1}{2F}\right)\cos\left(\frac{2\pi-2\theta+\varphi_1}{2F}\right)}\\ -\cos\left(\frac{\varphi_1}{2F}\right)\cos\left(\frac{\pi-2\theta+\varphi_1}{2F}\right)-K\cos\left(\frac{\pi}{2F}\right)\end{bmatrix}\end{cases}$$

Mode III
$$\begin{cases}Q_1=\frac{NU_iU_o}{\pi^2KZ_r}F\sec\left(\frac{\pi}{2F}\right)\begin{bmatrix}\cos\left(\frac{\pi}{2F}\right)-K\sin\left(\frac{\varphi_2-2\theta}{2F}\right)\sin\left(\frac{\varphi_2-\pi}{2F}\right)\\ -\sqrt{1+K^2\sin^2\left(\frac{\pi-\varphi_2}{2F}\right)+K\left[\cos\left(\frac{\pi-\theta}{F}\right)-\cos\left(\frac{\varphi_2-\theta}{F}\right)\right]}\end{bmatrix}\\ Q_2=0\end{cases}$$

Mode IV
$$\begin{cases}Q_1=\frac{NU_iU_o}{\pi^2KZ_r}F\sec\left(\frac{\pi}{2F}\right)\begin{bmatrix}\cos\left(\frac{\pi}{2F}\right)+K\cos\left(\frac{\varphi_2}{2F}\right)\cos\left(\frac{\pi-2\theta-\varphi_2}{2F}\right)\\ -\sqrt{1+K^2\cos^2\left(\frac{\varphi_2}{2F}\right)+2K\cos\left(\frac{\varphi_2}{2F}\right)\cos\left(\frac{\varphi_2+2\theta-2\pi}{2F}\right)}\end{bmatrix}\\ Q_2=\frac{NU_iU_o}{\pi^2Z_r}F\sec\left(\frac{\pi}{2F}\right)\begin{bmatrix}\sqrt{1+K^2\cos^2\left(\frac{\varphi_2}{2F}\right)+2K\cos\left(\frac{\varphi_2}{2F}\right)\cos\left(\frac{\varphi_2+2\theta-2\pi}{2F}\right)}\\ -\cos\left(\frac{\pi-2\theta}{2F}\right)-K\cos\left(\frac{\varphi_2}{2F}\right)\cos\left(\frac{\varphi_2-\pi}{2F}\right)\end{bmatrix}\end{cases}$$

$$\begin{cases}\text{Mode I}: \varphi_1=\theta+\frac{\pi}{2}-Far\sin(T_1),\ P_{opu}\le\sqrt{1+(4K-4K^2)\tan^2(\pi/2F)}-1\\ \text{Mode II}: \varphi_1=-\frac{\pi}{2}+Far\sin(T_1),\ P_{opu}>\sqrt{1+(4K-4K^2)\tan^2(\pi/2F)}-1\\ \text{Mode III}: \varphi_2=\frac{\pi}{2}+\theta-Far\sin(T_2),\ P_{opu}\le\sqrt{1+(4/K-4/K^2)\tan^2(\pi/2F)}-1\\ \text{Mode IV}: \varphi_2=\frac{\pi}{2}-\theta-Far\sin(T_2),\ P_{opu}>\sqrt{1+(4/K-4/K^2)\tan^2(\pi/2F)}-1\end{cases}$$

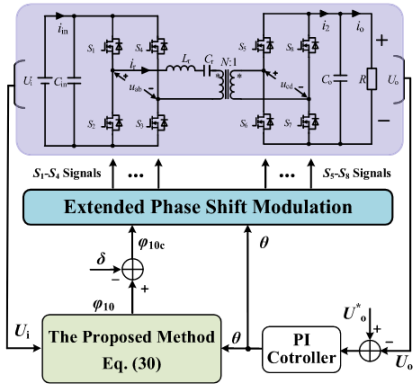

Time domain model based reactive power elimination for EPS controlled DAB-SRC

Y. Deng, W. Song, S. Yin, M. Zhong, J. Chen, and X. Feng, "Zero-Backflow Power Control Scheme of Dual Bridge Series Resonant DC–DC Converters With High-Accuracy Time Domain Modeling," *IEEE Transactions on Power Electronics*, vol. 38, no. 9, pp. 10985–10996, Sep. 2023, doi: 10.1109/TPEL.2023.3279435.

DAB-SRC: load transient optimization with trajectory control

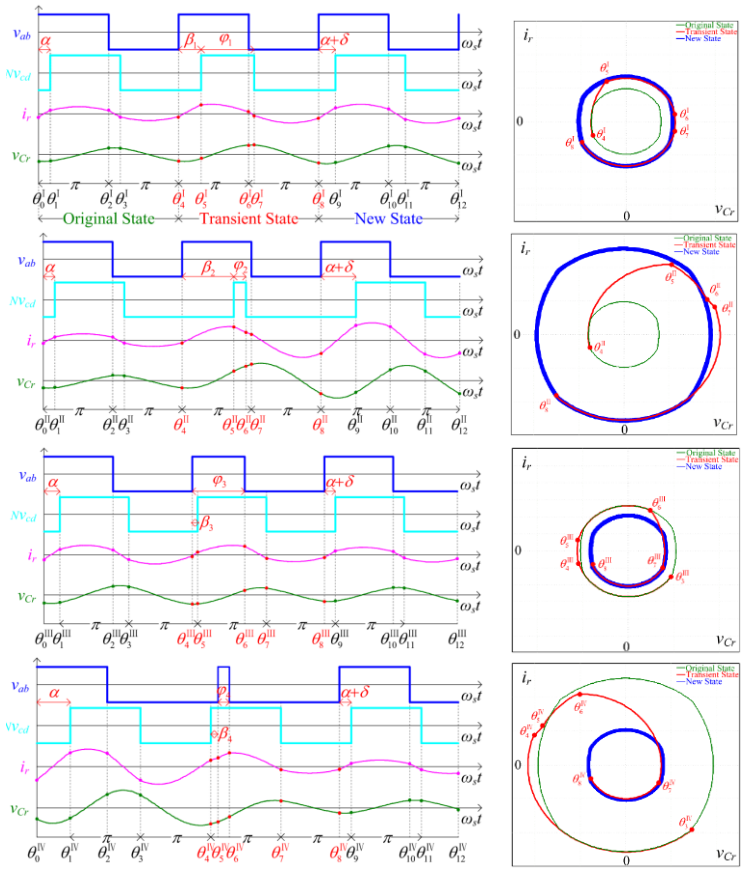

$$\varphi = 2F \cdot \arcsin\left[\frac{1}{2}\sec\left(\frac{\pi}{2F}\right)\sin\left(\frac{2\pi+|\delta|}{2F}\right)\right]$$

$$\beta_1 = \frac{\pi + 2\alpha + \delta - \varphi_1}{2}.$$

$$\varphi_1 = 2F \cdot \arcsin\left[\frac{1}{2}\sec\left(\frac{\pi}{2F}\right)\sin\left(\frac{2\pi+\delta}{2F}\right)\right]$$

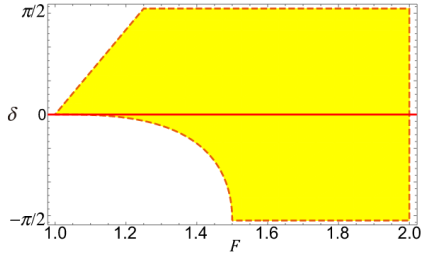

$$\beta_3 = \frac{\pi - 2\alpha - \delta - \varphi_3}{2}$$

$$\varphi_3 = 2F \cdot \arcsin\left[\frac{1}{2}\sec\left(\frac{\pi}{2F}\right)\sin\left(\frac{2\pi-\delta}{2F}\right)\right]$$

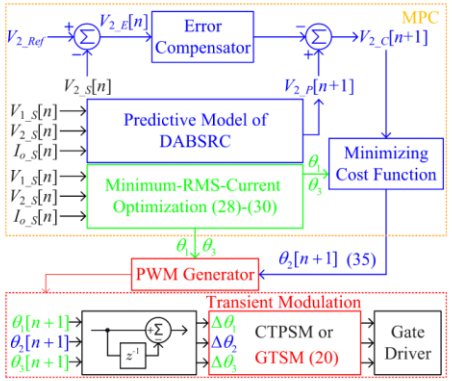

Fig. 7. Block diagram of MPC with minimum-rms-current optimization.

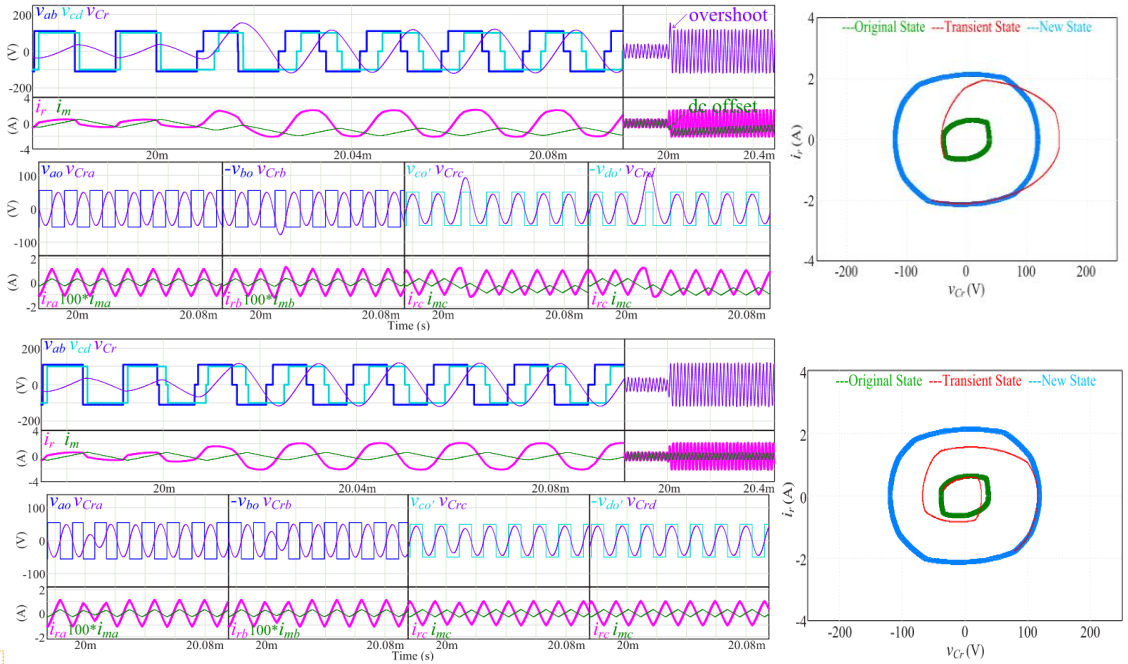

Fig. 6. Open-loop simulation examples from SPS mode to TPS mode under TSM [13] and GTSM with V1 = 110 V, V2 = 100 V, fs = 60 kHz, and F = 1.54. Simulated transient waveforms under (a) TSM and (b) GTSM.

TABLE I
COMPARISON OF DIFFERENT TRANSIENT MODULATION SCHEMES

Desirable properties	GTSM	TSM [13]	Methods in [17]–[19]
Oscillation suppression	✓	✓	✓
DC-offset elimination	✓	✗	✗
Generic method	✓	✗	✗
Analytical expression	✓	✓	✗
Sensorless algorithm	✓	✓	✗
Closed-loop implementation	✓	✓	✗
Wide feasible region	✓	✗	Not applicable

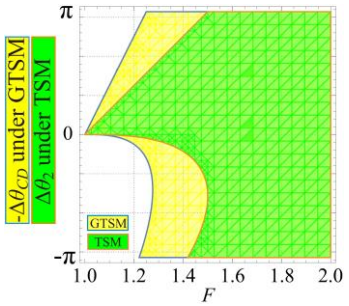

C. Sun, X. Jiang, L. Cao, and K. H. Loo, "Total Suppression of High-Frequency Transient Oscillations in Dual-Active-Bridge Series-Resonant Converter by Trajectory-Switching Modulation," *IEEE Transactions on Power Electronics*, vol. 37, no. 6, pp. 6511–6529, Jun. 2022, doi: 10.1109/TPEL.2021.3138150.

C. Sun *et al.*, "Generalized Multiphase-Shift Transient Modulation for Dual-Active-Bridge Series-Resonant Converter," *IEEE Transactions on Power Electronics*, vol. 38, no. 7, pp. 8291–8309, Jul. 2023, doi: 10.1109/TPEL.2023.3267297.

DAB-SRC control patent review

Delta Electronics Inc

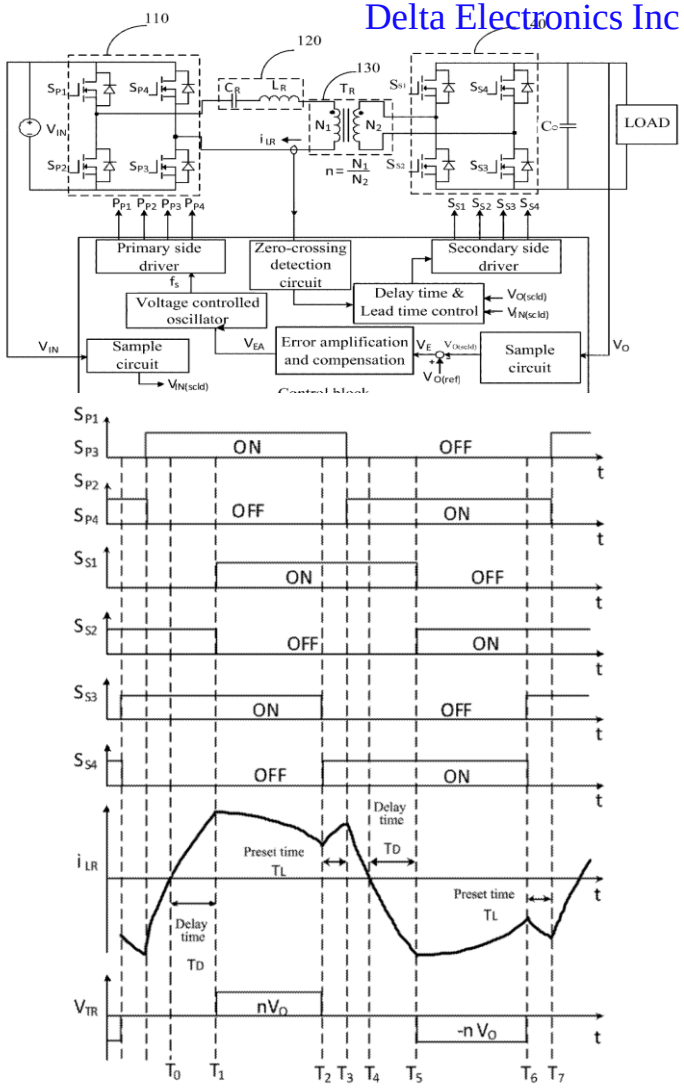

T. Wei and H. Lu, "Resonant converter and control method for realizing soft switching," US10756617B2, Aug. 25, 2020. [Online]. Available: https://patents.google.com/patent/US10756617B2/en?oq=US+Patent+10%2c756%2c617+

Siemens AG

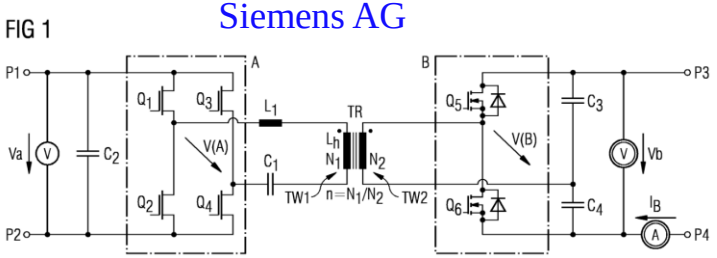

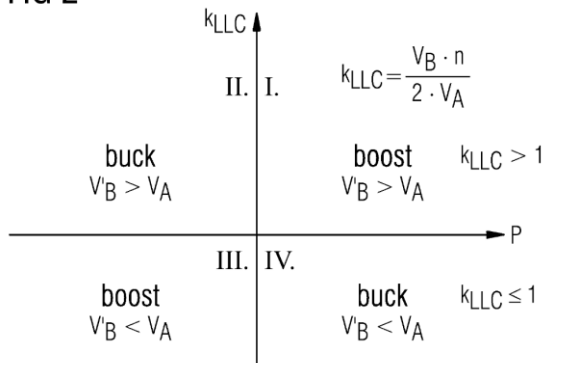

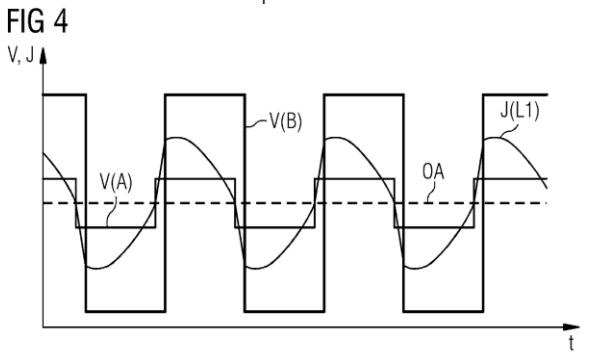

C. Fromme, F. Döbler, D. Malane, and M. Tannhäuser, "Bidirektionaler LLC-Resonanzwandler und Verfahren," DE102020213206A1, Apr. 21, 2022. [Online]. Available: https://patents.google.com/patent/DE102020213206A1/en?oq=US20150229225A1

Delta Electronics Inc

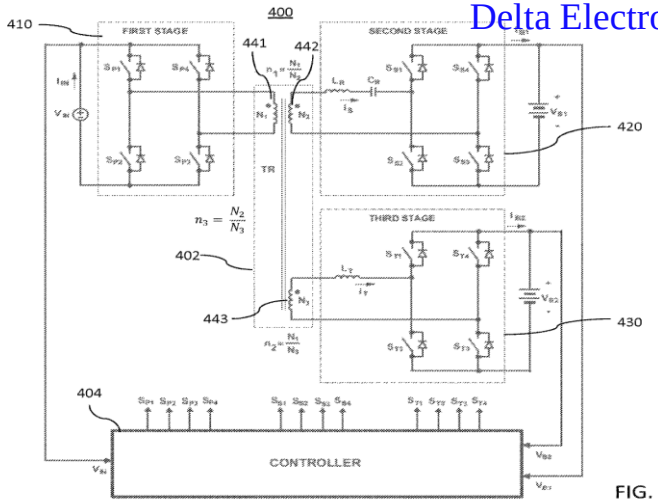

FIG. 4

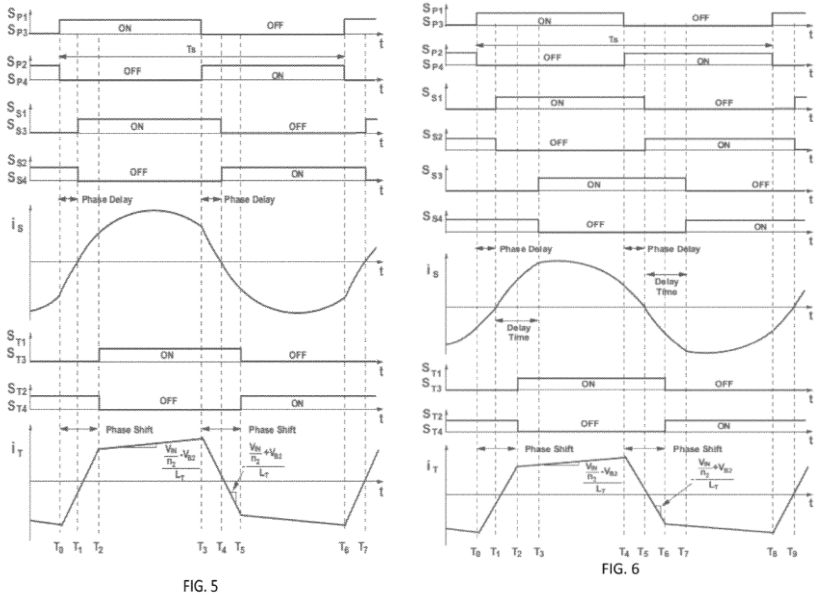

FIG. 5

FIG. 6

M. Kumar, Y. Jang, P. M. BARBOSA, M. Jia, and H. Sun, "Multiple-port bidirectional converter and control method thereof," US11594973B2, Feb. 28, 2023 Accessed: Jan. 23, 2025. [Online]. Available: https://patents.google.com/patent/US11594973B2/en?oq=US+Patent+10%2c756%2c617+

DAB-SRC patent review

Delta Electronics Inc

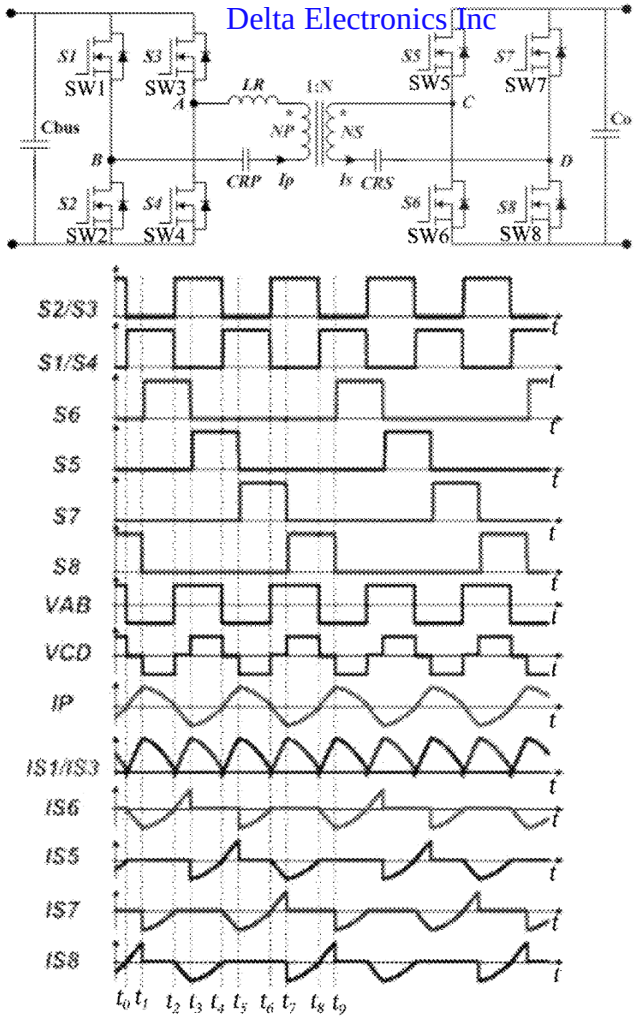

FIG. 6

H. Sun, M. Jia, and J. Zhang, “Control method for DC/DC converter and DC/DC converter,” US11070134B2, Jul. 20, 2021. [Online]. Available: https://patents.google.com/patent/US11070134B2/en?oq=US20150229225A1

Delta Electronics Inc

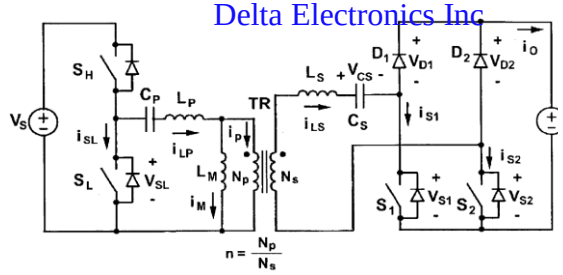

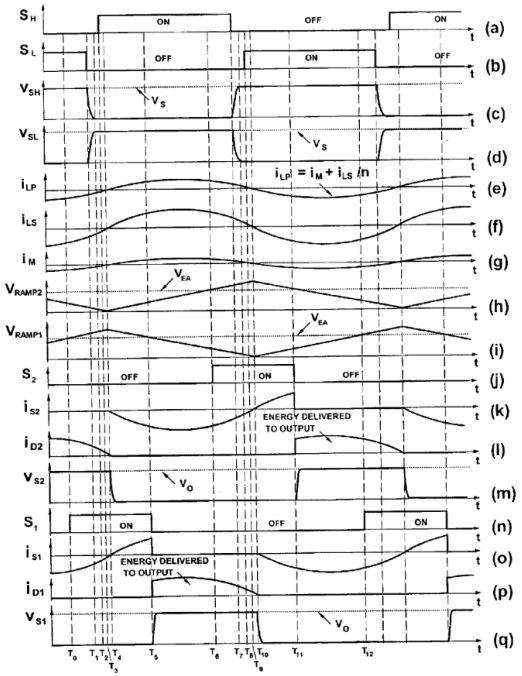

Fig. 7

Y. Jang and M. M. Jovanovic, “Contactless electrical energy transmission system having a primary side current feedback control and soft-switched secondary side rectifier,” US6934167B2, Aug. 23, 2005. [Online]. Available: https://patents.google.com/patent/US6934167B2/en?oq=US20150229225A1

Hangzhou Weisibo System Technology Co ltd

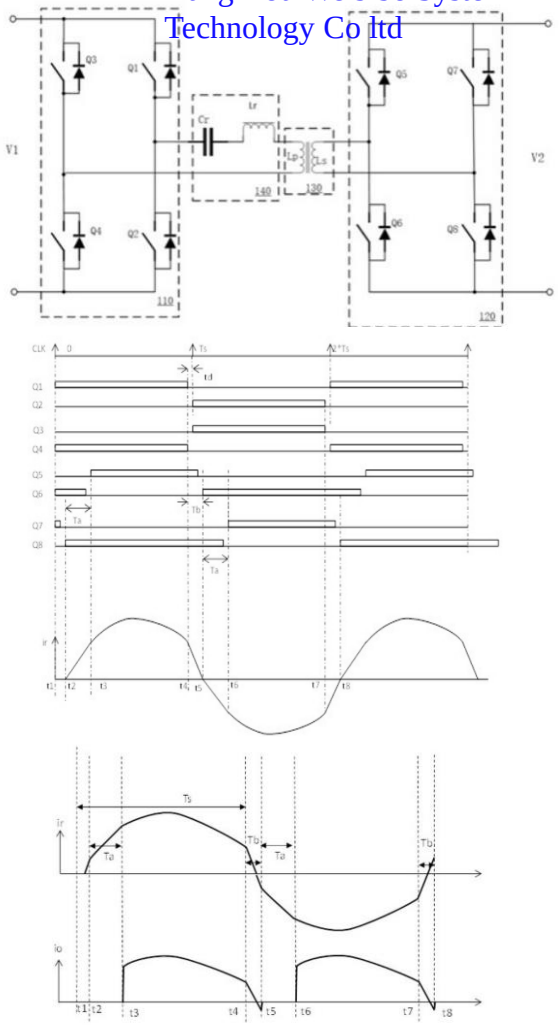

黄贵松 and 刘钢, “桥式谐振变换器的控制方法及桥式谐振变换器,” CN117240105B, Mar. 01, 2024. [Online]. Available: https://patents.google.com/patent/CN117240105B/en?oq=US+Patent+10%2c756%2c617+

Delta Electronics Inc

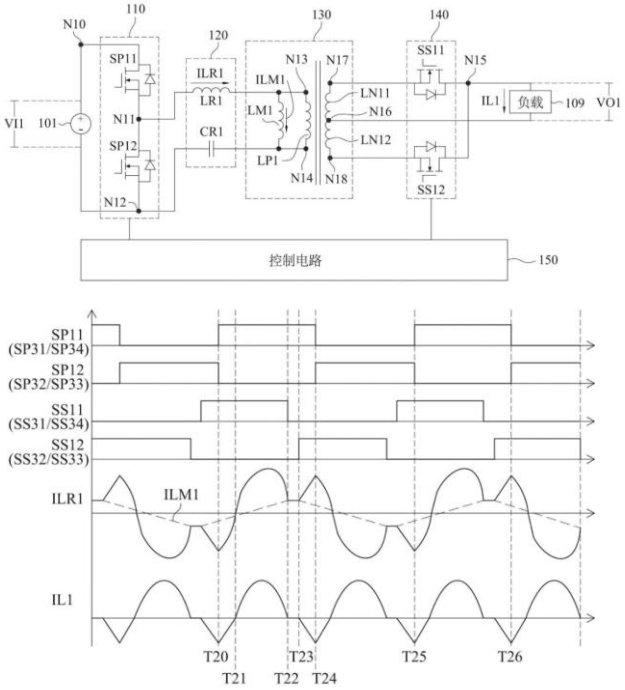

黄辉 *et al.*, “谐振变换器及其操作方法,” CN115776234A, Mar. 10, 2023. [Online]. Available: https://patents.google.com/patent/CN115776234A/en?oq=US+Patent+10%2c756%2c617+

DAB-SRC patent review

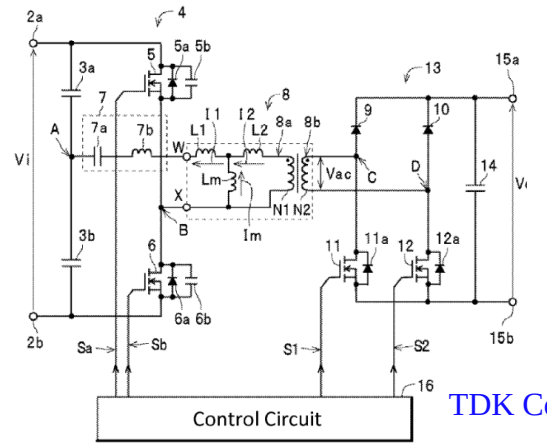

TDK Corp

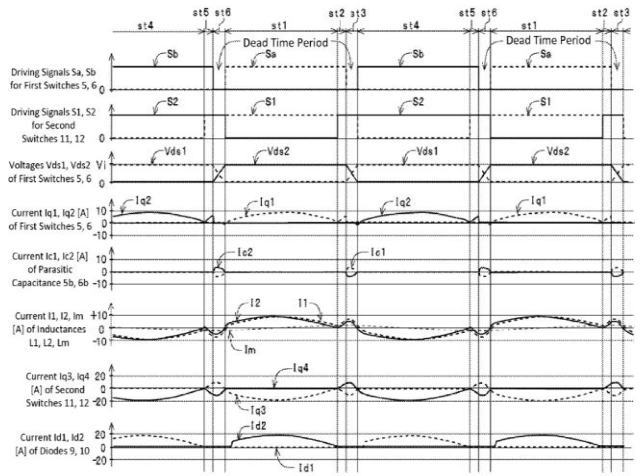

Fig. 2

K. Matsuura, Y. ISHIZUKA, and A. HARIYA, "Current resonance dc-dc converter," US20150263631A1, Sep. 17,. 2015. [Online]. Available: https://patents.google.com/patent/US20150263631A1/en?oq=US+Patent+10%2c756%2c617+

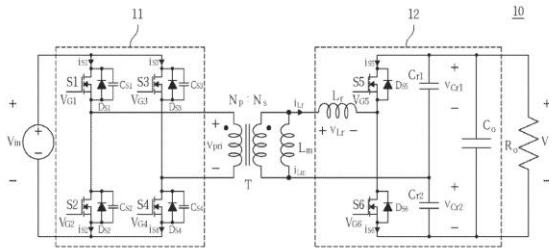

POSTECH

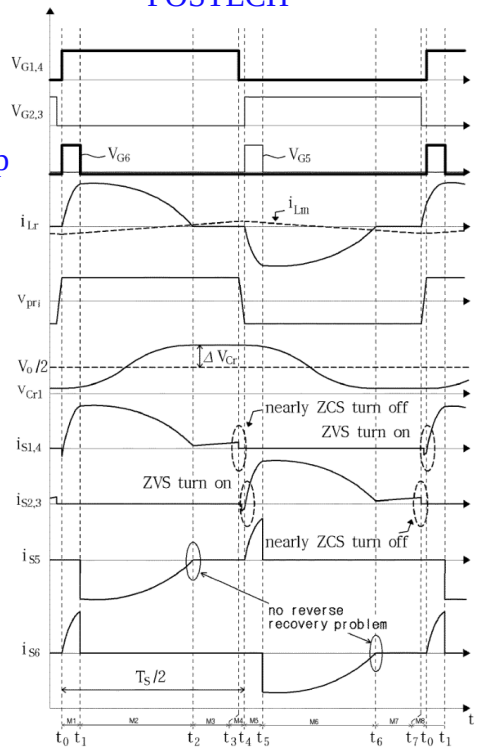

M. Kim, S. KIM, and B. KIM, "Power conversion circuit for photovoltaic power generation with high efficiency over wide ... voltage range," US10476398B1, Nov. 12, 2019. [Online]. Available: https://patents.google.com/patent/US10476398B1/en?oq=US20150229225A1

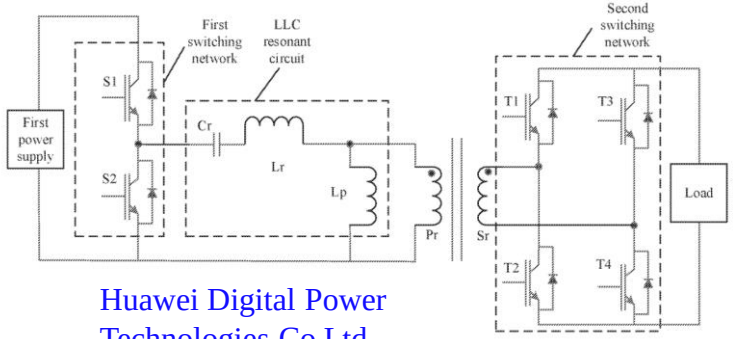

Huawei Digital Power Technologies Co Ltd

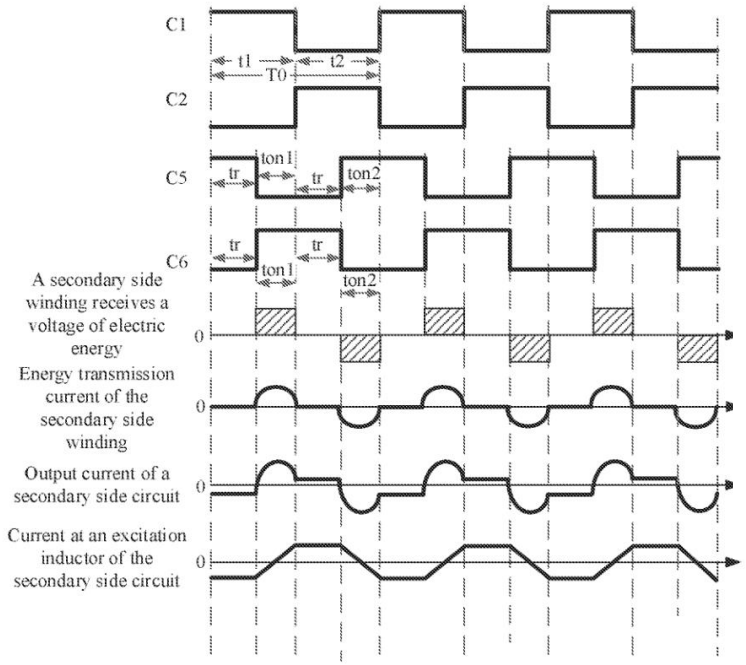

FIG. 9

T. Wang and W. Liu, "Power Converter, Method for Increasing Inverse Gain Range, Apparatus, and Medium," US20220345046A1, Oct. 27, 2022. [Online]. Available: https://patents.google.com/patent/US20220345046A1/en?oq=US20150229225A1

Infineon Technologies Austria AG

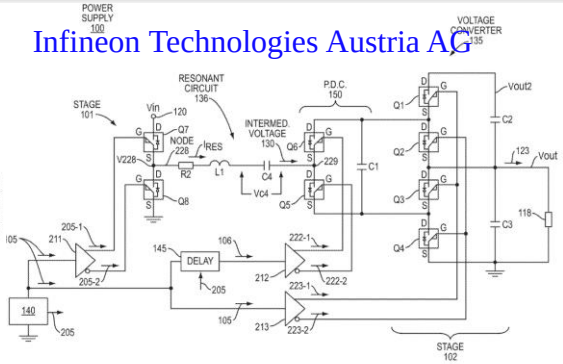

FIG. 2

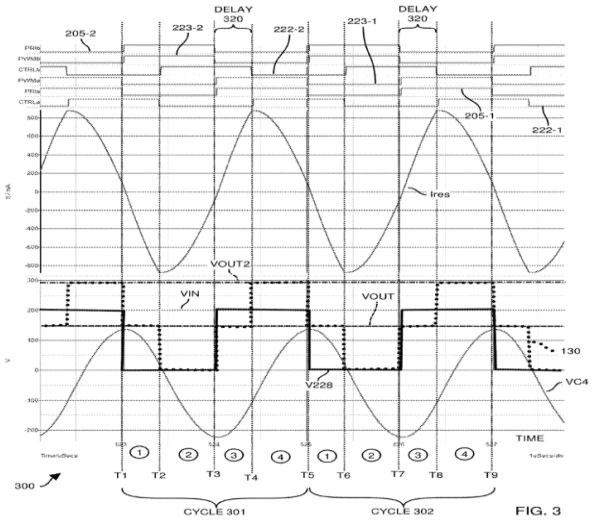

FIG. 3

P. Ausseresse, "Hybrid resonant power supply," US12051972B2, Jul. 30, 2024. [Online]. Available: https://patents.google.com/patent/US12051972B2/en?oq=US20150229225A1

Current Fed APM : non-resonant current fed converter

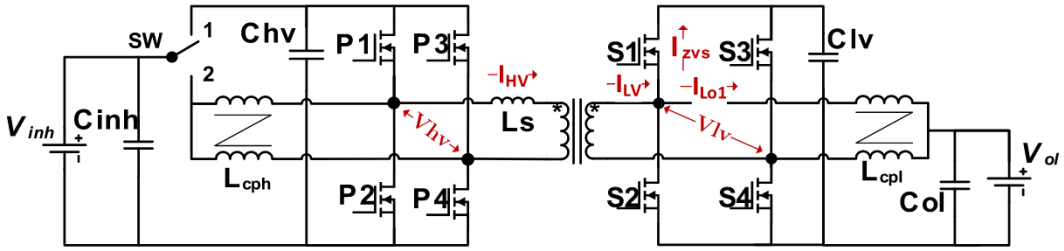

reconfigurable topologies are illustrated in Fig. 19. The VF/CF configuration boundary is also marked. Clearly, the reconfigurable design improves the efficiency of corner cases effectively

$$\frac{V_{inh}}{V_{ol}} < \frac{N_t}{\max(D_h)}. \tag{36}$$

Ultra-high Gain Current-fed Universal Auxiliary Power Module

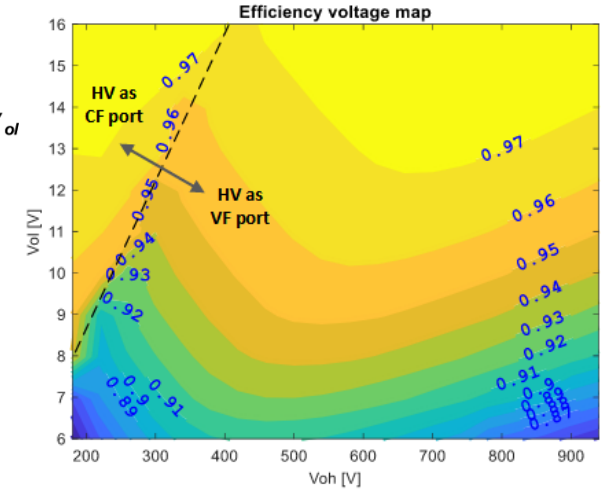

Fig. 8 The boundary of VF/CF mode and estimated efficiency map

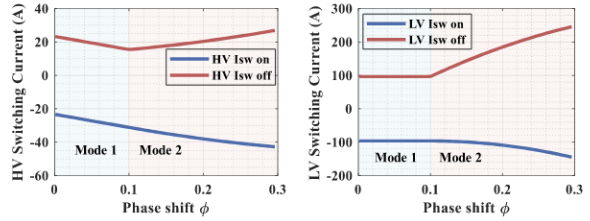

Fig. 15. Impact of the ϕ on switching current, fixed D_h and D_l, CF configuration.

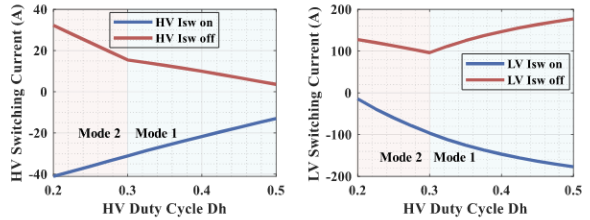

Fig. 16. Impact of D_h on switching current, fixed D_l, CF-CFDAB.

L. Zhu, H. Bai, and A. Brown, "Model and control of a current-fed dual active bridge based ultrawide-voltage-range auxiliary power module for 400 V/800 V electric vehicles," *IEEE Transactions on Power Electronics*, vol. 39, no. 3, pp. 3263–3276, Mar. 2024, doi: 10.1109/TPEL.2023.3337712.

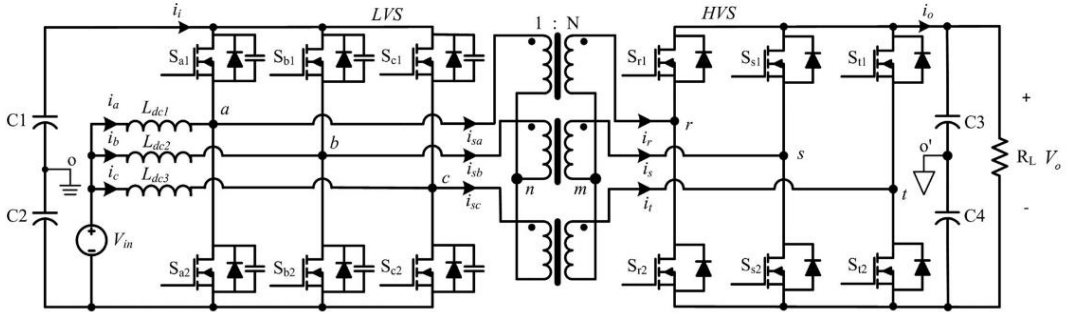

Three-phase Current-fed Bidirectional DC-DC Converter With High Efficiency Over a Wide Input Voltage Range

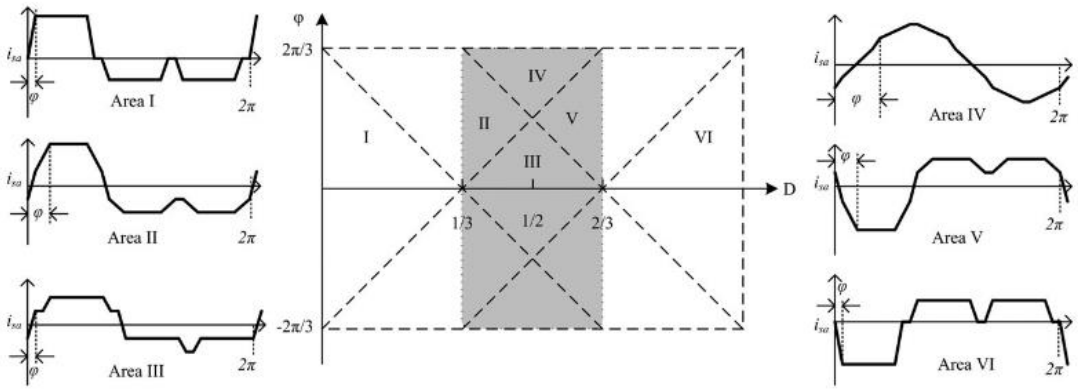

Z. Wang and H. Li, "A soft switching three-phase current-fed bidirectional DC-DC converter with high efficiency over a wide input voltage range," *IEEE Transactions on Power Electronics*, vol. 27, no. 2, pp. 669–684, Feb. 2012, doi: 10.1109/TPEL.2011.2160284.

Current Fed APM : resonant current fed converter

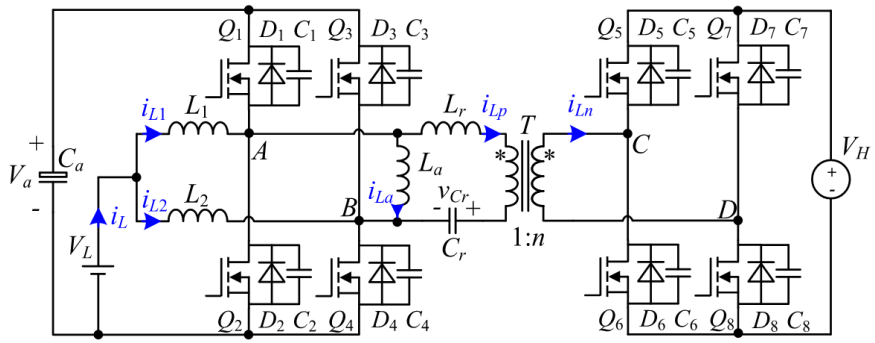

TABLE I
OPERATING MODES DEFINITION

Mode	Duty cycle	Voltage gain
Buck	D_L>0.5, D_H=0.5	M<2
Boundary	D_L=0.5, D_H=0.5	M=2
Boost	D_L=0.5, D_H>0.5	M>2
	D_L=0.5, D_H<0.5	
	D_L<0.5, D_H>0.5	
	D_L<0.5, D_H<0.5	
	D_L<0.5, D_H=0.5	

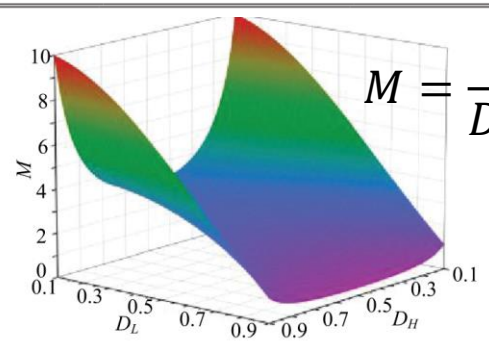

$$M = \frac{sin(D_L\pi)}{D_L sin(D_H\pi)}$$

Hybrid-PWM-Controlled Current-Fed Bidirectional Series Resonant Converter With Low Current Ripple and Wide Voltage Gain

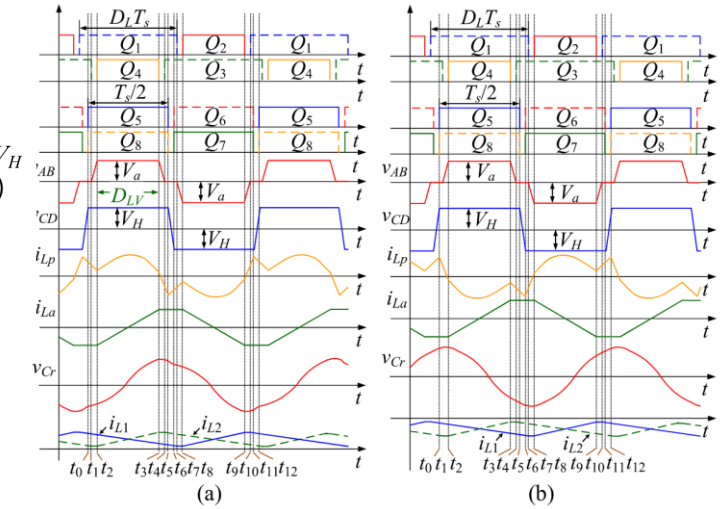

CF-SR BDC in Buck Mode. (a) Forward Mode. (b) Backward Mode.

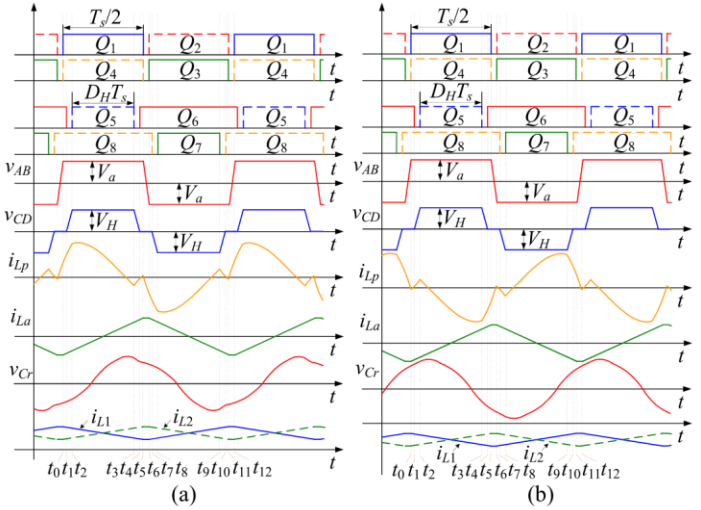

CF-SR BDC in Boost Mode. (a) Forward Mode. (b) Backward Mode.

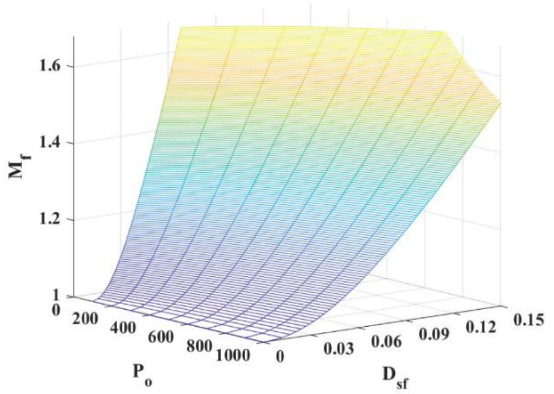

$$D_{sf} = \frac{2M_f}{V_H}\sqrt{\frac{L_r P_o}{T_s}\left(1-\frac{1}{M_f}\right)}$$

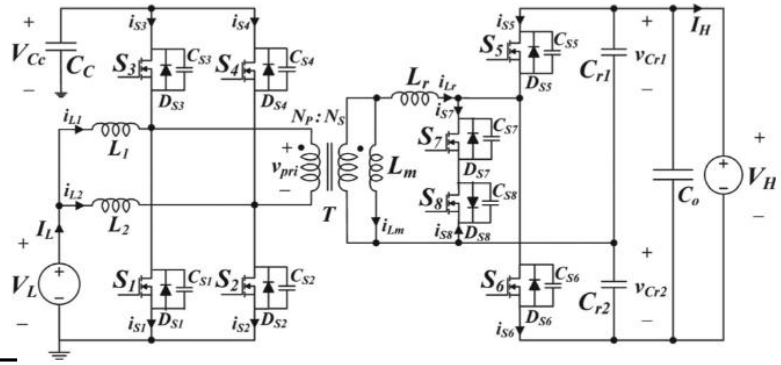

Highly Efficient Bidirectional Current-Fed Resonant Converter Over a Wide Voltage Gain Range

L. Gu, X. Zhang, and P. Li, "Hybrid-PWM-Controlled Current-Fed Bidirectional Series Resonant Converter With Low Current Ripple and Wide Voltage Gain," *IEEE Transactions on Industrial Electronics*, vol. 68, no. 8, pp. 7125–7136, Aug. 2021, doi: 10.1109/TIE.2020.3000090.

Current Fed APM : modified resonant current fed converter

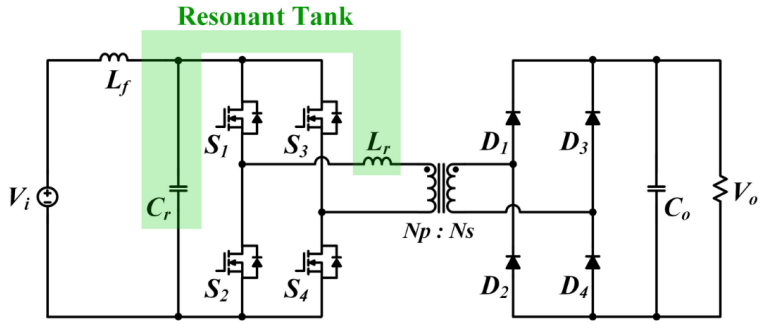

New Interleaved Current-Fed Resonant Converter With Significantly Reduced High Current Side Output Filter for EV and HEV Applications

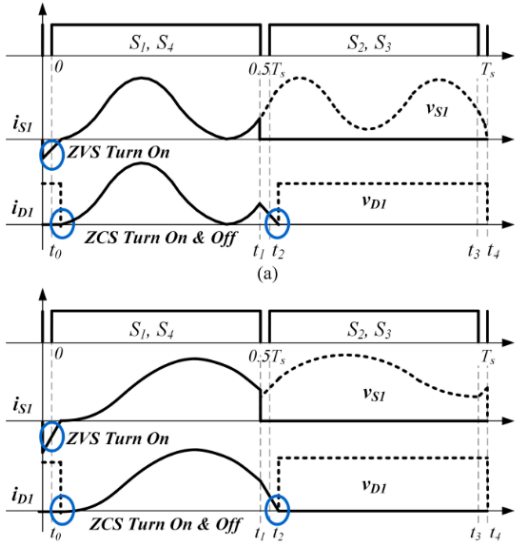

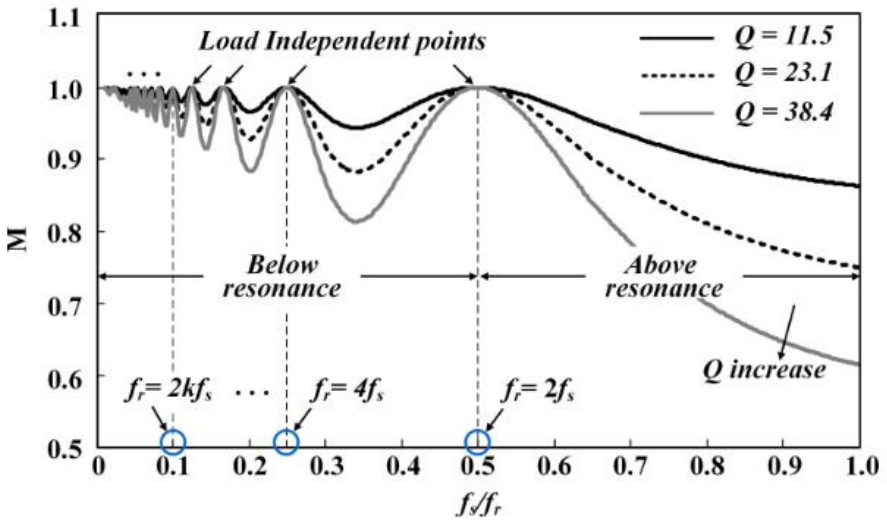

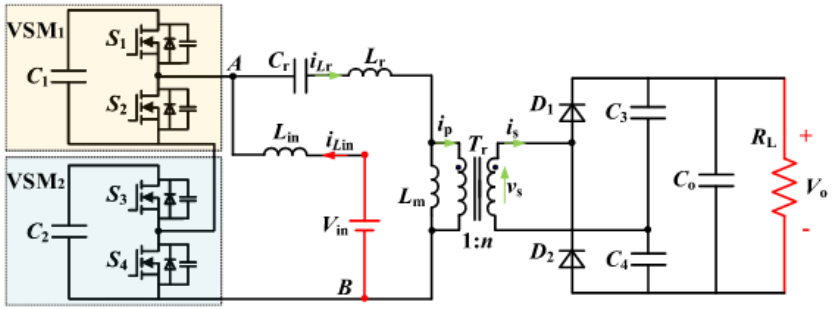

Fixed-Frequency Circulant Phase-Shift Controlled Current-Fed Resonant Converter With Wide Voltage Gain Range

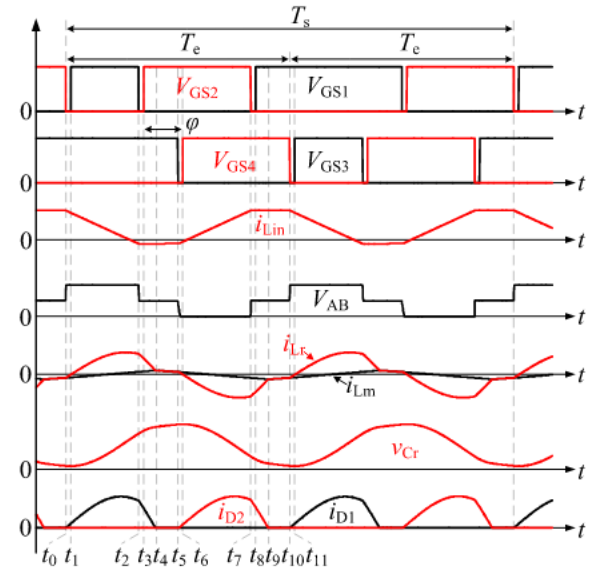

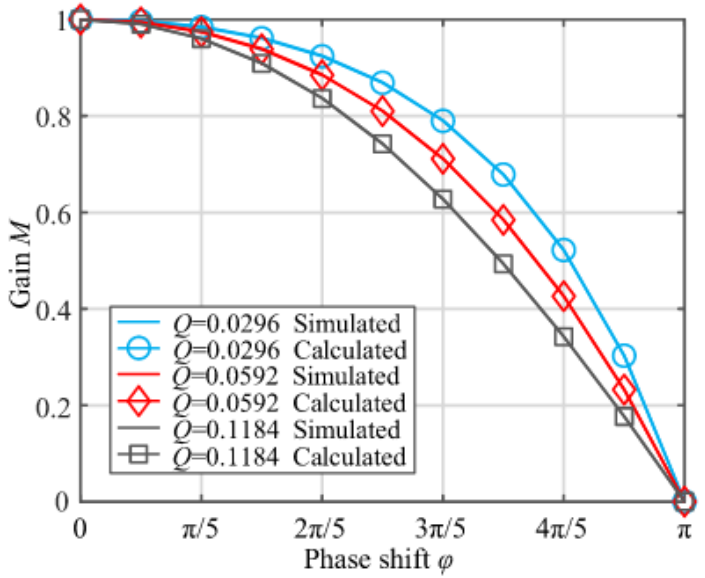

D. Moon, J. Park, and S. Choi, "New interleaved current-fed resonant converter with significantly reduced high current side output filter for EV and HEV applications," *IEEE Transactions on Power Electronics*, vol. 30, no. 8, pp. 4264–4271, Aug. 2015, doi: 10.1109/TPEL.2014.2360470.

R. Gu, D. Zhang, J. Duan, R. Qu, and A. Li, "Fixed-frequency circulant phase-shift controlled current-fed resonant converter with wide voltage gain range," *IEEE Transactions on Industrial Electronics*, pp. 1–11, 2023, doi: 10.1109/TIE.2023.3322011.

Current Fed APM : Direct Power Transfer (coupled boost inductor)

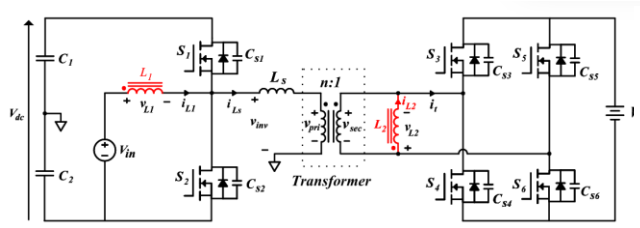

$$P_{DPT} = \frac{MV_o}{L_t^2 f_s}\left[V_{in}(\phi - 0.25) + V_{dc}\left(\frac{1}{8} - \phi^2\right)\right]$$

Bidirectional Current-Fed Converter With Direct Power Transfer

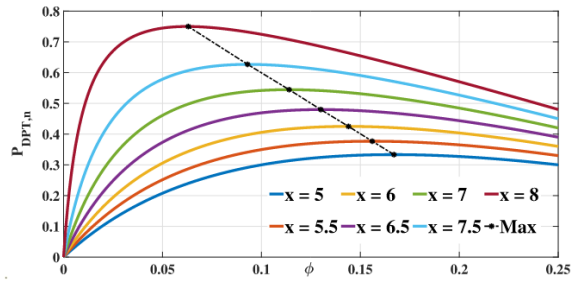

FIGURE 5. The normalized direct power transfer curve with respect to ϕ for different values of x parameter.

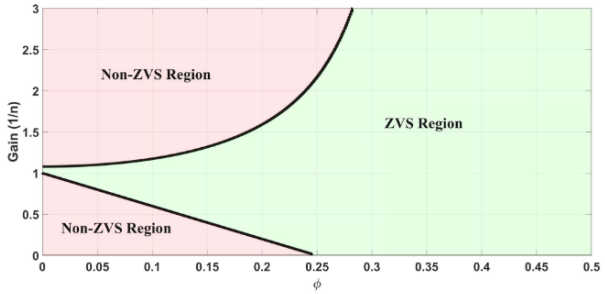

FIGURE 7. ZVS region of the proposed converter.

S. Goudarzitaemeh and M. Pahlevani, "A Bidirectional DC–DC Converter With Direct Power Transfer," *IEEE Open J. Power Electron.*, vol. 5, pp. 232–249, 2024, doi: 10.1109/OJPEL.2024.3359971.

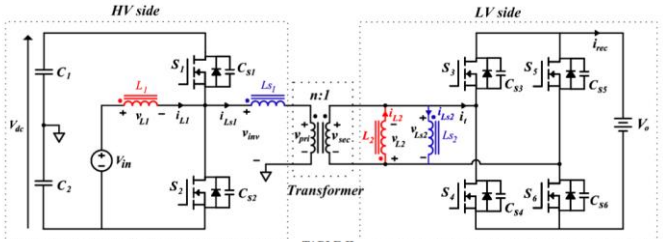

TABLE II
COMPARISON OF THE EQUATIONS IN EPS AND SPS MODES

Variable	SPS	EPS
P_{tr}	$\frac{V_{in}(nLs_2+Ls_M)V_o}{2f_sLs_t^2}[2n_\phi(1-2n_\phi)]$	$\frac{V_{in}(nLs_2+Ls_M)V_o}{2f_sLs_t^2}[n_\phi(1-2n_\phi)+n_\theta(1-2n_\theta)]$
P_{DPT}	$\frac{V_{in}MV_o}{2f_sL_t^2}[2n_\phi(1-2n_\phi)]$	$\frac{V_{in}MV_o}{2f_sL_t^2}[n_\phi(1-2n_\phi)+n_\theta(1-2n_\theta)]$
$P_{slope,adjust}$	$\frac{V_{in}Ls_MV_o}{2f_sLs_t^2}[2n_\phi(1-2n_\phi)]$	$\frac{V_{in}Ls_MV_o}{2f_sLs_t^2}[n_\phi(1-2n_\phi)+n_\theta(1-2n_\theta)]$
I_{in}	$\frac{MV_o}{4L_t^2f_s}(4n_\phi-1)+\frac{L_2V_{in}}{4L_t^2f_s}$	$\frac{MV_o}{4L_t^2f_s}(2n_\phi+2n_\theta-1)+\frac{L_2V_{in}}{4L_t^2f_s}$
P_{out}	$\frac{V_{in}V_o}{2f_sL_t^2Ls_t^2}[(nLs_2+2Ls_M)L_t^2+MLs_t^2]\times[2n_\phi(1-2n_\phi)]$	$\frac{V_{in}V_o}{2f_sL_t^2Ls_t^2}[(nLs_2+2Ls_M)L_t^2+MLs_t^2]\times[n_\phi(1-2n_\phi)+n_\theta(1-2n_\theta)]$
$P_{DPT,n}$	$\frac{2MV_o[2n_\phi(1-2n_\phi)]}{MV_o(4n_\phi-1)+L_2V_{in}}$	$\frac{2MV_o[n_\phi(1-2n_\phi)+n_\theta(1-2n_\theta)]}{MV_o(2n_\phi+2n_\theta-1)+L_2V_{in}}$
P_{BFP}	$\frac{V_o}{4f_sL_t^2Ls_t^2(a_1V_{in}+a_2V_o)}\times[a_1V_{in}(2n_\phi-0.5)+0.5a_2V_o]^2$	$\frac{V_o}{4f_sL_t^2Ls_t^2(a_1V_{in}+a_2V_o)}\times[a_1V_{in}(2n_\theta-0.5)+a_2V_o(-n_\phi+n_\theta+0.5)]^2$

Extended Phase Shift Control Current-Fed Converter With Direct Power Transfer

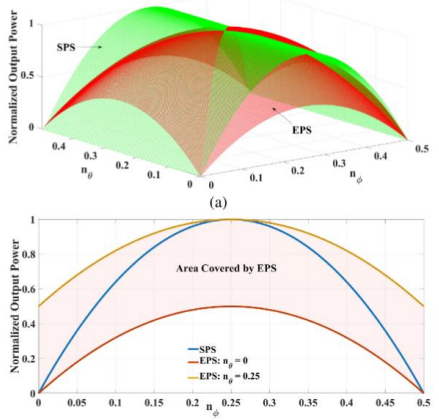

Fig. 6. Curves of the output power with variation in ϕ and θ for SPS and EPS controls: (a) 3-D and (b) 2-D.

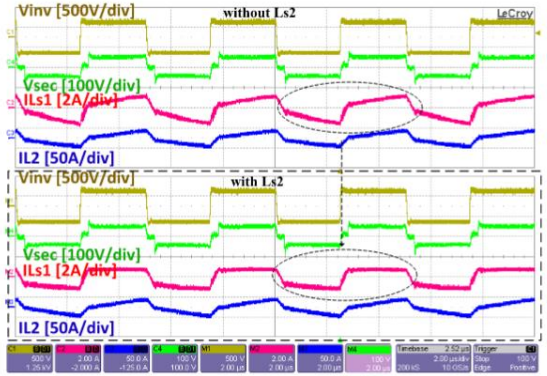

Fig. 20. Experimental waveforms v_{inv}, v_{sec}, i_{Ls1}, and i_{L2} of the proposed converter at $V_{in} = 400$ V, $V_o = 48$ V, and $P = 1$ kW with the EPS control in the HV2LV mode: (top) Ls_2 is shorted and (bottom) Ls_2 is in the circuit.

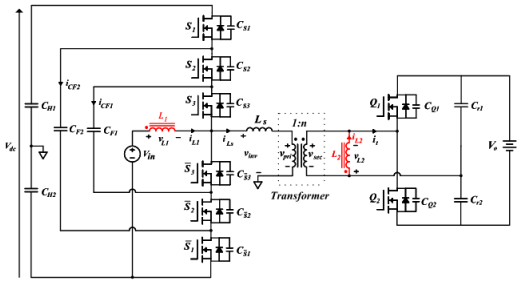

Multilevel Current-Fed DAB Converter With Direct Power Transfer

S. Goudarzitaemeh and M. Pahlevani, "Extended Phase Shift Control of a Novel Bidirectional DC–DC Converter With Direct Power Transfer," *IEEE Journal of Emerging and Selected Topics in Power Electronics*, vol. 12, no. 5, pp. 4521–4537, Oct. 2024, doi: 10.1109/JESTPE.2024.3439098.

S. Goudarzitaemeh, L. Melanson, J. Woelfle, and M. Pahlevani, "A Multilevel Current-Fed DAB Converter With Direct Power Transfer," *IEEE Open Journal of Power Electronics*, vol. 5, pp. 1612–1628, 2024, doi: 10.1109/OJPEL.2024.3476496.

Two-stage APM: Regulated DC/DC + isolated LLC

Boost regulated stage + LLC isolated stage

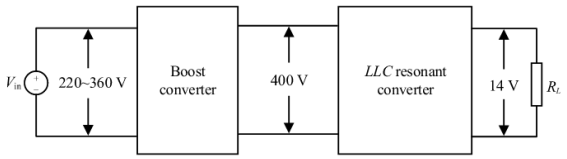

Fig. 2. Structure of two-level automotive auxiliary converter.

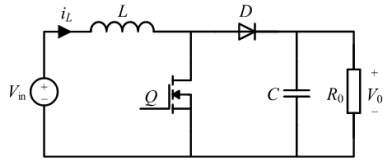

Fig. 3. Typology of the boost converter.

C. Wu, J. Liu, L. Wang, Y. Su, and J. Yue, "An Online Proactive CTR Monitoring Method for Optocoupler in Automotive Auxiliary Converter," *IEEE Transactions on Instrumentation and Measurement*, vol. 70, pp. 1–13, 2021, doi: 10.1109/TIM.2021.3115582.

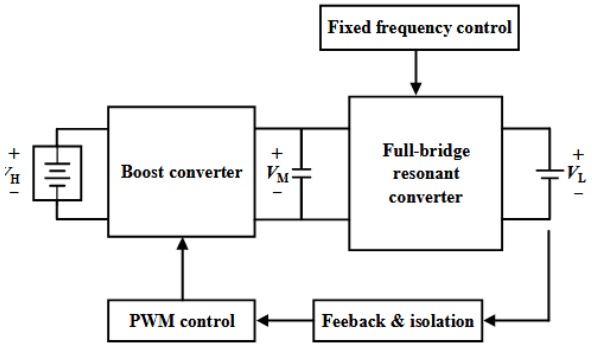

Fig. 2. Two-stage converter for APM

C.-Y. Chen, T.-J. Liang, K.-F. Liao, K.-H. Chen, and Y.-H. Yeoh, "Design and Implementation of Two-Stage Boost and Full-Bridge Resonant Converter for Wide-Range APMs," in *2021 IEEE International Future Energy Electronics Conference (IFEEC)*, Nov. 2021, pp. 1–6. doi: 10.1109/IFEEC53238.2021.9662017.

Buck regulated stage + LLC isolated stage

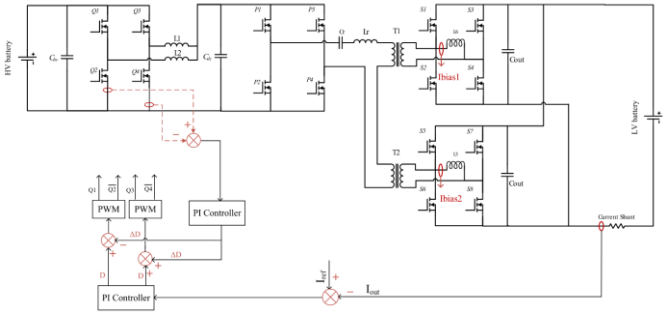

L. Zhu, H. Bai, A. Brown, and M. McAmmond, "Design a 400 V–12 V 6 kW bidirectional auxiliary power module for electric or autonomous vehicles with fast precharge dynamics and zero DC-bias current," *IEEE Transactions on Power Electronics*, vol. 36, no. 5, pp. 5323–5335, May 2021, doi: 10.1109/TPEL.2020.3028361.

Vin=250-450V, Vo=10-16V,
Buck stage fs =100-500kHz;
LLC stage fs = 200kHz

Power=6kW, PD=2.22 kW/L,
Eff_pk=0.962%

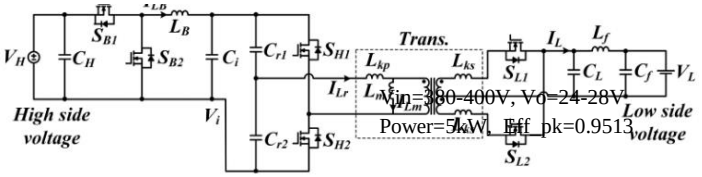

Vin=380-400V, Vo=24-28V
Power=5kW, Eff_pk=0.9513

Fig. 2. Proposed two-stage BDC.

J. Park and S. Choi, "Design and control of a bidirectional resonant DC–DC converter for automotive engine/battery hybrid power generators," *IEEE Transactions on Power Electronics*, vol. 29, no. 7, pp. 3748–3757, Jul. 2014, doi: 10.1109/TPEL.2013.2281826.

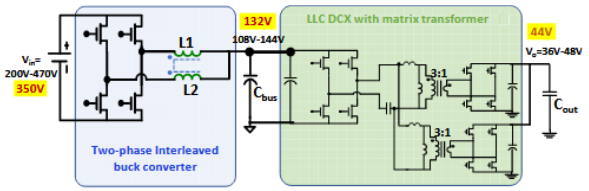

P. R. Prakash, A. Nabih, S. Wang, P. P. Hieu, Y. Ruan, and Q. Li, "GaN-Based 400V/48V DC-DC Converter with 97% Efficiency and PCB Magnetics for Automotive Applications," in *2023 IEEE Applied Power Electronics Conference and Exposition (APEC)*, Mar. 2023, pp. 3201–3208. doi: 10.1109/APEC43580.2023.10131189.

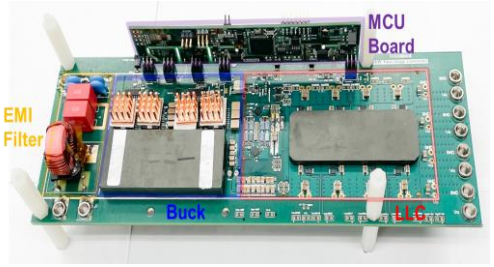

Vin=200-470V, Vo=36-48V

Power=2kW, PD=5kW/L, Eff_pk=0.966

LLC isolated (SAC) + non-isolated 48-12V regulator

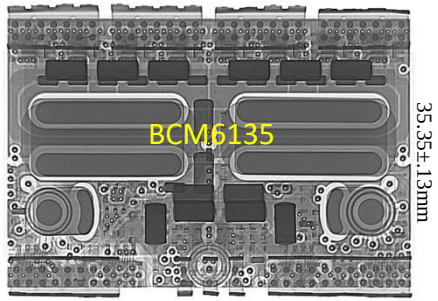

61.33±.13mm H = 7.417mm

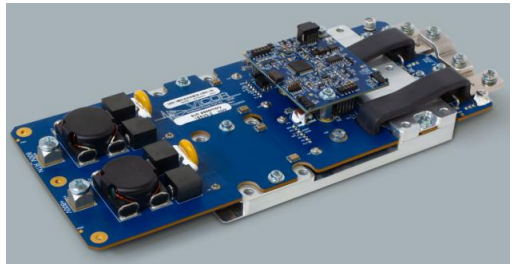

HV to LV 4kW system

BCM6135 65A BCM Bus Converter - Vicor | Mouser

DCM3735 48V to PoL DC-DC Converter - Vicor | Mouser

Topology	LLC resonant converter
Rated Power	4kW
HV range	800V
LV range	13.8V
Switch Freq.	--
Peak Eff.	>0.95
Power Density	3.63 kW/L

"Power modules meet EV power demands that have increased by 20x." May 24, 2024. Accessed: Nov. 06, 2024. [Online]. Available: https://www.vicorpower.com/resource-library/articles/automotive/power-modules-for-uncharted-ev-power-challenges

Two stage may have higher component cost, but better regulation and possibly higher density

https://www.vicorpower.com/documents/event-presentation/2024-AID-Maximizing-vehicle-weight-reduction.pdf

EV DC-DC APM Performance Map – Product

A Giant leap from 400 to 800V architecture

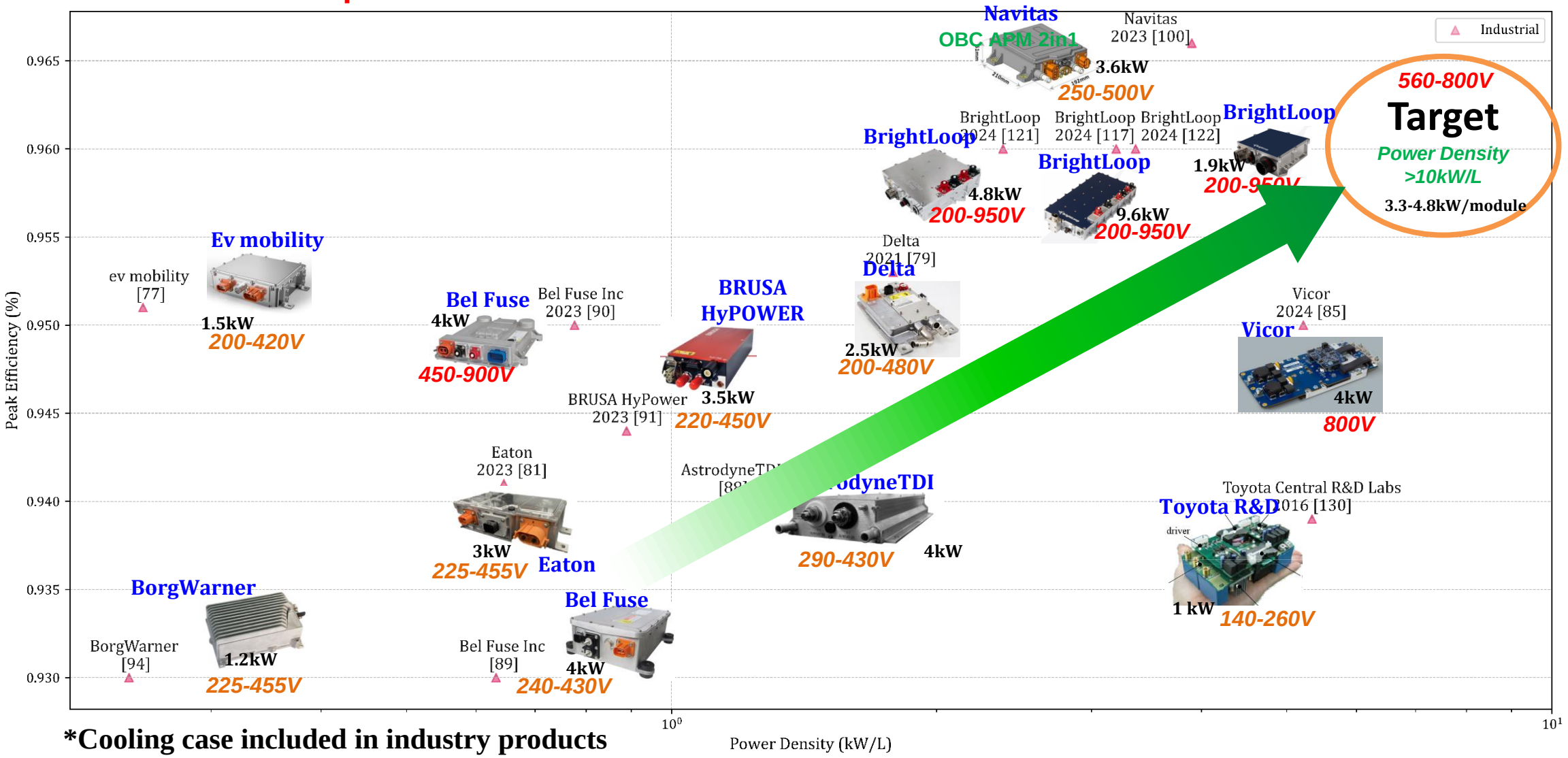

*Cooling case included in industry products

EV DC-DC APM Performance Map – Research

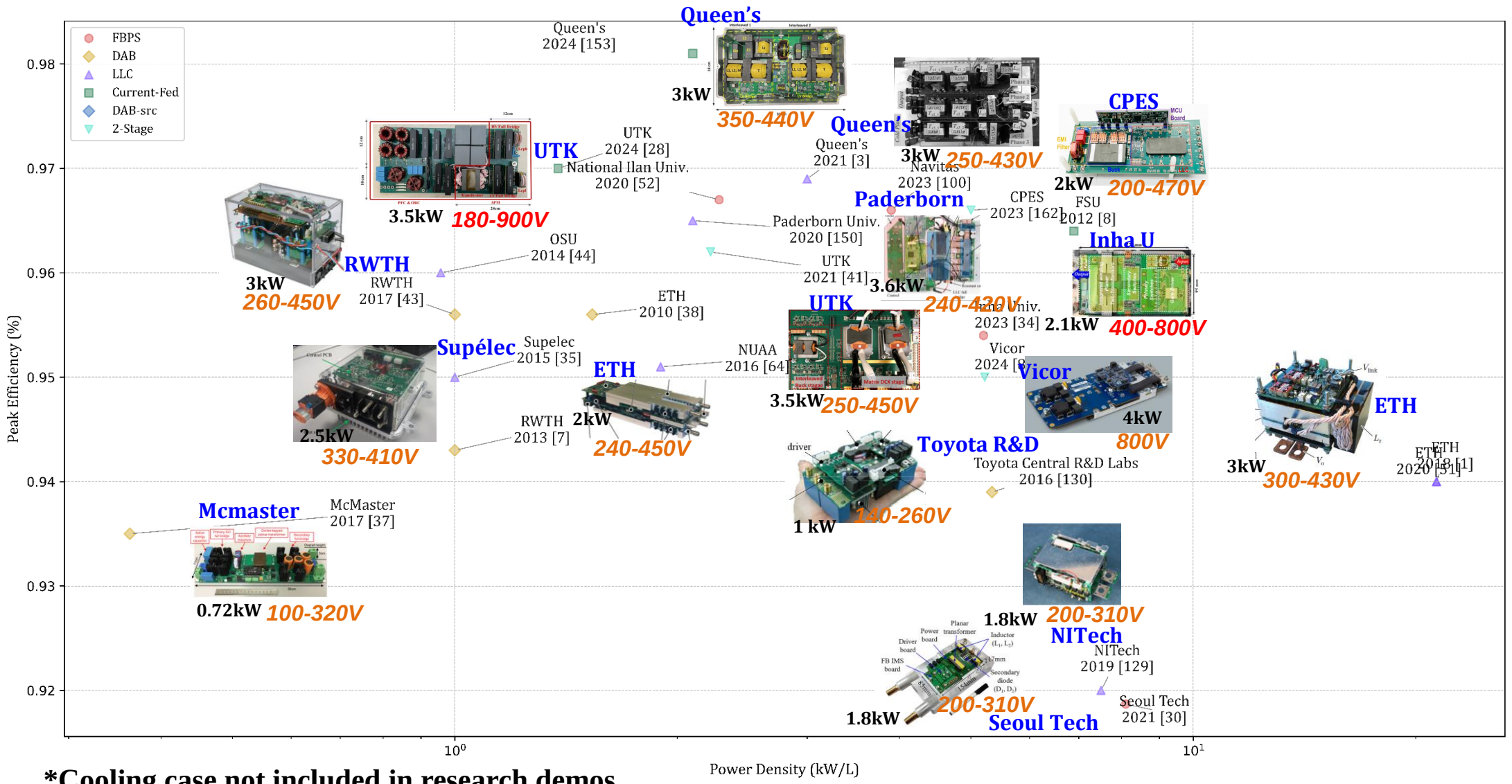

*Cooling case not included in research demos

Topology Comparison – perspective of Peak Efficiency

Queen's U | Queen's U | Delta | Queen's U | RWTH | UTK

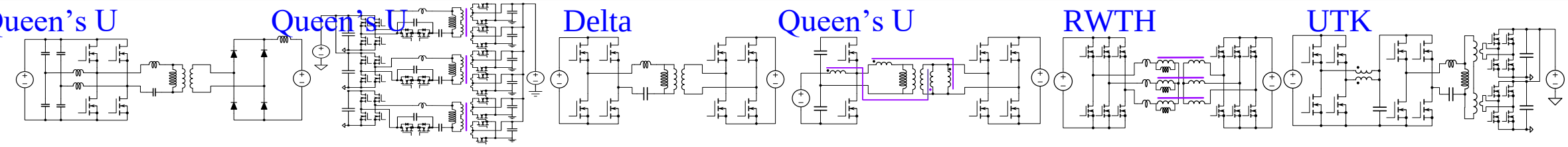

Topology	Aux-inductor ZVS Full bridge Phase shift	3-phase SCC balanced interleaved LLC converter	Series-Resonant DAB	Current-Fed with Direct Power Transfer	Non-resonant 3-phase interleaved DAB	2-stage (Interleaved Buck + LLC)
Rated Power	3kW	3phases x 1kW	3kW	2phases x 1.5kW	3kW	6kW
HV range	235-431V	250-430V	250-450V	350-450V	260-450V	250-450V
LV range	11.5-15V	9-16V	9.5-15.5V	45-60V	10-16V	10-16V
Switch Freq.	220kHz	260-400kHz (fr=546kHz)	300-400kHz (fr=270kHz)	200kHz	100kHz	140-400kHz buck/ 200kHz LLC
Peak Eff.	**0.975**	0.969	0.961	**0.981**	0.956	0.962
Power Density	--(very low)	3kW/L	--	2.648kW/L	1kW/L	2.22kW/L

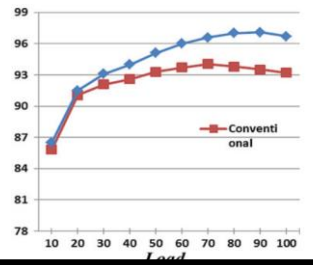

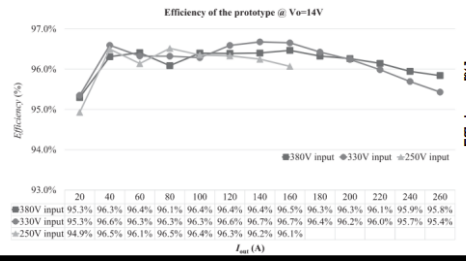

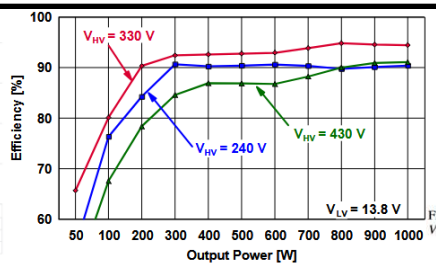

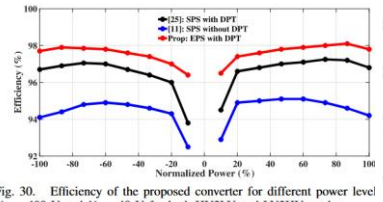

Fig. 30. Efficiency of the proposed converter for different power level V_{in} = 400 V and V_o = 48 V for both HV2LV and LV2HV modes.

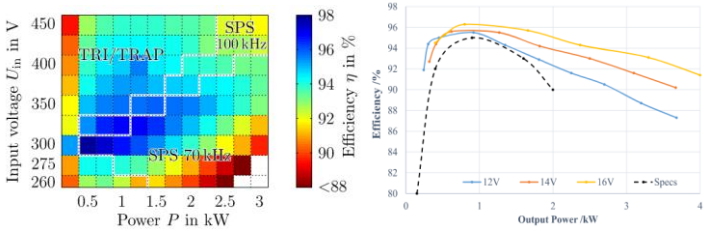

Advantage	• Good efficiency • Neat control principle • Full pri ZVS and sec ZCS	• Flat efficiency by phase-shedding • Good efficiency even at light load • Low turn-off loss, pri ZVS + sec ZCS	• Very wide 3-L or FB/HB operation • Inherent bidirectional operation • Narrow frequency vs traditional LLC	• Flexible voltage regulation • Good overall efficiency over wide load range	• Very wide voltage regulation • Inherent bidirectional operation	• wide voltage regulation • Possibly higher efficiency if well designed
Drawbacks	• Excessive components, low power density • Triangular current, high stress	• Wide freqency range, bad regulation • Extra phase balancing required	• Relative high turn-off current at high input volt (triangular current) • Complex control principle	• Complex control principle • Relative high turn-off current	• High turn-off current • Complex control principle • Bad light load efficiency	• Higher cost

doi: 10.1109/TPEL.2011.2178103. doi: 10.1109/TPEL.2021.3076773. doi: 10.1109/APEC.2019.8722067. doi: 10.1109/JESTPE.2024.3439098. doi: 10.1109/TPEL.2013.2251905. doi: 10.1109/TPEL.2020.3028361.

Topology Comparison – perspective of Power Density

Inha U

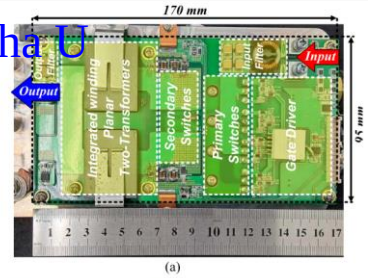

ETH

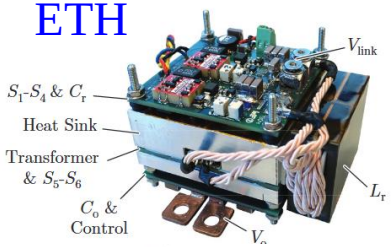

ETH

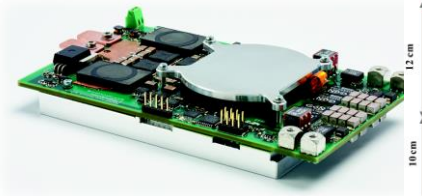

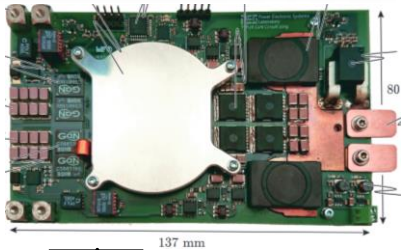

UTK

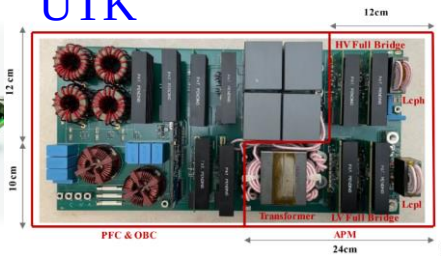

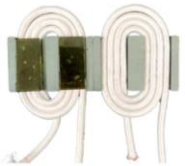

ETH

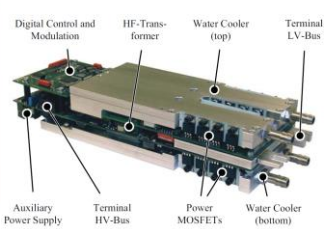

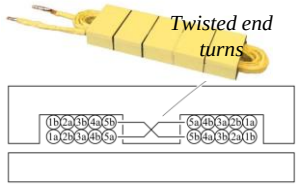

CPES

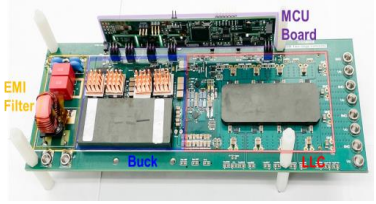

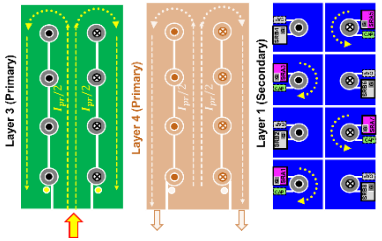

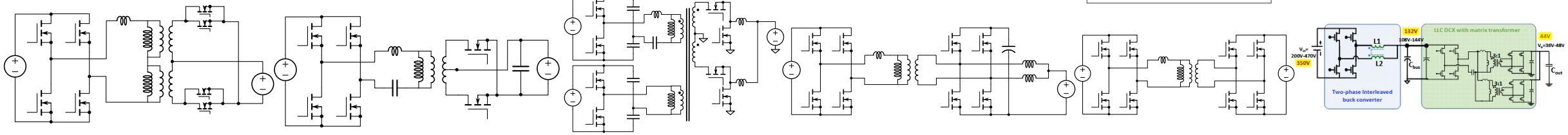

Topologys	2 xfrm full bridge phase shift	LLC resonant converter	Series-Resonant TAB	Non-resonant Current-Fed	Non-resonant DAB	2-stage (Interleaved Buck + LLC)
Rated Power	2.1kW	3kW	1.5kW	3.2kW	2kW	2kW
HV range	400-800V	300-430V	250-500V	180-900V	240-450V	200-470V
LV range	13-15V	12V	10.5-15V	6-16V	11-16V	36-48V
Switch Freq.	200kHz	320-500kHz (fr=300kHz)	155-750kHz (fr=430kHz)	80kHz	100kHz	200kHz buck/ 500kHz LLC
Peak Eff.	0.954	0.94	0.966	0.97	0.95	0.966
Power Density	5.2kW/L	**21.35 kW/L**	8.2kW/L	2.66 kW/L	1.535kW/L	5kW/L

doi: 10.1109/TTE.2022.3190968. doi: 10.1109/APEC39645.2020.9124410. [Online]. Available: https://ieeexplore.ieee.org/document/9861943 doi: 10.1109/TPEL.2023.3337712. doi: 10.1109/TIE.2009.2025284. doi: 10.1109/APEC43580.2023.10131189.

Conclusion

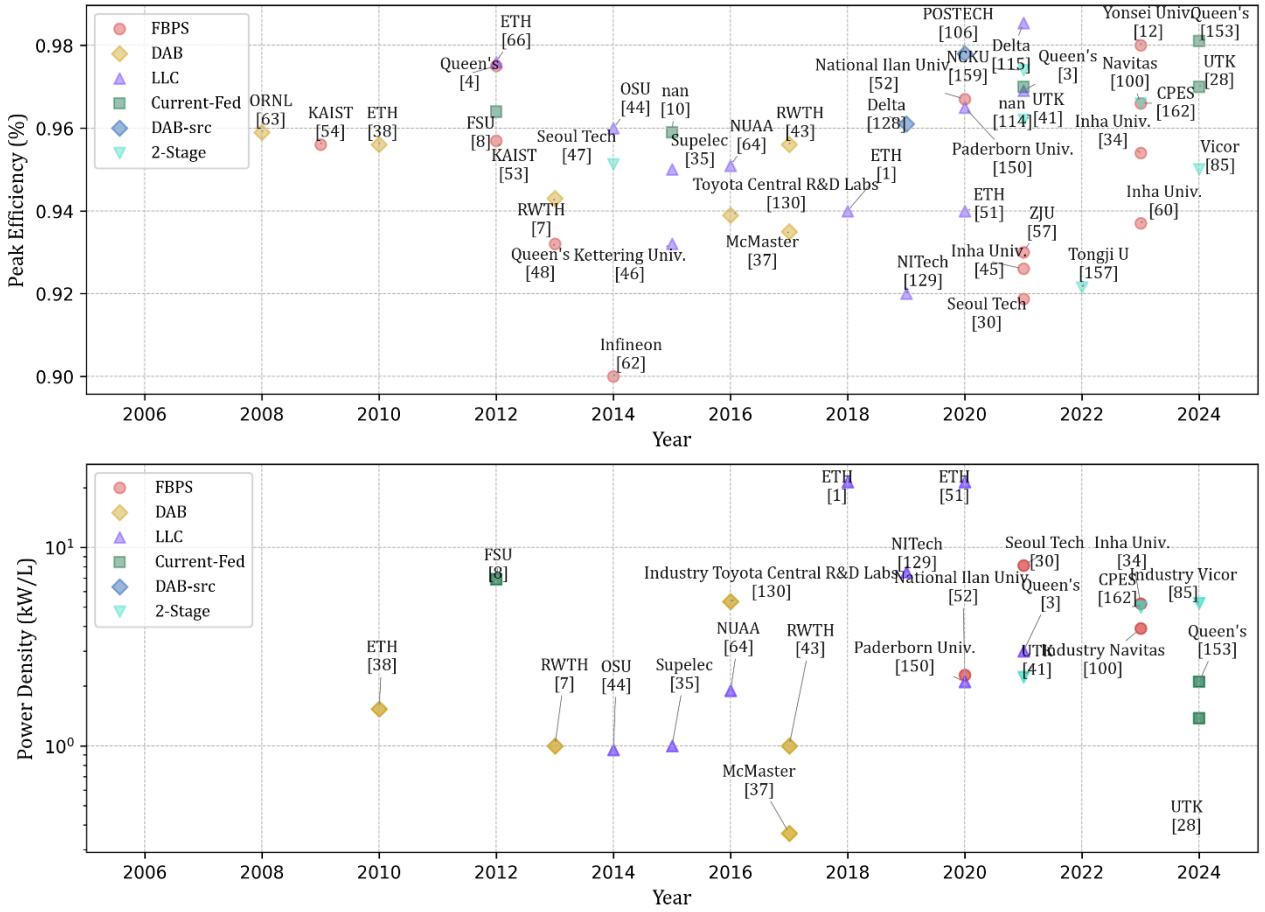

Among the five mainstream topologies, DAB-SRC and Current-Fed have been gaining more awareness in recent years

Possible candidates for future study!

Five main-stream APM topologies with the corresponding improvement are investigated:

- (FBPS) Full Bridge Phase Shift Converter with its rectifier, and magnetic integration
- (LLC/CLLC) LLC, multiphase LLC converter with variable frequency control for wide voltage gain
- (DAB) Non-resonant Dual Active Bridge and its variants
- (DAB-SRC) Series Resonant Converter with both primary and secondary active switch control
- (Current-Fed) Current-Fed DAB converter, non-resonant and resonant

Question and Answer

Reference

References

[1] G. C. Knabben, J. Schafer, L. Peluso, J. W. Kolar, M. J. Kasper, and G. Deboy, "New PCB Winding "Snake-Core" Matrix Transformer for Ultra-Compact Wide DC Input Voltage Range Hybrid B+DCM Resonant Server Power Supply," in *2018 IEEE International Power Electronics and Application Conference and Exposition (PEAC)*. Shenzhen: IEEE, Nov. 2018, pp. 1–6.

[2] T. Jiang, J. Zhang, X. Wu, K. Sheng, and Y. Wang, "A Bidirectional Three-Level LLC Resonant Converter With PWAM Control," *IEEE Transactions on Power Electronics*, vol. 31, no. 3, pp. 2213–2225, Mar. 2016.

[3] X. Zhou, B. Sheng, W. Liu, Y. Chen, L. Wang, Y.-F. Liu, and P. C. Sen, "A high-efficiency high-power-density on-board low-voltage DC–DC converter for electric vehicles application," *IEEE Transactions on Power Electronics*, vol. 36, no. 11, pp. 12 781–12 794, Nov. 2021.

[4] M. Pahlevaninezhad, P. Das, J. Drobnik, P. K. Jain, and A. Bakhshai, "A Novel ZVZCS Full-Bridge DC/DC Converter Used for Electric Vehicles," *IEEE Transactions on Power Electronics*, vol. 27, no. 6, pp. 2752–2769, Jun. 2012.

[5] X. Yu, Z. Lan, J. Zeng, C. Tu, and D. He, "Time-domain based Superposition Analysis for Triple Active Bridge and its Application for ZVS and Current Stress Optimization," *IEEE Transactions on Power Electronics*, pp. 1–13, 2023.

[6] Z. Lin, S. Pan, M. Wang, W. Lin, J. Gong, L. Yao, and P. Jain, "A Three-Port LCC Resonant Converter for the 380-V/48-V Hybrid DC System," *IEEE Transactions on Power Electronics*, vol. 37, no. 9, pp. 10 864–10 876, Sep. 2022.

[7] H. van Hoek, M. Neubert, and R. W. De Doncker, "Enhanced modulation strategy for a three-phase dual active bridge—boosting efficiency of an electric vehicle converter," *IEEE Transactions on Power Electronics*, vol. 28, no. 12, pp. 5499–5507, Dec. 2013.

[8] Z. Wang and H. Li, "A soft switching three-phase current-fed bidirectional DC-DC converter with high efficiency over a wide input voltage range," *IEEE Transactions on Power Electronics*, vol. 27, no. 2, pp. 669–684, Feb. 2012.

[9] P. Purgat, S. Bandyopadhyay, Z. Qin, and P. Bauer, "Zero Voltage Switching Criteria of Triple Active Bridge Converter," *IEEE Transactions on Power Electronics*, vol. 36, no. 5, pp. 5425–5439, May 2021.

[10] D. Moon, J. Park, and S. Choi, "New interleaved current-fed resonant converter with significantly reduced high current side output filter for EV and HEV applications," *IEEE Transactions on Power Electronics*, vol. 30, no. 8, pp. 4264–4271, Aug. 2015.

[11] H. Yu, Y. Wang, H. Zhang, and Z. Chen, "Impedance Modeling and Stability Analysis of Triple-Active-Bridge-Converter-Based Renewable-Electricity-Hydrogen-Integrated Metro DC Traction Power System," *IEEE Transactions on Industrial Electronics*, vol. 70, no. 12, pp. 12 340–12 353, Dec. 2023.

[12] I. Kim and J.-W. Park, "New integrated DC–DC conversion system for electric vehicles," *IEEE Transactions on Industrial Electronics*, pp. 1–10, 2023.

[13] X. Tang, H. Wu, W. Hua, Z. Yu, and Y. Xing, "Three-Port Bidirectional Series-Resonant Converter With First-Harmonic-Synchronized PWM," *IEEE Journal of Emerging and Selected Topics in Power Electronics*, vol. 9, no. 2, pp. 1410–1419, Apr. 2021.

[14] J. Andrade, D. S. Y Rosas, D. Frey, and J.-P. Ferrieux, "Modified triple active bridge DC/AC three-phase converter with a series-resonant LC circuit on the AC-side," in *2017 IEEE Southern Power Electronics Conference (SPEC)*. Puerto Varas, Chile: IEEE, Dec. 2017, pp. 1–6.

[15] K. Wang, W. Liu, and F. Wu, "Topology-Level Power Decoupling Three-Port Isolated Current-Fed Resonant DC-DC Converter," *IEEE Transactions on Industrial Electronics*, vol. 69, no. 5, pp. 4859–4868, May 2022.

[16] F. Wu, W. Liu, K. Wang, and G. Wang, "Modeling and Closed-Loop Control of Three-Port Isolated Current-Fed Resonant DC–DC Converter," *IEEE Transactions on Transportation Electrification*, vol. 9, no. 1, pp. 1341–1349, Mar. 2023.

[17] N. D. Dao, D.-C. Lee, and Q. D. Phan, "High-Efficiency SiC-Based Isolated Three-Port DC/DC Converters for Hybrid Charging Stations," *IEEE Transactions on Power Electronics*, vol. 35, no. 10, pp. 10 455–10 465, Oct. 2020.

[18] P. Wang, X. Lu, W. Wang, and D. Xu, "Hardware Decoupling and Autonomous Control of Series-Resonance-Based Three-Port Converters in DC Microgrids," *IEEE Transactions on Industry Applications*, vol. 55, no. 4, pp. 3901–3914, Jul. 2019.

[19] Y.-K. Tran, F. D. Freijedo, and D. Dujic, "Open-Loop Power Sharing of Three-Port DC-DC Resonant Converters," in *2019 IEEE Applied Power Electronics Conference and Exposition (APEC)*, Mar. 2019, pp. 2138–2144.

[20] J. Wu, X. Yan, X. Sun, X. Su, H. Du, and X. Wang, "A Series Resonant Three-Port DC–DC Converter With Decoupling Function and Magnetic Integration," *IEEE Transactions on Power Electronics*, vol. 37, no. 12, pp. 14 720–14 737, Dec. 2022.

[21] X. Zhang, H. Liu, P. Wheeler, and F. Wu, "Research on Power Decoupling and Parameter Mismatch of Three-Port Isolated Resonant DC–DC Converter Applied Switch-Controlled Capacitor," *IEEE Transactions on Industrial Electronics*, vol. 70, no. 8, pp. 8098–8107, Aug. 2023.

[22] S. S. Chakraborty, S. Dey, and K. Hatua, "Design of a Three-Winding Transformer for Power Decoupling of a Three-Port Series Resonant Converter for an Integrated On-Board EV Charger," *IEEE Transactions on Power Electronics*, vol. 38, no. 11, pp. 14 262–14 273, Nov. 2023.

[23] H. Tao, A. Kotsopoulos, J. L. Duarte, and M. A. M. Hendrix, "Transformer-Coupled Multiport ZVS Bidirectional DC–DC Converter With Wide Input Range," *IEEE Transactions on Power Electronics*, vol. 23, no. 2, pp. 771–781, Mar. 2008.

[24] H. Cao, G. Zhu, F. Diao, and Y. Zhao, "Novel Power Decoupling Methods for Three-Port Triple-Active-Bridge Converters," in *2022 IEEE Applied Power Electronics Conference and Exposition (APEC)*, Mar. 2022, pp. 1833–1837.

[25] L. Wang, Z. Wang, and H. Li, "Asymmetrical Duty Cycle Control and Decoupled Power Flow Design of a Three-port Bidirectional DC-DC Converter for Fuel Cell Vehicle Application," *IEEE Transactions on Power Electronics*, vol. 27, no. 2, pp. 891–904, Feb. 2012.

[26] Y. Cai, C. Gu, J. Li, J. Yang, G. Buticchi, and H. Zhang, "Dynamic Performance Enhancement of a Triple Active Bridge With Power Decoupling-Based Configurable Model Predictive Control," *IEEE Transactions on Transportation Electrification*, vol. 9, no. 2, pp. 3338–3349, Jun. 2023.

[27] S. Goudarzitaemeh and M. Pahlevani, "A Bidirectional DC–DC Converter With Direct Power Transfer," *IEEE Open Journal of Power Electronics*, vol. 5, pp. 232–249, 2024.

[28] L. Zhu, H. Bai, and A. Brown, "Model and control of a current-fed dual active bridge based ultrawide-voltage-range auxiliary power module for 400 V/800 V electric vehicles," *IEEE Transactions on Power Electronics*, vol. 39, no. 3, pp. 3263–3276, Mar. 2024.

[29] M. Salato and P. Kowalyk, "Double-clamp ZVS converter interfaces high voltage traction batteries with 12V legacy system in hybrid and pure-electric vehicles," in *2012 IEEE Vehicle Power and Propulsion Conference*, Oct. 2012, pp. 667–670.

[30] A. M. Naradhipa, S. Kim, D. Yang, S. Choi, I. Yeo, and Y. Lee, "Power density optimization of 700 kHz GaN-based auxiliary power module for electric vehicles," *IEEE Transactions on Power Electronics*, vol. 36, no. 5, pp. 5610–5621, May 2021.

[31] C. C. D. Viana, M. Pathmanathan, and P. W. Lehn, "Auxiliary power module elimination in evs using dual inverter drivetrain," *IEEE Transactions on Power Electronics*, vol. 37, no. 10, pp. 12 513–12 524, Oct. 2022.

[32] R. Hou and A. Emadi, "Evaluation of integrated active filter auxiliary power modules in electrified vehicle applications," in *2015 IEEE Energy Conversion Congress and Exposition (ECCE)*, Sep. 2015, pp. 6314–6319.

[33] ——, "Applied integrated active filter auxiliary power module for electrified vehicles with single-phase onboard chargers," *IEEE Transactions on Power Electronics*, vol. 32, no. 3, pp. 1860–1871, Mar. 2017.

[34] D.-W. Lee, H.-S. Youn, and J.-K. Kim, "Development of phase-shift full-bridge converter with integrated winding planar two-transformer for LDC," *IEEE Transactions on Transportation Electrification*, vol. 9, no. 1, pp. 1215–1226, Mar. 2023.

[35] G. Yang, P. Dubus, and D. Sadarnac, "Double-phase high-efficiency, wide load range high- voltage/low-voltage LLC DC/DC converter for electric/hybrid vehicles," *IEEE Transactions on Power Electronics*, vol. 30, no. 4, pp. 1876–1886, Apr. 2015.

[36] L. Zhu, H. Bai, A. Brown, and A. Körner, "An ultra-high gain current-fed universal auxiliary power module for 400V/800V electric vehicles," in *2023 IEEE Applied Power Electronics Conference and Exposition (APEC)*, Mar. 2023, pp. 885–891.

[37] R. Hou and A. Emadi, "A primary full-integrated active filter auxiliary power module in electrified vehicles with single-phase onboard chargers," *IEEE Transactions on Power Electronics*, vol. 32, no. 11, pp. 8393–8405, Nov. 2017.

[38] F. Krismer and J. W. Kolar, "Accurate power loss model derivation of a high-current dual active bridge converter for an automotive application," *IEEE Transactions on Industrial Electronics*, vol. 57, no. 3, pp. 881–891, Mar. 2010.

[39] M. Pahlevaninezhad, J. Drobnik, P. K. Jain, and A. Bakhshai, "A load adaptive control approach for a zero-voltage-switching DC/DC converter used for electric vehicles," *IEEE Transactions on Industrial Electronics*, vol. 59, no. 2, pp. 920–933, Feb. 2012.

[40] F. Krismer and J. W. Kolar, "Accurate small-signal model for the digital control of an automotive bidirectional dual active bridge," *IEEE Transactions on Power Electronics*, vol. 24, no. 12, pp. 2756–2768, Dec. 2009.

[41] L. Zhu, H. Bai, A. Brown, and M. McAmmond, "Design a 400 V–12 V 6 kW bidirectional auxiliary power module for electric or autonomous vehicles with fast precharge dynamics and zero DC-bias current," *IEEE Transactions on Power Electronics*, vol. 36, no. 5, pp. 5323–5335, May 2021.

[42] E. Stolt, W. Braun, K. Nguyen, V. Chulukhadze, R. Lu, and J. Rivas-Davila, "A spurious-free piezoelectric resonator based 3.2 kW DC–DC converter for EV on-board chargers," *IEEE Transactions on Power Electronics*, vol. 39, no. 2, pp. 2478–2488, Feb. 2024.

[43] H. van Hoek, "Design and operation considerations of three-phase dual active bridge converters for low-power applications with wide voltage ranges," Ph.D. dissertation, Shaker Verlag, Aachen, 2017.

[44] X. Zhang, C. Yao, C. Li, L. Fu, F. Guo, and J. Wang, "A wide bandgap device-based isolated quasi-switched-capacitor DC/DC converter," *IEEE Transactions on Power Electronics*, vol. 29, no. 5, pp. 2500–2510, May 2014.

[45] S.-H. Lee, B.-S. Lee, D.-H. Kwon, J.-H. Ahn, and J.-K. Kim, "Two-mode low-voltage DC/DC converter with high and wide input voltage range," *IEEE Transactions on Industrial Electronics*, vol. 68, no. 12, pp. 12 088–12 099, Dec. 2021.

[46] C. Duan, H. Bai, W. Guo, and Z. Nie, "Design of a 2.5-kW 400/12-V high-efficiency DC/DC converter using a novel synchronous rectification control for electric vehicles," *IEEE Transactions on Transportation Electrification*, vol. 1, no. 1, pp. 106–114, Jun. 2015.

[47] J. Park and S. Choi, "Design and control of a bidirectional resonant DC–DC converter for automotive engine/battery hybrid power generators," *IEEE Transactions on Power Electronics*, vol. 29, no. 7, pp. 3748–3757, Jul. 2014.

[48] D. Hamza, M. Pahlevaninezhad, and P. K. Jain, "Implementation of a novel digital active EMI technique in a DSP-based DC–DC digital controller used in electric vehicle (EV)," *IEEE Transactions on Power Electronics*, vol. 28, no. 7, pp. 3126–3137, Jul. 2013.

[49] Y.-S. Kim, C.-Y. Oh, W.-Y. Sung, and B. K. Lee, "Topology and control scheme of OBC–LDC integrated power unit for electric vehicles," *IEEE Transactions on Power Electronics*, vol. 32, no. 3, pp. 1731–1743, Mar. 2017.

[50] D.-H. Kim, M.-J. Kim, and B.-K. Lee, "An integrated battery charger with high power density and efficiency for electric vehicles," *IEEE Transactions on Power Electronics*, vol. 32, no. 6, pp. 4553–4565, Jun. 2017.

[51] G. C. Knabben, J. Scahfer, J. W. Kolar, G. Zulauf, M. J. Kasper, and G. Deboy, "Wide-input-voltage-range 3 kW DC-DC converter with hybrid LLC & boundary / discontinuous mode control," in *2020 IEEE Applied Power Electronics Conference and Exposition (APEC)*. New Orleans, LA, USA: IEEE, Mar. 2020, pp. 1359–1366.

[52] Y.-C. Liu, C.-Y. Xiao, C.-C. Huang, P.-C. Chi, and H.-J. Chiu, "Integrated magnetics design for a full-bridge phase-shifted converter," *Energies*, vol. 14, no. 1, p. 183, Dec. 2020.

[53] K.-M. Cho, Y.-D. Kim, I.-H. Cho, and G.-W. Moon, "Transformer integrated with additional resonant inductor for phase-shift full-bridge converter with primary clamping diodes," *IEEE Transactions on Power Electronics*, vol. 27, no. 5, pp. 2405–2414, May 2012.

[54] Young-Do Kim, Chong-Eun Kim, Kyu-Min Cho, Ki-Bum Park, and Gun-Woo Moon, "ZVS phase shift full bridge converter with separated primary winding," in *2009 IEEE Energy Conversion Congress and Exposition*. San Jose, CA: IEEE, Sep. 2009, pp. 484–489.

[55] D.-W. Lee, B.-S. Lee, J.-H. Ahn, J.-Y. Kim, and J.-K. Kim, "New combined OBC and LDC system for electric vehicles with 800 V battery," *IEEE Transactions on Industrial Electronics*, vol. 69, no. 10, pp. 9938–9951, Oct. 2022.

[56] V. B. Gandluru, K. Autkar, and Y. Hu, "Identifying suitable PSFB topology for HVLV auxiliary power supply (APS) application in evs," in *2024 IEEE Applied Power Electronics Conference and Exposition (APEC)*, Feb. 2024, pp. 2069–2076.

[57] Q. Ding, Y. Gao, and H. Ma, "Self-adaptive synchronous rectifier control algorithm of phase-shifted full bridge current double rectifier converter," in *2021 IEEE 1st International Power Electronics and Application Symposium (PEAS)*, Nov. 2021, pp. 1–6.

[58] S. Mukherjee, V. Sujan, S. Chowdhury, and O. Onar, "Multiport converter based auxiliary power supply for heavy duty fuel cell power train," in *2024 IEEE Transportation Electrification Conference and Expo (ITEC)*, Jun. 2024, pp. 1–6.

[59] G. Yu and S. Choi, "An effective integration of APM and OBC with simultaneous operation and entire ZVS range for electric vehicle," *IEEE Transactions on Power Electronics*, vol. 36, no. 9, pp. 10 343–10 354, Sep. 2021.

[60] S.-W. Jeong, S.-H. Lee, D.-H. Kwon, J.-Y. Kim, and J.-K. Kim, "Two-transformer phase-shift full-bridge converter with a new rectifier for reducing conduction loss," *IEEE Transactions on Power Electronics*, vol. 38, no. 12, pp. 15 634–15 644, Dec. 2023.

[61] F. Krismer and J. W. Kolar, "Efficiency-optimized high-current dual active bridge converter for automotive applications," *IEEE Transactions on Industrial Electronics*, vol. 59, no. 7, pp. 2745–2760, Jul. 2012.

[62] S. Zeljkovic, T. Reiter, and D. Gerling, "Efficiency optimized single-stage reconfigurable DC/DC converter for hybrid and electric vehicles," *IEEE Journal of Emerging and Selected Topics in Power Electronics*, vol. 2, no. 3, pp. 496–506, Sep. 2014.

[63] G.-J. Su and L. Tang, "A three-phase bidirectional DC-DC converter for automotive applications," in *2008 IEEE Industry Applications Society Annual Meeting*, Oct. 2008, pp. 1–7.

[64] Z. Pang, X. Ren, J. Xiang, Q. Chen, X. Ruan, and W. Chen, "High-frequency DC-DC converter in electric vehicle based on GaN transistors," in *2016 IEEE Energy Conversion Congress and Exposition (ECCE)*. Milwaukee, WI, USA: IEEE, Sep. 2016, pp. 1–7.

[65] H. Wouters, H. Pervaiz, T. Geboers, Y. Zuo, W.-R. Lin, and W. Martinez, "Interleaved PCB Winding Planar Transformer for Electric Vehicle Charging CLLC Converters," in *2024 IEEE Applied Power Electronics Conference and Exposition (APEC)*, Feb. 2024, pp. 3216–3223.

[66] A. Hillers, D. Christen, and J. Biela, "Design of a Highly efficient bidirectional isolated LLC resonant converter," in *2012 15th International Power Electronics and Motion Control Conference (EPE/PEMC)*, Sep. 2012, pp. DS2b.13–1–DS2b.13–8.

[67] "Vitesco Technologies - High Voltage DC/DC Converter - 4th Generation." [Online]. Available: https://www.vitesco-technologies.com/en-us/products/high-voltage-dc-dc-converter-4th-generation

[68] "Vitesco Technologies - High Voltage Power Electronics Inverter + DC/DC Converter." [Online]. Available: https://www.vitesco-technologies.com/en-us/products/high-voltage-power-electronics-(epf2-8)

[69] "PC32_Power supply_Passenger car solution_Products and Solutions_Suzhou Inovance Automotive Co., Ltd." [Online]. Available: https://en.inovance-automotive.com/content/details86_843.html

[70] "PC41_Power supply_Passenger car solution_Products and Solutions_Suzhou Inovance Automotive Co., Ltd." [Online]. Available: https://en.inovance-automotive.com/content/details86_842.html

[71] "PP30_Power supply_Passenger car solution_Products and Solutions_Suzhou Inovance Automotive Co., Ltd." 2018. [Online]. Available: https://en.inovance-automotive.com/content/details86_839.html

[72] "PC36_Power supply_Passenger car solution_Products and Solutions_Suzhou Inovance Automotive Co., Ltd." [Online]. Available: https://en.inovance-automotive.com/content/details86_838.html

[73] "Charger-converter." [Online]. Available: https://www.bosch-mobility.com/en/solutions/power-electronics/charger-converter/

[74] "High-voltage DC/DC converter generation 3evo," 2021. [Online]. Available: https://www.bosch-mobility.com/en/solutions/power-electronics/high-voltage-dc-dc-converter-generation-3evo/

[75] "Integrate SiC power electronics into EV fast chargers | Wolfspeed." [Online]. Available: https://www.wolfspeed.com/knowledge-center/article/maximize-efficiency-in-isolated-dc-converters-for-ev-fast-charging-systems/

[76] "CRD-60DD12N-K 60 kW Discrete Interleaved LLC DC-DC Converter | Wolfspeed." [Online]. Available: https://www.wolfspeed.com/products/power/reference-designs/crd-60dd12n-k/

[77] "DC DC Converter 1500w | EMP EV MOBILITY." [Online]. Available: https://www.empevmobility.com/products/1.5kw-dc-dc-converter-unit.html

[78] "EV OBC DCD PDU 3 in 1 CDU Unit, Electric Drive Unit | EMP EV MOBILITY." [Online]. Available: https://www.empevmobility.com/products/obc-dcd-pdu-3-in-1-cdu-unit.html

Reference

[79] "400V DC/DC Converter - Delta," 2021. [Online]. Available: https://www.deltaww.com/en-US/products/ev-dc-dc-converters/ALL/

[80] "48V DC/DC converter." [Online]. Available: https://www.eaton.com/us/en-us/catalog/emobility/48v-dc-dc-converter.html

[81] "High-voltage DC/DC converter," Jun. 2023. [Online]. Available: https://www.eaton.com/us/en-us/catalog/emobility/high-voltage-dc-dc-converter.html

[82] "800V DC/DC Converter - Delta," 2022. [Online]. Available: https://www.deltaww.com/en-US/products/ev-dc-dc-converters/ALL/

[83] "Learn more about Technology Innovation for the Next Gen of EVs." [Online]. Available: https://www.vicorpower.com/ja-jp/resource-library/videos/technology-innovations-next-gen-evs-green

[84] G. Greg, "Unprecedented levels of miniaturization in automotive electronics," May 2024. [Online]. Available: https://www.vicorpower.com/documents/event-presentation/ICPE-2023-Impact-miniaturized-power-modules-electrification-Green.pdf

[85] "Power modules meet EV power demands that have increased by 20x," May 2024. [Online]. Available: https://www.vicorpower.com/resource-library/articles/automotive/power-modules-for-uncharted-ev-power-challenges

[86] "Automotive Innovation Day 2024 in Seoul, Korea." [Online]. Available: https://www.vicorpower.com/resource-library/events/aid-2024

[87] YK. Choi, "Optimize your vehicle power distribution network by integrating the DC-DC converter into the battery pack."

[88] "LSM4k0-400-2, 4kW LSM DC-DC - 400V in, 24V Out, Droop CS." [Online]. Available: https://store.astrodynetdi.com/4kw-lsm-dc-dc-400v-in-24v-out-droop-cst100103677-lf.html

[89] "350DNC40-12 - 4000W, 12V, DC-DC HEV Down Converter | Bel Fuse." [Online]. Available: https://www.belfuse.com/product-detail/power-solutions-custom-value-added-solutions-emobility-350dnc40-down-converter

[90] "700DNG40-24-8 - 4000W, 24V, DC-DC HEV Down Converter | Bel Fuse," Dec. 2023. [Online]. Available: https://www.belfuse.com/product-detail/power-solutions-custom-value-added-solutions-emobility-700dng40-24-down-converter?navCategory=eMobilityDcdcConvertersundefined

[91] "Bsc6xx, DC/DC Converter - 125 A, 220 - 450 V, 24 V," Jun. 2023. [Online]. Available: https://www.brusahypower.com/portfolio/bsc614/

[92] "BSC7xx, DC/DC converter - 190 - 480 V / 350 - 890 V." [Online]. Available: https://www.brusahypower.com/portfolio/bsc7xx/

[93] "DC/DC Converter - 3×400 VAC / 32 A, 700 VDC, 22 kW." [Online]. Available: https://www.brusahypower.com/portfolio/nlg667/

[94] "Gen5 High Voltage DC/DC." [Online]. Available: https://www.borgwarner.com/technologies/power-electronics#isolated-converter

[95] P. Xuewei and A. K. Rathore, "Naturally Clamped Soft-Switching Current-Fed Three-Phase Bidirectional DC/DC Converter," *IEEE Transactions on Industrial Electronics*, vol. 62, no. 5, pp. 3316–3324, May 2015.

[96] C.-Y. Lim, Y. Jeong, and G.-W. Moon, "Phase-Shifted Full-Bridge DC–DC Converter With High Efficiency and High Power Density Using Center-Tapped Clamp Circuit for Battery Charging in Electric Vehicles," *IEEE Transactions on Power Electronics*, vol. 34, no. 11, pp. 10 945–10 959, Nov. 2019.

[97] H. Zou, R. Yu, R. Anand, J. Tong, and A. Q. Huang, "A GaN Variable-Frequency Series Resonant Dual-Active-Bridge Bidirectional AC-DC Converter for Battery Energy Storage System," in *2023 IEEE Applied Power Electronics Conference and Exposition (APEC)*, Mar. 2023, pp. 150–157.

[98] C. Sun, X. Jiang, L. Cao, and K. H. Loo, "Total Suppression of High-Frequency Transient Oscillations in Dual-Active-Bridge Series-Resonant Converter by Trajectory-Switching Modulation," *IEEE Transactions on Power Electronics*, vol. 37, no. 6, pp. 6511–6529, Jun. 2022.

[99] J. Minli and S. Hao, "GaN-based High Frequency 6.6kW Bi-directional DC/DC Converter for OBC Application," in *2022 IEEE International Power Electronics and Application Conference and Exposition (PEAC)*, Nov. 2022, pp. 1330–1335.

[100] M. Jia and H. Sun, "GaN-based High-Frequency, High-Power-Density, 2-in-1 Bi-directional OBC Design for EV Applications," in *PCIM Europe 2023; International Exhibition and Conference for Power Electronics, Intelligent Motion, Renewable Energy and Energy Management*, May 2023, pp. 1–10.

[101] E. L. Carvalho, A. Chub, A. Blinov, S. N. Banavath, and D. Vinnikov, "Comparative Evaluation of a DAB Converter and SRC for DC Buildings Application," in *2024 IEEE 21st International Power Electronics and Motion Control Conference (PEMC)*, Sep. 2024, pp. 1–6.

[102] J. Xu, G. Xu, Y. Sun, and M. Su, "A Family of Bidirectional Series Resonant Converter With Sine-Wave Modulation in Wide Voltage Range," *IEEE Transactions on Power Electronics*, vol. 38, no. 4, pp. 5013–5023, Apr. 2023.

[103] L. Gu, X. Zhang, and P. Li, "Hybrid-PWM-Controlled Current-Fed Bidirectional Series Resonant Converter With Low Current Ripple and Wide Voltage Gain," *IEEE Transactions on Industrial Electronics*, vol. 68, no. 8, pp. 7125–7136, Aug. 2021.

[104] Z. Pei, D. Guo, T. Cui, C. Liu, D. Kong, D. Zhu, Y. Jiang, and N. Chen, "Phase-Shift Full-Bridge (PSFB) Converter Integrated Double-Inductor Rectifier With Separated Resonant Circuits (SRCs) for 800-V High-Power Electric Vehicles," *IEEE Journal of Emerging and Selected Topics in Power Electronics*, vol. 12, no. 1, pp. 269–282, Feb. 2024.

[105] K. Qiu, P. Jia, and Y. Zhang, "Dynamic Response Optimization of a DABSRC Based on Feedforward Control," in *2023 IEEE 2nd International Power Electronics and Application Symposium (PEAS)*, Nov. 2023, pp. 1635–1639.

[106] C. Bai, B. Han, B.-H. Kwon, and M. Kim, "Highly Efficient Bidirectional Series-Resonant DC/DC Converter Over Wide Range of Battery Voltages," *IEEE Transactions on Power Electronics*, vol. 35, no. 4, pp. 3636–3650, Apr. 2020.

[107] G. Liu, Y. Jang, M. M. Jovanovi, and J. Q. Zhang, "Implementation of a 3.3-kW DC–DC Converter for EV On-Board Charger Employing the Series-Resonant Converter With Reduced-Frequency-Range Control," *IEEE Transactions on Power Electronics*, vol. 32, no. 6, pp. 4168–4184, Jun. 2017.

[108] R. Gu, D. Zhang, J. Duan, and A. Li, "An Interleaved Current-Fed Integrated LLC Resonant Converter With Input Current Ripple Cancellation," *IEEE Transactions on Industrial Electronics*, pp. 1–11, 2024.

[109] W. Han and L. Corradini, "General Closed-Form ZVS Analysis of Dual-Bridge Series Resonant DC–DC Converters," *IEEE Transactions on Power Electronics*, vol. 34, no. 9, pp. 9289–9302, Sep. 2019.

[110] ——, "Wide-Range ZVS Control Technique for Bidirectional Dual-Bridge Series-Resonant DC–DC Converters," *IEEE Transactions on Power Electronics*, vol. 34, no. 10, pp. 10 256–10 269, Oct. 2019.

[111] S. Gurudiwan, A. Zade, R. Hatch, H. Wang, and R. Zane, "ZVS Boundary Assessment for T-type-based Dual Active Bridge Series Resonant Converters using State-Plane Analysis," in *2024 IEEE Applied Power Electronics Conference and Exposition (APEC)*, Feb. 2024, pp. 2098–2105.

[112] L. Corradini, D. Seltzer, D. Bloomquist, R. Zane, D. Maksimović, and B. Jacobson, "Minimum Current Operation of Bidirectional Dual-Bridge Series Resonant DC/DC Converters," *IEEE Transactions on Power Electronics*, vol. 27, no. 7, pp. 3266–3276, Jul. 2012.

[113] Y. Gao, L. Zhou, Z. Zhou, Q. Ding, X. Zhang, and H. Ma, "Low-Side-Extended-Phase-Shift-Under-Resonant Modulation Scheme for Dual-Bridge-Series-Resonant Converter," *IEEE Transactions on Industrial Electronics*, vol. 71, no. 12, pp. 15 554–15 567, Dec. 2024.

[114] N.-G. Kim, S.-W. Jo, B. Han, H.-H. Choi, and M. Kim, "Highly Efficient Bidirectional Current-Fed Resonant Converter Over a Wide Voltage Gain Range," *IEEE Transactions on Industrial Electronics*, vol. 68, no. 11, pp. 10 913–10 927, Nov. 2021.

[115] J.-W. Kim and P. Barbosa, "PWM-Controlled Series Resonant Converter for Universal Electric Vehicle Charger," *IEEE Transactions on Power Electronics*, vol. 36, no. 12, pp. 13 578–13 588, Dec. 2021.

[116] I.-O. Lee and G.-W. Moon, "Analysis and Design of a Three-Level LLC Series Resonant Converter for High- and Wide-Input-Voltage Applications," *IEEE Transactions on Power Electronics*, vol. 27, no. 6, pp. 2966–2979, Jun. 2012.

[117] "DCDC LP Converters," 2024. [Online]. Available: https://brightloop.fr/products/hv-lv-dc-dc-converters/dcdc-lp/

[118] "BRIGHTLOOP | Automotive Application for GaN Semiconductors," 2024. [Online]. Available: https://gansystems.com/gan-applications/brightloop/

[119] "VITESCO TECHNOLOGIES | Automotive Application for GaN Semiconductors." [Online]. Available: https://gansystems.com/gan-applications/vitesco-technologies/

[120] "HELLA | Automotive Application for GaN Semiconductors." [Online]. Available: https://gansystems.com/gan-applications/hella-22-kw-ev-onboard-charger/

[121] "DCDC MP Converters," 2024. [Online]. Available: https://brightloop.fr/products/hv-lv-dc-dc-converters/dcdc-mp/

[122] "DCDC SP Converters," 2024. [Online]. Available: https://brightloop.fr/products/hv-lv-dc-dc-converters/dcdc-sp/

[123] A. Chandwani, A. Mallik, and A. Akturk, "Steady-State Model-Derived Multivariable Loss Optimization for Triple Active C^3L^3 Resonant Converter," *IEEE Transactions on Transportation Electrification*, vol. 10, no. 1, pp. 1729–1746, Mar. 2024.

[124] L. Jiang, L. Gong, J. Xu, J. Chen, H. Tang, M. Nie, and Y. Wang, "A Variable Tertiary DC-Link Voltage Control for Integrated APM in EV Charger Systems Featuring Full ZVS Range," *IEEE Transactions on Transportation Electrification*, vol. 10, no. 4, pp. 8962–8977, Dec. 2024.

[125] A. Jung, D. Moon, C. Bai, J. Jang, M. Oh, S. Lee, S. Hwang, and H. Moon, "Bi-directional Operation Mode of LLC/CLLC DC/DC Converter for On Board Charger of 800V Battery Systems," in *2023 11th International Conference on Power Electronics and ECCE Asia (ICPE 2023 - ECCE Asia)*, May 2023, pp. 2814–2819.

[126] C. Bai and M. Kim, "Bidirectional Resonant Converter With Minimized Switching Loss Over Wide Operating Voltage Range," *IEEE Journal of Emerging and Selected Topics in Power Electronics*, vol. 10, no. 3, pp. 2975–2988, Jun. 2022.

[127] J. Schaefer and J. W. Kolar, "Highly Integrated Ultra-Compact Three-Port Converter Systems for Automotive Applications," in *CIPS 2022; 12th International Conference on Integrated Power Electronics Systems*, Mar. 2022, pp. 1–4. [Online]. Available: https://ieeexplore.ieee.org/document/9861943

[128] Y. Jang, M. M. Jovanović, M. Kumar, J. M. Ruiz, R. Lu, and T. Wei, "Isolated, Bi-Directional DC-DC Converter for Fuel Cell Electric Vehicle Applications," in *2019 IEEE Applied Power Electronics Conference and Exposition (APEC)*, Mar. 2019, pp. 1674–1681.

[129] H. Matsumori, T. Kosaka, K. Sekido, K. Kim, T. Egawa, and N. Matsui, "Isolated DC-DC Converter utilizing GaN power device for Automotive Application," in *2019 IEEE Applied Power Electronics Conference and Exposition (APEC)*, Mar. 2019, pp. 1704–1709.

[130] K. Itoh, S. Inoue, T. Sugiyama, and M. Sugai, "Design and modulation method of Multi-port DC/DC converter for next generation HV sub system," in *IECON 2016 - 42nd Annual Conference of the IEEE Industrial Electronics Society*, Oct. 2016, pp. 1318–1323.

[131] Y. Jang and M. M. Jovanovic, "Resonant converters and control methods thereof," US Patent US20 150 229 225A1, Aug., 2015. [Online]. Available: https://patents.google.com/patent/US20150229225A1/en?q=(patent)&inventor=Yungtaek+Jang&oq=Yungtaek+Jang+us+patent&sort=new

[132] T. Wei and H. Lu, "Resonant converter and control method for realizing soft switching," US Patent US10 756 617B2, Aug., 2020. [Online]. Available: https://patents.google.com/patent/US10756617B2/en?oq=US+Patent+10%2c756%2c617+

[133] Y. Jang and M. M. Jovanovic, "Contactless electrical energy transmission system having a primary side current feedback control and soft-switched secondary side rectifier," US Patent US6 934 167B2, Aug., 2005. [Online]. Available: https://patents.google.com/patent/US6934167B2/en?oq=US20150229225A1

[134] H. Seong, "Synchronous rectifier type series resonant converter for operating in intermittence mode," US Patent US7 843 708B2, Nov., 2010. [Online]. Available: https://patents.google.com/patent/US7843708B2/en?oq=US20150229225A1

[135] L. Ye, H. Dai, D. Fu, and D. Chen, "Resonant Converters with an Improved Voltage Regulation Range," US Patent US20 160 294 294A1, Oct., 2016. [Online]. Available: https://patents.google.com/patent/US20160294294A1/en?oq=US+Patent+10%2c756%2c617+

[136] W. Hu and C. Lu, "DC/DC converter and control method thereof," US Patent US11 063 523B2, Jul., 2021. [Online]. Available: https://patents.google.com/patent/US11063523B2/en?oq=US20150229225A1

[137] M. Jia, H. Sun, C. Zhang, J. Zhang, and P. M. BARBOSA, "Three-level rectification dc/dc converter," US Patent US20 230 179 107A1, Jun., 2023. [Online]. Available: https://patents.google.com/patent/US20230179107A1/en?oq=US+Patent+10%2c756%2c617+

[138] H. Liu, B. SONG, S. OUYANG, and C. Lu, "Resonant converter, and controlling method for the same," EP Patent EP4 322 382A1, Feb., 2024. [Online]. Available: https://patents.google.com/patent/EP4322382A1/en?oq=US+Patent+10%2c756%2c617+

[139] M. Kumar, Y. Jang, P. M. BARBOSA, M. Jia, and H. Sun, "Multiple-port bidirectional converter and control method thereof," US Patent US11 594 973B2, Feb., 2023. [Online]. Available: https://patents.google.com/patent/US11594973B2/en?oq=US+Patent+10%2c756%2c617+

[140] T. Wang and W. Liu, "Power Converter, Method for Increasing Inverse Gain Range, Apparatus, and Medium," US Patent US20 220 345 046A1, Oct., 2022. [Online]. Available: https://patents.google.com/patent/US20220345046A1/en?oq=US20150229225A1

[141] M. Kim, S. KIM, and B. KIM, "Power conversion circuit for photovoltaic power generation with high efficiency over wide input voltage range," US Patent US10 476 398B1, Nov., 2019. [Online]. Available: https://patents.google.com/patent/US10476398B1/en?oq=US20150229225A1

[142] H. Sun, M. Jia, and J. Zhang, "Control method for DC/DC converter and DC/DC converter," US Patent US11 070 134B2, Jul., 2021. [Online]. Available: https://patents.google.com/patent/US11070134B2/en?oq=US20150229225A1

[143] C. Fromme, F. Döbler, D. Malane, and M. Tannhäuser, "Bidirektionaler LLC-Resonanzwandler und Verfahren," DE Patent DE102 020 213 206A1, Apr., 2022. [Online]. Available: https://patents.google.com/patent/DE102020213206A1/en?oq=US20150229225A1

[144] P. REHLAENDER, F. Schafmeister, and J. Boecker, "Power balancing in interleaved llc converters via duty cycle variation," EP Patent EP3 965 279A1, Mar., 2022. [Online]. Available: https://patents.google.com/patent/EP3965279A1/en?oq=US20150229225A1

[145] C. Zhang and P. Barbosa, "Isolated dc/dc converters for wide output voltage range and control methods thereof," EP Patent EP3 916 984A1, Dec., 2021. [Online]. Available: https://patents.google.com/patent/EP3916984A1/en?oq=US20150229225A1

[146] P. Ausseresse, "Hybrid resonant power supply," US Patent US12 051 972B2, Jul., 2024. [Online]. Available: https://patents.google.com/patent/US12051972B2/en?oq=US20150229225A1

[147] C. Zhang and P. Barbosa, "Isolated DC/DC converters for wide output voltage range and control methods thereof," US Patent US11 901 826B2, Feb., 2024. [Online]. Available: https://patents.google.com/patent/US11901826B2/en?oq=US20150229225A1

[148] S.-K. YANG, H.-K. WANG, and Y.-W. Lin, "Llc resonance converter and method of controlling the same," US Patent US20 220 416 677A1, Dec., 2022. [Online]. Available: https://patents.google.com/patent/US20220416677A1/en?oq=US20150229225A1

[149] K. D. T. Ngo, X. Cao, and Y. Wang, "Pulse width modulated resonant power conversion," US Patent US20 120 014 138A1, Jan., 2012. [Online]. Available: https://patents.google.com/patent/US20120014138A1/en?oq=US+Patent+10%2c756%2c617+

[150] P. Rehlaender, T. Grote, S. Tikhonov, M. Schroeder, F. Schafmeister, and J. Boecker, "A 3,6 kW Single-Stage LLC Converter Operating in Half-Bridge, Full-Bridge and Phase-Shift Mode for Automotive Onboard DC-DC Conversion," in *PCIM Europe Digital Days 2020; International Exhibition and Conference for Power Electronics, Intelligent Motion, Renewable Energy and Energy Management*, Jul. 2020, pp. 1–8. [Online]. Available: https://ieeexplore.ieee.org/document/9177997/?arnumber=9177997

[151] A. Chandwani and A. Mallik, "Fabrication Tradeoff Based Optimal Synthesis of Winding Configurations for Planar Transformer in CLLC DC–DC Converter," *IEEE Transactions on Power Electronics*, vol. 38, no. 5, pp. 6243–6258, May 2023.

[152] S. Goudarzitaemeh, L. Melanson, J. Woelfle, and M. Pahlevani, "A Multilevel Current-Fed DAB Converter With Direct Power Transfer," *IEEE Open Journal of Power Electronics*, vol. 5, pp. 1612–1628, 2024.

[153] S. Goudarzitaemeh and M. Pahlevani, "Extended Phase Shift Control of a Novel Bidirectional DC–DC Converter With Direct Power Transfer," *IEEE Journal of Emerging and Selected Topics in Power Electronics*, vol. 12, no. 5, pp. 4521–4537, Oct. 2024.

[154] D. Sha, X. Wang, and Y. Xu, "Unequal PWM control for a current-fed dc-dc converter for battery application," in *2017 IEEE Applied Power Electronics Conference and Exposition (APEC)*, Mar. 2017, pp. 3373–3377.

[155] D. Sha, Y. Xu, J. Zhang, and Y. Yan, "Current-Fed Hybrid Dual Active Bridge DC–DC Converter for a Fuel Cell Power Conditioning System With Reduced Input Current Ripple," *IEEE Transactions on Industrial Electronics*, vol. 64, no. 8, pp. 6628–6638, Aug. 2017.

[156] C. Yu, S. Jang, H. Kim, T. Kim, S. Son, C. Kwon, I. Jang, and H. Cha, "High Efficiency Bidirectional Dual Active Bridge (DAB) Converter Adopting Boost-Up Function for Increasing Output Power," *IEEE Transactions on Power Electronics*, vol. 37, no. 12, pp. 14 678–14 691, Dec. 2022.

[157] C. Wu, J. Yue, J. Liu, and L. Wang, "An Online Proactive Health Monitoring Method for Output Capacitors of Vehicular Auxiliary Converter," *IEEE Journal of Emerging and Selected Topics in Power Electronics*, vol. 10, no. 1, pp. 1219–1231, Feb. 2022.

[158] C. Wu, J. Liu, L. Wang, Y. Su, and J. Yue, "An Online Proactive CTR Monitoring Method for Optocoupler in Automotive Auxiliary Converter," *IEEE Transactions on Instrumentation and Measurement*, vol. 70, pp. 1–13, 2021.

[159] C.-Y. Chen, T.-J. Liang, K.-F. Liao, K.-H. Chen, and Y.-H. Yeoh, "Design and Implementation of Two-Stage Boost and Full-Bridge Resonant Converter for Wide-Range APMs," in *2021 IEEE International Future Energy Electronics Conference (IFEEC)*, Nov. 2021, pp. 1–6.

[160] L. Zhu, H. Bai, A. Brown, and M. McAmmond, "Two-stage vs One-stage Design for A Bidirectional 400V/12V 6kW Auxiliary Power Module in Electric Vehicles," in *2020 IEEE Transportation Electrification Conference & Expo (ITEC)*, Jun. 2020, pp. 1222–1226.

[161] S. Wang, P. H. Pham, Q. Li, A. Nabih, and P. R. Prakash, "PCB Winding-Based Coupled Inductor for a High-Frequency DC/DC Converter with 99% Efficiency," in *2023 IEEE Applied Power Electronics Conference and Exposition (APEC)*, Mar. 2023, pp. 420–425.

[162] P. R. Prakash, A. Nabih, S. Wang, P. P. Hieu, Y. Ruan, and Q. Li, "GaN-Based 400V/48V DC-DC Converter with 97% Efficiency and PCB Magnetics for Automotive Applications," in *2023 IEEE Applied Power Electronics Conference and Exposition (APEC)*, Mar. 2023, pp. 3201–3208.